Available online at www.sciencedirect.com

ScienceDirect

Journal of Magnesium and Alloys 10 (2022) 1737–1785

www.elsevier.com/locate/jma

Review

Effects of heat treatment on the corrosion behavior and mechanical properties of biodegradable Mg alloys

Meysam Mohammadi Zerankeshi[a], Reza Alizadeh[a,*], Ehsan Gerashi[a], Mohammad Asadollahi[a], Terence G. Langdon[b]

[a] *Department of Materials Science and Engineering, Sharif University of Technology, Tehran, Iran*
[b] *Materials Research Group, Department of Mechanical Engineering, University of Southampton, Southampton SO17 1BJ, United Kingdom*

Received 5 December 2021; received in revised form 1 April 2022; accepted 9 April 2022
Available online 8 June 2022

Abstract

Biodegradable magnesium (Mg) alloys exhibit great potential for use as temporary structures in tissue engineering applications. Such degradable implants require no secondary surgery for their removal. In addition, their comparable mechanical properties with the human bone, together with excellent biocompatibility, make them a suitable candidate for fracture treatments. Nevertheless, some challenges remain. Fast degradation of the Mg-based alloys in physiological environments leads to a loss of the mechanical support that is needed for complete tissue healing and also to the accumulation of hydrogen gas bubbles at the interface of the implant and tissue. Among different methods used to improve the performance of the biodegradable Mg alloys to address these challenges, it appears that heat treatment is the most effective way to modify the microstructure and thus the corrosion behavior and mechanical properties without changing the composition or shape of the alloys. A desirable combination of corrosion and mechanical properties can be obtained through a precise control of the heat treatment parameters. In this report, the effects of different heat treatments (T4 and T6) on the microstructure, corrosion behavior, and mechanical properties of some of the most important heat-treatable biodegradable Mg alloys (Mg-Zn, Mg-Gd, Mg-Y, Mg-Nd, Mg-Al and Mg-Ag) are examined as well as new perspectives to enhance their clinical implementation.

Keywords: Biodegradable implants; Corrosion rate; Heat treatment; Mechanical properties; Mg alloys.

1. Introduction

Regenerative medicine needs a further development of novel biomaterials to help the process of recovery of the damaged tissues, where this has become of special importance and interest in recent years as a consequence of the aging and overall longevity of the world's population. The biodegradable implants have attracted too much attention in recent years due to their outstanding performance in the process of tissue regeneration. Such implants can act as a temporary structure which helps the damaged tissue to carry the loads, and after the execution of their clinical function they will degrade gradually within the biological media to be replaced by the native tissue. As a consequence, the issues concerning the use of permanent implants, such as the chronic inflammation, physical irritation, endothelial dysfunctions and the need for secondary surgery for the implant removal, are effectively avoided [1–8].

Mg-based alloys as biodegradable implants exhibit a significant potential for use as temporary structures for tissue engineering purposes. In this regard, the Mg alloys are considered as an exceptional candidate for fracture treatments due to their comparable density (1.74-2.0 g/cm^3) and tensile strength (100-200 MPa) to those of the human bone. The stress shielding effect and associated problems, such as implant loosening, skeleton thickening and serious impediments to the healing process, would be mitigated by the similar elastic modulus (41-45 GPa) of the Mg alloys to that of natural bone (10-30 GPa) [9]. Magnesium, as the fourth most abundant cation

* Corresponding author.
E-mail address: r.alizadeh@sharif.edu (R. Alizadeh).

https://doi.org/10.1016/j.jma.2022.04.010

in the human body, is essential to human metabolism and its daily recommended intake for an adult is of the order of 240-420 mg/day, where the excess Mg cations can be excreted in the urine without any toxicity [10–12]. The Mg alloys would be degraded in biological environments due to the presence of Cl^- [13,14]. The associated mechanical properties, together with the biocompatibility characteristics of the Mg alloys, like osteogenesis inductivity [15], antibacterial [16] and anti-tumor effects [17] and anti-inflammatory properties [18], make them a distinctive choice in biomedical applications such that extensive research has been conducted in this area. A summary of the numbers of published articles containing "biodegradable Mg" or "biodegradable magnesium" expressions in the title is presented in Fig. 1a, implying a very significant growth after 2005.

The success in the regeneration of damaged bone tissue is strongly related to attaining a balance between the corrosion rate of the implant and the bone healing rate, the presence of an adequate mechanical support during the healing time, a through degradation of the implant after complete bone healing and the absence of any signs of a systematic response (e.g., chronic inflammation and allergy) due to the created by-products. Despite the outstanding properties of the biodegradable Mg-based implants and their extensive development in clinical applications in recent years, several challenges remain unaddressed that inhibit their extensive use in biomedical applications [19]. For example, it is generally believed that the corrosion rate of the biodegradable Mg alloys is too high for implant applications since fast corroding implants cannot provide sufficient mechanical support for the tissue. The localized corrosion processes, such as pitting and stress corrosion cracking, lead to a reduction in the mechanical strength of the implant in the early stages of implantation. Furthermore, rapid corrosion of the Mg in the physiological environment leads to the generation of large quantities of hydrogen gas bubbles between the implant and the bone interface and this may hinder the healing process [3,20].

Many different ways and methods have been suggested for improving the properties of biodegradable Mg alloys through the use of procedures such as coatings [21,22] and alloying [23,24]. However, it appears that the use of heat treatment is the most valuable tool for manipulating the mechanical properties and corrosion behavior of the biodegradable Mg alloys. The reason is because a heat treatment does not alter the chemical composition or the shape of the alloys but instead, it simply modifies the microstructure. The well-established solid solution treatment (T4) and the solid solution with subsequent aging treatment (T6) are two common heat treatments that have been widely conducted on biodegradable Mg alloys [14]. Changes in the morphology and volume fraction of the secondary phases, the introduction of a protective corrosion film and the effect on grain size during the heat treatment may all affect the corrosion performance of the Mg alloys. Moreover, solid solution strengthening, precipitation strengthening and grain growth are three important factors determining the overall mechanical properties of the heat-treated Mg alloys.

Depending on the chemical composition of the alloy and the heat treatment that was used, significantly different combinations of mechanical and corrosion properties may be obtained. Fig. 1b demonstrates a noticeable progress in applying the heat treatment process to biodegradable Mg alloys where the number of published articles in this area from 2007 to 2020 is presented. A summary of the properties and challenges of biodegradable Mg alloys is given in Fig. 2. Accordingly, this review aims to provide a comprehensive summary of the different effects of the T4 and T6 heat treatments on the corrosion performance and mechanical properties of the biodegradable Mg alloys. A detailed understanding of the effects of heat treatment on each alloying system will help to control the properties of the biodegradable Mg alloys in order to achieve the desired properties for biomedical applications without the need to change the composition or shape of the alloys.

2. Clinical applications

Mg alloys have been used for biomedical applications since the 1800s. Initially, Mg wires were devised by Edward C. Huse as ligatures to hinder bleeding [25]. Moreover, in 1900, Erwin Payr proposed that Mg implants can be employed for the fabrication of fixator pins, plates and nails [26]. However, since the early 2000s, the modern era of the research on Mg alloys for biomedical applications has been initiated. Currently, Mg alloys are used in two main categories of biomedical applications: vascular stents [27], and orthopedic applications [28]. In this regard, the Mg stenting procedure was employed for 63 patients who had plaque in their arteries, and the results obtained indicated that such stents can be used safely [29]. There is also a great potential for Mg alloys, as surgical implant materials, to be used for bone repair [30]. Mg alloys have been utilized in different types of fixation devices for orthopedic surgery, including as fasteners, screws, and plates. These extensive biomedical practices of Mg-based alloys are due to their excellent biocompatibility, such as their minimal effect on blood composition change, which does not lead to damage of excretory organs like the liver or the kidneys [31].

To make biodegradable Mg alloys suitable for these applications, there is a need to adjust some properties, where the most important one is the degradation rate. The acceptable corrosion rate for biomedical implants depends on many factors and there is not a specific rate for all applications [32]. As Mg alloys produce hydrogen in the body, the acceptable corrosion rate can be determined by the evolved hydrogen. For example, according to [33], when the hydrogen evolution rate is 0.01 $mL/cm^2/day$ it can be tolerated by the human body and there will not be a serious threat. Also, it has been reported that the corrosion rate should be less than 0.5 mm/y in simulated body fluid (SBF) solution at 37 °C, which reflects a functionality time of 3-6 months [34]. It is worth mentioning that the pH, alloying element release and osmolality (caused by a high concentration of Mg^{2+} ions) of the medium are all affected by the degradation rate of Mg-based alloys, where

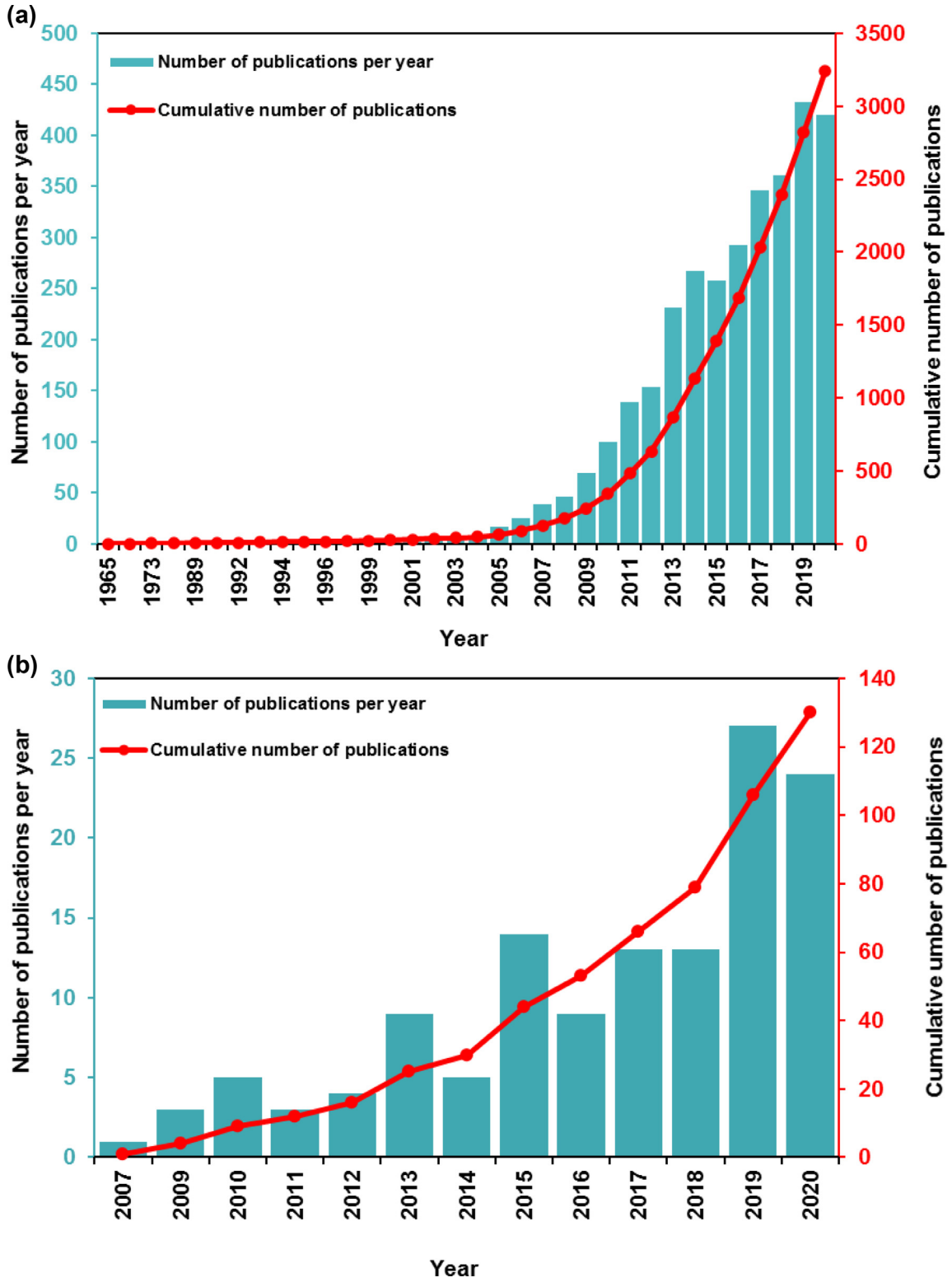

Fig. 1. The numbers of publications per year and the cumulative number of publications for (a) biodegradable Mg alloys and (b) the heat treatment of biodegradable Mg alloys.

a high degradation rate would result in an increment of pH, excess amount of alloying element and osmolality, leading to the cytotoxicity of human osteoblasts [35,36]. Therefore, tailoring the corrosion rate of biodegradable Mg alloys is of great significance.

Mechanical integrity of an orthopedic implant is of great importance to provide structural support during the bone reconstruction process. It has been reported [14,37] that biodegradable implants should have tensile strength and ductility higher than 200 MPa and 10%, respectively. Fortunately,

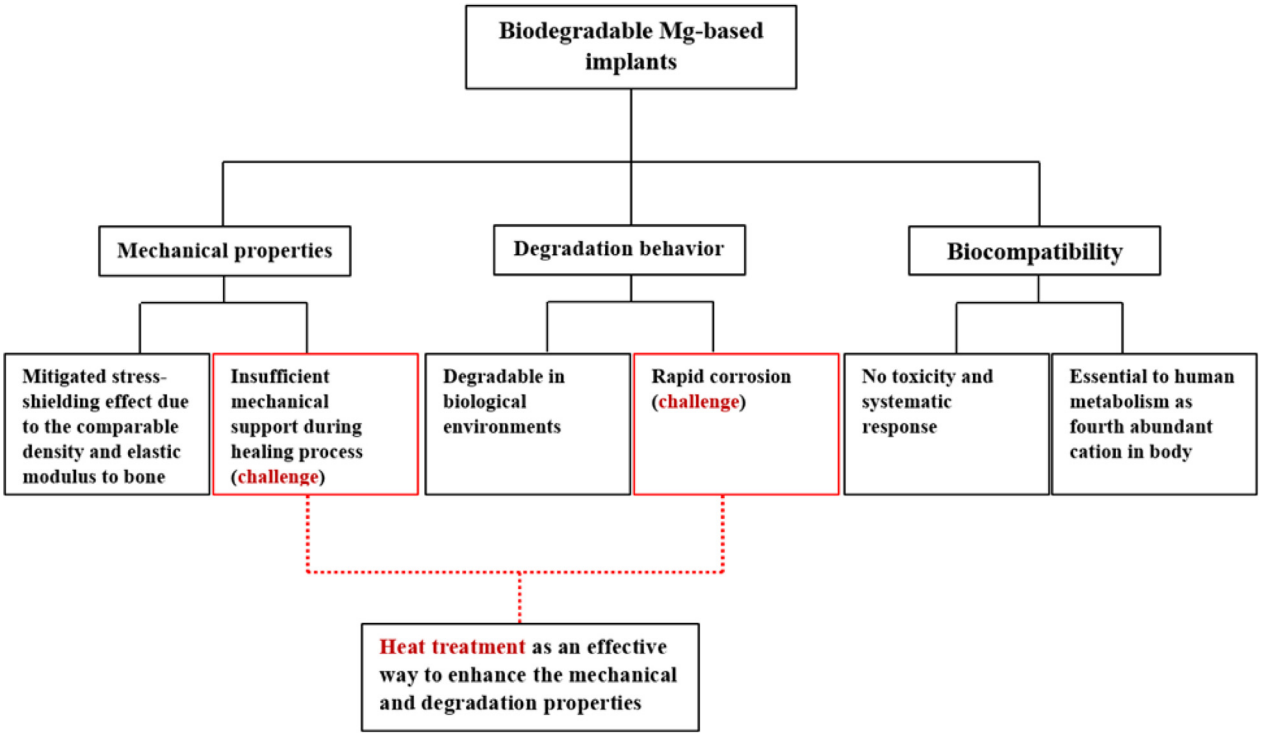

Fig. 2. Properties and challenges associated with biodegradable Mg alloys and the potential role for addressing these challenges through the use of heat treatment.

Mg-based alloys usually can be designed to reach these properties [38]. However, loss of the load-bearing ability of Mg implants as the result of fast degradation is still challenging. Most of the biodegradable Mg-based alloys would be thoroughly degraded within 6-12 weeks, while the designed implant should maintain its support for 24-36 weeks, which is the bone regeneration duration [39,40]. As will be reviewed and discussed in the following sections, heat treatment, as an effective implement, can control and further improve the corrosion and mechanical properties of the Mg alloys to the limits required for use as biodegradable implants.

3. The general effects of heat treatment

Although a heat treatment affects different Mg alloys in distinct ways, some effects of T4 and T6 treatments on microstructure and hence the characteristics of biodegradable Mg-based alloys are common and will be discussed here.

3.1. The general effects of a T4 heat treatment

The solid solution heat treatment T4 removes the dendritic structure and the associated segregations in addition to reducing the density of dislocations, twins and other defects with the overall driving force of decreasing the internal energy of the as-cast alloy. The effect of a solid solution heat treatment will become more significant by increasing the concentration of the alloying elements [41,42]. After the T4 heat treatment, the alloying elements are more homogeneously distributed and some or all of the precipitates are dissolved in the matrix as the result of the increased solubility of the alloying elements with temperature. Fig. 3 depicts a single-phase microstructure and complete dissolution of intermetallic compounds of the Mg-2.49 at% Gd alloy into the matrix by the solution treatment at 535 °C for 9 h [43].

The rearrangement of the alloying elements and secondary phases during the solution treatment can be very beneficial for the corrosion resistance since finely and uniformly distributed secondary phases may effectively improve the corrosion resistance of the Mg alloys. In fact, the distribution and size of the secondary phase particles remarkably affect the corrosion performance of the biodegradable Mg alloys [44]. Thus, large particles deteriorate the corrosion resistance of the Mg alloys with respect to the micro-galvanic corrosion and this is an effect that will be discussed in detail in this review.

The following eq. (1) demonstrates the relation between the corrosion rate and the cathodic area:

$$\mathrm{Ln}\ \gamma = \frac{(E_{corr2} - E_{corr})}{(\beta_{a1} + \beta_{c2})} + \frac{\beta_{c2}}{(\beta_{a1} + \beta_{c2})} \ln \frac{I_{corr2}}{I_{corr1}} + \frac{\beta_{c2}}{(\beta_{a1} + \beta_{c2})} \ln \frac{A_2}{A_1} \quad (1)$$

where γ is the galvanic corrosion effect, E_{corr2} and E_{corr1} are the cathodic corrosion potential and the anodic corrosion potential, respectively, I_{corr2} and I_{corr1} are the cathodic corrosion current density and the anodic corrosion current density, re-

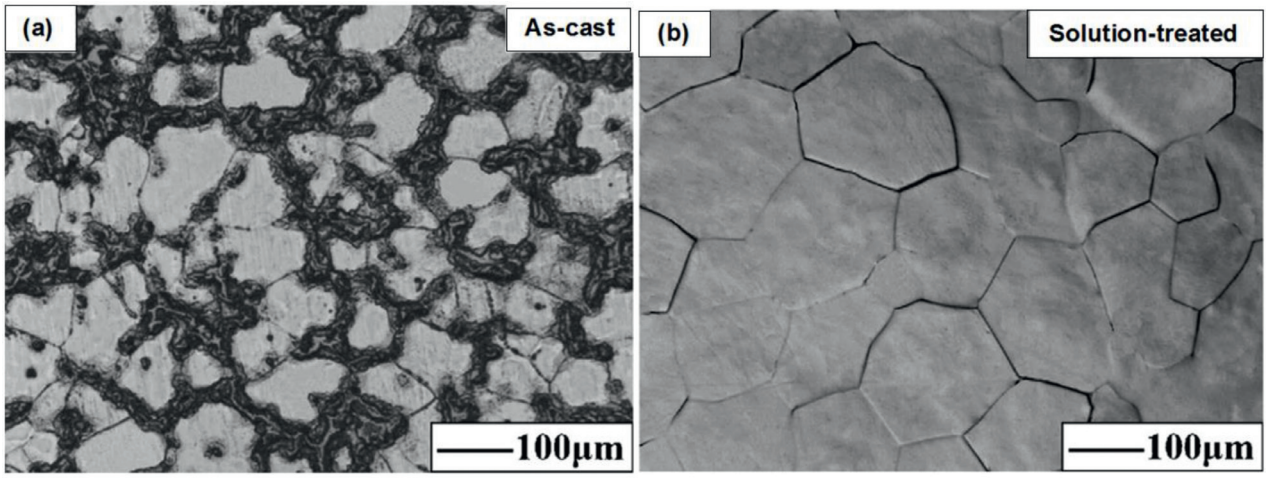

Fig. 3. Optical microstructure of the Mg–2.49 at% Gd alloy in (a) the as-cast and (b) the solution-treated conditions. Reproduced from [43].

spectively, β_{a1} and β_{c2} are the anodic slope and the cathodic slope, respectively, and A_2 and A_1 are the cathode area and the anode area, respectively [45].

In addition to the effect of the morphology of the particles on the galvanic corrosion in Mg-based alloys, the grain size distribution is also an important factor. A non-uniform grain size distribution is highly destructive due to the formation of galvanic corrosion between the fine and coarse grains. During the T4 heat treatment, due to the coalescence of the small grains, the smaller grains are gradually removed and the grain size becomes more uniform and larger [46,47]. As the time/temperature of the solid solution heat treatment increases, grain growth becomes more severe while the rate of growth will be a function of both the temperature and time of the heat treatment as well as the type of alloy. On the other hand, the corrosion rate is usually improved by reducing the grain size of magnesium alloys. Accordingly, the corrosion behavior of Mg alloys after a T4 heat treatment will be affected by these two parameters.

The solution heat treatment affects the strength of the Mg alloys from two important aspects. First, the solution treatment establishes a supersaturated solid solution where the atomic size difference between the Mg atoms and the solute atoms generates a lattice distortion in the α-Mg matrix and this leads to solid solution hardening. Second, due to the high annealing temperatures, the casting precipitates dissolve in the α-Mg matrix and this produces some softening [48]. This means in effect that the mechanical properties of the solution-treated biodegradable Mg alloys originate from attaining a balance between these two factors. Grain growth and the loss of some strengthening from the grain boundaries should also be added to these factors. In this respect, it is generally considered that after a solid solution treatment the yield strength (YS) of magnesium alloys is slightly reduced compared with the as-cast condition due to the occurrence of grain growth and also the dissolution of some of the precipitates [49].

3.2. The general effects of a T6 heat treatment

During aging, the secondary phases precipitate again from the supersaturated solid solution formed during the T4 treatment, and as the aging time increases so the size of the precipitates and the distance between them also increases due to the enhanced diffusion [48]. In this process, the morphology of the precipitates changes continuously with time. This is accompanied by grain growth while the growth kinetics are smaller compared to the solution treatment due to the lower temperatures typically used in aging. The temperature and time of the aging heat treatment also significantly affect the morphology of the precipitates and thus the final properties of the alloy: this effect will be discussed in detail in this review.

Regarding the influence of the T6 treatment on the corrosion resistance of Mg alloys, it is believed that the precipitates may play different roles with respect to their homogeneity, morphology, distribution and the type of alloy. Thus, they may act both as micro-cathodes which cause an acceleration in the corrosion rate of the alloy and also as barriers against corrosion propagation [50].

There are many factors that may affect the efficiency and also the amount of precipitate strengthening. For example, these factors include the precipitate size, precipitate shape, precipitate volume fraction and distribution, the nature of the interface with the surrounding matrix, the elastic modulus, the strength of the precipitates and the precipitate crystal structure [50,51]. Usually, these parameters change during aging and this will appear in the aging curve where the strength or hardness is plotted against time.

The proper selection of time and temperature of heat treatment is a critical factor to obtain the best results. It is well-established that phase diagrams, which are based on equilibrium phases, are the most practical tools to define the temperature of heat treatment for each alloy. Since the conditions may deviate from equilibrium due to kinetic considera-

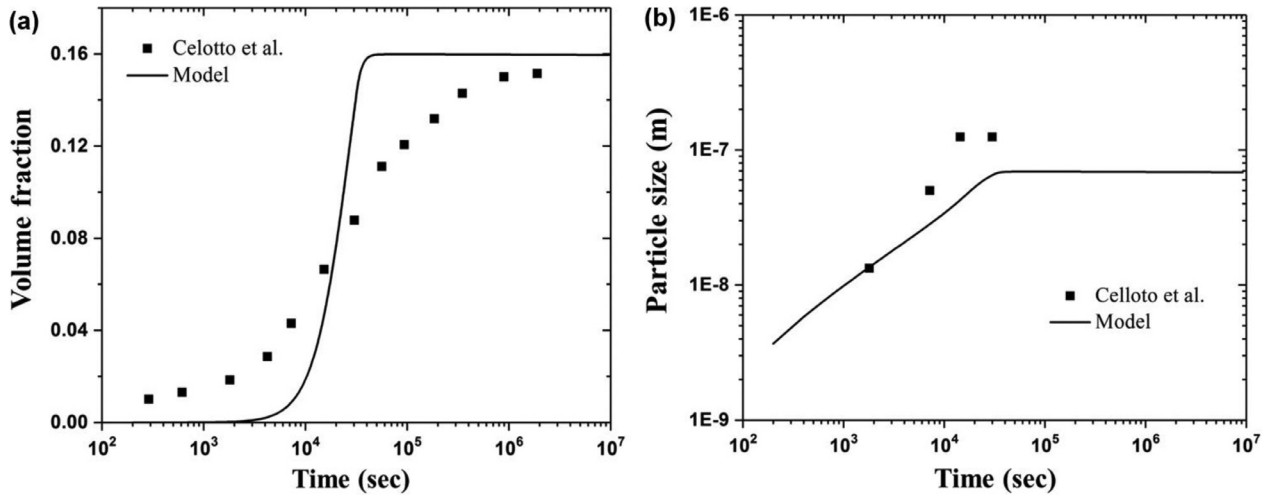

Fig. 4. Comparison of the experimental results with model predictions for the evolved $Mg_{17}Al_{12}$ phase in T6 treatment of AZ91 alloy at 200 °C: (a) volume fraction, and (b) particle size are plotted against time of T6 heat treatment. Reproduced from [54].

tions, different experimental techniques such as thermal analysis, X-ray diffraction (XRD), electrical conductivity, scanning electron microscopy (SEM) and transmission electron microscopy (TEM) can also be employed to determine the appropriate time and temperature of the heat treatment. All of these techniques rely on measuring changes in physical, chemical and structural properties of a material when a phase transformation occurs [52]. For instance, electrical resistivity and hardness tests have been utilized to assess the optimum solid solution time for a biodegradable Mg-Y-Ag alloy [53]. It was realized that electrical resistivity and hardness significantly decreased and increased, respectively, after 3 h of T4 treatment at 500 °C (determined according to phase diagram) and no remarkable changes were noticed after that, indicating that most of the precipitates were dissolved by 3 h of solution treatment at 500 °C, which was chosen as the heat treatment time and temperature.

In addition to experimental techniques, models and simulations are also being developed and performed respectively to further predict the appropriate time and temperature of heat treatment. Interestingly, a novel microstructure model has been devised to predict the microstructure evolution of some Mg-based systems such as Mg-Zn and Mg-Al alloys during T6 treatment [54,55]. This model is mainly based on thermodynamic calculations for the physical phenomena of nucleation, growth and coarsening, which can give valuable information for deciding the time and temperature of the heat treatment. Fig. 4 shows a reasonable fit between experimental data and model predictions, where volume fraction and size of $Mg_{17}Al_{12}$ phase in an Mg-9Al-1Zn alloy aged at 200 °C (obtained by TEM measurement) are plotted against time of heat treatment [56], implying the potential of this model for developing for other Mg alloys. However, some important parameters such as the morphology of precipitates are not included in these nascent models, which necessitate future investigations for higher predictive accuracy.

4. The effects of heat treatment on Mg-Zn alloys

4.1. The corrosion behavior

4.1.1. The corrosion behavior of Mg-Zn alloys in the as-cast condition

Zinc is a common alloying element in biodegradable Mg alloys that is omnipresent in all of the human body tissues as a vital nutritional element [57]. In practice, the addition of Zn improves the corrosion performance of biodegradable Mg alloys by enhancing the nobility. In addition, it appears that Zn increases the stability of the corrosion film by reducing impurities and also boosts the charge transfer resistance of the Mg alloys and thereby improves the corrosion resistance [58,59].

The general microstructure of the as-cast Mg-Zn alloys includes Mg-Zn secondary phases embedded in an Mg-Zn solid solution matrix together with some zinc-rich segregation areas. The secondary phases can be found both at the grain boundaries and within the grains [51]. The corrosion behavior of the Mg-Zn alloys is mainly determined by three factors: the purity, the zinc concentration and the morphology and composition of the secondary phases in the microstructure.

The role of the Zn content in enhancing the corrosion resistance of as-cast Mg-Zn alloys is more evident in Fig. 5. In this diagram, the surfaces of the binary Mg-xZn alloys (x = 1.25, 2.50, and 4.00 wt%) are shown after immersion in a Kokubo solution for 144 h. In this respect, it was concluded that the addition of 4 wt% Zn can significantly improve the corrosion resistance of Mg-Zn alloys for biomedical applications by forming a protective film . It was also noted that the number of cracks appearing on the surface of alloys decreases through the addition of Zn. A uniform corrosion product is formed on the surface of the Mg-4Zn alloy where it is much thicker than in other alloys with less Zn content. The volume fraction of the secondary phases and the thickness of the Zn

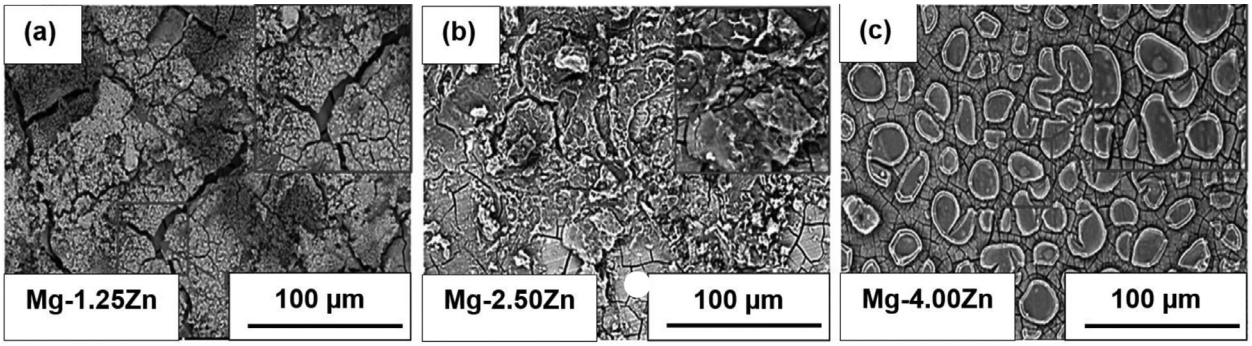

Fig. 5. The morphology of the corroded surfaces of the Mg-1.25Zn (a), Mg-2.5Zn (b) and Mg-4Zn (c) alloys after immersion for 144 h in a Kokubo solution. Reproduced from [60].

oxide layer will assess the corrosion resistance of the Mg-Zn alloys. However, due to the presence of different phases and also the dendritic character of the microstructure of the as-cast Mg-Zn alloys, these alloys in the as-cast condition are very vulnerable to galvanic corrosion and usually have insufficient surface layer protection and passivation [60]. The use of heat treatment effects is an effective way to modify the microstructure of the Mg-Zn alloys and this will be reviewed and discussed in the following sections.

4.1.2. The corrosion behavior of Mg-Zn alloys after a T4 heat treatment

Irrespective of the location of the secondary phases, whether at the grain boundaries or within the grains, they can act as micro-cathodes and thus increase the corrosion rate. From this point of view, a solid solution heat treatment will be the most suitable option for improving the corrosion resistance of as-cast Mg-Zn alloys as it can significantly reduce the volume fraction of the secondary phases [45,61]. In some cases, an incomplete dissolution of the secondary phases has been reported due to the excellent thermal stability of the secondary phases at the temperature used for the solution treatment. For example, there are reports of an incomplete dissolution of the $Mg_{70}Zn_{25}Sr_5$ particles in the Mg-4.0Zn-0.5Sr alloy [62] and the $Mg_{12}Zn_{13}$ particles in the Mg-1.5Zn alloy [42]). Nevertheless, by precisely controlling and adjusting the heat treatment parameters it is also possible to dissolve these phases.

In a comparative study [63], the corrosion resistance of an Mg-2Zn-1Mn (ZM21) alloy was studied and compared in the solution-treated, the extruded and the T5 heat-treated states. The results showed that the alloy in the solution-treated condition had the lowest amount of secondary phases, impurities, dislocations and other defects. In addition, the solution-treated alloy exhibited the best film protection according to the higher breakdown potential (E_b) value from the polarization curves (Fig. 6). Therefore, an alloy solution-treated at 510 °C for 4 h showed the best corrosion resistance.

An investigation was conducted on the effect of temperature and time of the solid solution heat treatment on the corrosion behavior of an Mg-3Zn-0.3Ca alloy 44. The results demonstrated that the optimum properties may be achieved by

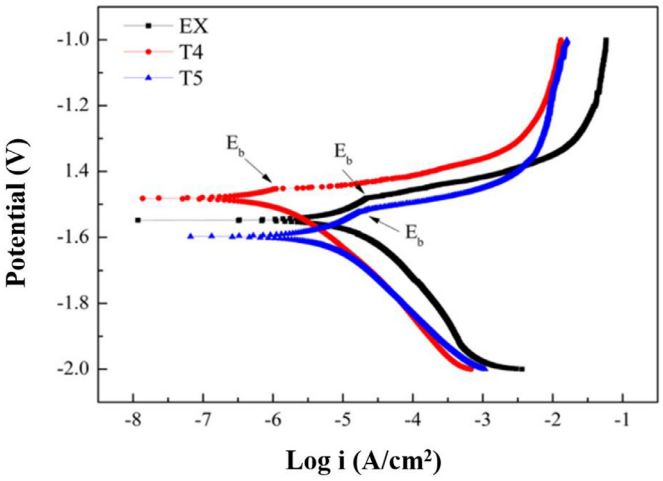

Fig. 6. Comparative polarization curves of the Mg-2Zn-1Mn alloy in the T4, the extruded and the T5 states. Reproduced from [63].

properly controlling the time and temperature of the solution treatment. In this respect, the as-cast alloy had the smallest grain size but the largest fraction of the secondary phases and the alloy experiencing the solution treatment at the highest temperature for the maximum time had the lowest fraction of secondary phases but the largest grain size. Both of these samples possessed an inappropriate corrosion rate and optimum properties were achieved for a sample with a balanced secondary phase volume fraction and grain size. Fig. 7a shows the results of a hydrogen evolution test during a 240 h immersion in SBF solution in which the T4-treated alloy at 420 °C for 24 h exhibited the best corrosion resistance. As shown schematically in Fig. 7b, the results obtained show how the corrosion rate decreases with a reduction in the secondary phase content and an increase in the grain size. According to Fig. 7c, a solution-treated alloy after 420 °C for 24 h, with a balanced secondary phase content and grain size, demonstrated a lower density and depth of the corrosion pits where this is in accordance with the sample showing the best corrosion resistance. Therefore, the conditions of time and temperature associated with the solid solution heat treatment play a significant role in determining the corrosion behavior of the Mg-Zn alloys [64].

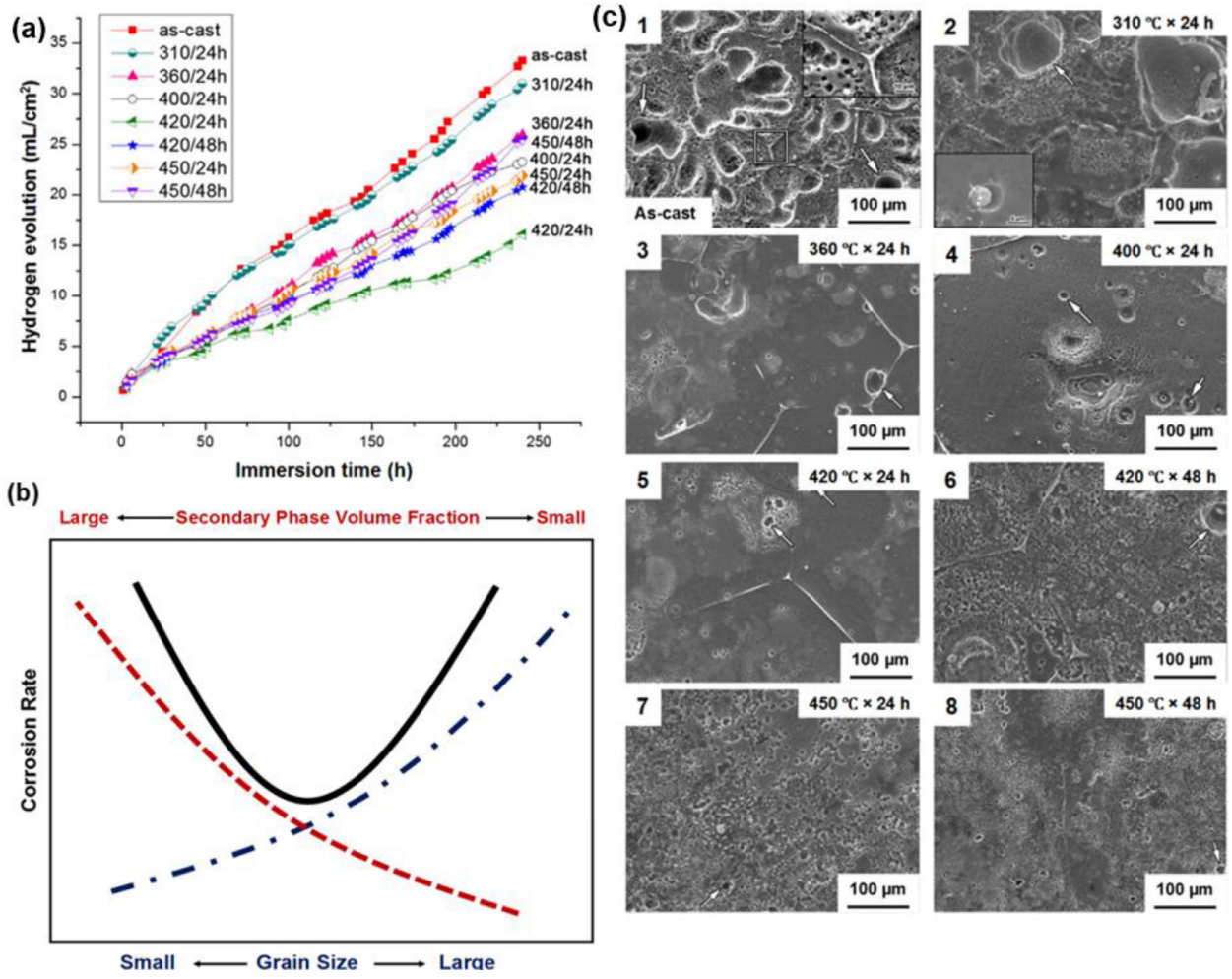

Fig. 7. (a) The effect of heat treatment on the corrosion rate (evaluated as the evolved hydrogen gas during immersion in SBF) of an as-cast Mg-3Zn-0.3Ca alloy. (b) Schematic plot showing the variations of the corrosion rate with the volume fraction of the secondary phases (dashed red curve) and grain size (dashed blue curve). The black solid curve refers to the overall effect of the solution treatment on the corrosion rate. (c) The corroded surfaces of the Mg-3Zn-0.3Ca alloy in the as-cast and heat-treated conditions (indicated in the top-right corner) after immersion in SBF for 240 h. All micrographs were obtained by SEM after removal of the corrosion products. Reproduced from [44].

It has been reported [49] that by increasing the time and temperature of the solution treatment some passivation is achieved and a protective film is formed on the alloy so that uniform corrosion occurs instead of pitting [25]. For example, passivation occurred in the T4-treated Mg-2Zn-0.5Nd-0.5Zr alloy after increasing the solution temperature up to 500 °C. The homogenous composition of the alloy after the solution heat treatment caused the formation of a uniform protective film. In this study, while many secondary phases exist in the untreated alloy (Fig. 8 a), following the solution treatment the volume fraction of the secondary phases decreased considerably (Fig. 8 b). With immersion in Hank's solution, the alloy corroded homogenously (Fig. 8 c) and a uniform protective corrosion layer formed on the alloy surface, which could inhibit the corrosion propagation (Fig. 8 e,d) [49].

It has been reported [42] that, after the solid solution heat treatment, a more protective film forms on the surface of the alloys with higher Zn content, and this covers the surface of the alloy and acts as a barrier against the penetration of chloride ions [19]. For example, the film formed on an Mg-9Zn alloy was reported to be more protective than a film formed on an Mg-1.5Zn alloy in the solid solution state. Adding other alloying elements such as Yb and Nd to the Mg-Zn alloys up to 1% and 0.6%, respectively, further strengthened the surface film and thus improved the corrosion resistance in the solid solution condition [65]. The corrosion resistance improvement during the solution treatment was mainly attributed to the stabilization of the Mg matrix by the addition of Yb. However, increasing the Yb content to 2 wt% resulted in some undissolved eutectic phases and relatively more severe corrosion compared with the alloy containing only 1 wt% Yb in the solution-treated state, where this is probably due to the microgalvanic corrosion between the undissolved secondary phases and the α-Mg matrix [66]. Therefore, the type and amount of the alloying elements, and the conditions of the solid solution heat treatment in terms of time and temperature, are very ef-

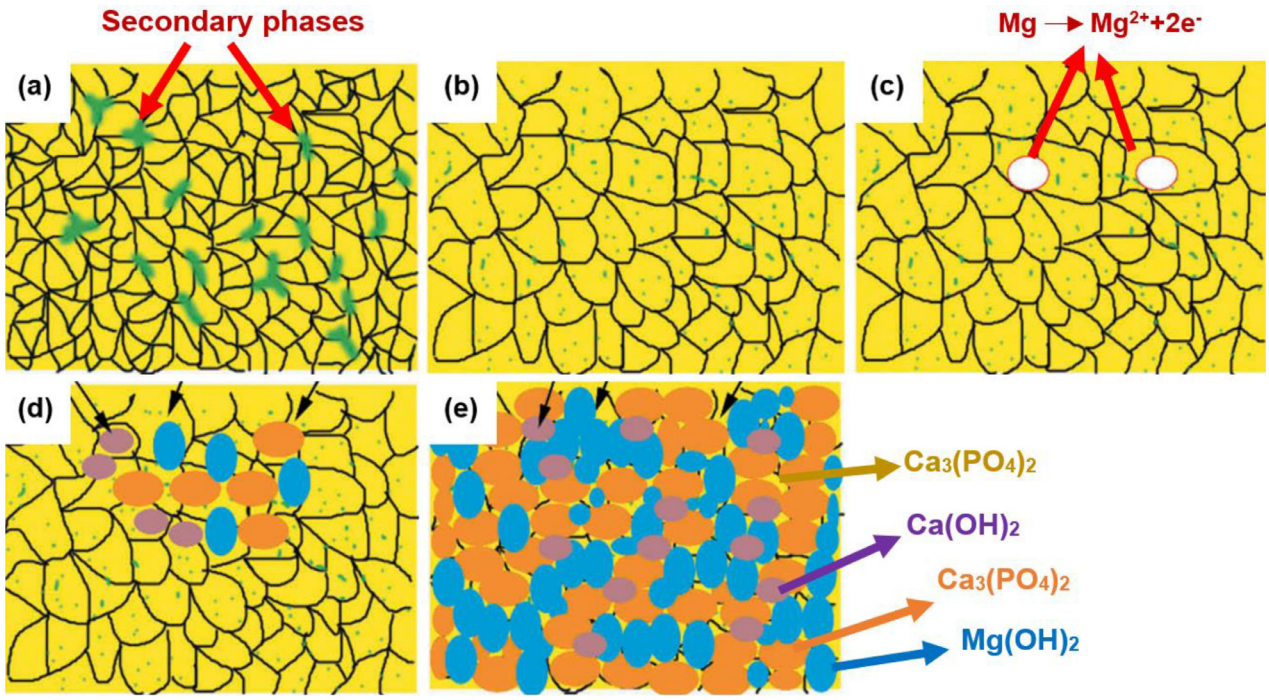

Fig. 8. Schematic representation of the corrosion process in the T4-treated Mg-2Zn-0.5Nd-0.5Zr alloy. While there were many secondary phases present in the untreated alloy (a), the volume fraction of the secondary phases decreased considerably after the solution treatment (b), which resulted in homogenous corrosion (c). The uniform film formation process on the surface of the T4-treated alloy is shown in (d) and (e). Reproduced from [49].

fective parameters in controlling the corrosion behavior of the Mg-Zn alloys and this should be considered in any attempt to achieve the optimum desired properties.

4.1.3. The corrosion behavior of the Mg-Zn alloys after a T6 heat treatment

The standard potential of magnesium is about -2.37 V and for zinc it is -0.762 V versus a standard hydrogen electrode (SHE). An Mg-Zn alloy containing secondary phases is susceptible to galvanic corrosion due to the formation of a galvanic battery between the secondary phases containing zinc as the cathode and the magnesium matrix as the anode [51]. An investigation compared the corrosion resistance of the Mg-5.2Zn-0.03Mn (ZK60) alloy in the as-cast and T6 conditions and it was reported that, while the amount of secondary phases were almost the same in both states, the T6-treated sample showed minor corrosion resistance due to the dispersed distribution of the precipitates along the grain boundaries [27]. By contrast, the concentrated distribution of the precipitates in the as-cast condition resulted in a better corrosion resistance. In another study [67], the higher volume fraction of the secondary phases in the T6-treated alloy compared to the as-cast alloy increased the amount of micro-galvanic couples which accelerated the galvanic corrosion. In this investigation, the presence of the Mg-Zn particles as a robust cathode triggered the micro-galvanic corrosion in the aged alloy. In addition, it was reported [68] that the aging process cannot produce a thick and protective film on the Mg-Zn-Ca-Mn alloys so pitting corrosion was activated to a great extent [36].

An Mg-5Zn alloy was aged for different times (4, 6 and 10 h) at 230 °C in order to study the effects of the morphology, distribution, and volume fraction of the Mg_xZn_y secondary phases on the corrosion behavior [50]. By extending the aging time, more secondary phases were precipitated and their dimensions increased up to ~2 μm after 10 h aging. Also, the distribution, morphology, and volume fraction of the secondary phases changed with time and after 10 h the Mg_xZn_y secondary phase appeared as a continuous network. However, the results from this study indicated that this continuous distribution of the Mg_xZn_y secondary phases were unable to act as a corrosion barrier hindering the corrosion propagation. Thus, by comparing different morphologies of the secondary phases in an aged Mg-5Zn alloy, it was concluded that irrespective of the distribution of the Mg_xZn_y secondary phases whether discrete or continuous, in both cases these phases act as micro-cathodes and deteriorate the overall corrosion resistance of the alloy. Fig. 9 shows severe corrosion pits in the T6-treated alloy located at the grain boundaries and within the grains at a high magnification. In this case, each corrosion pit is the result of a micro-galvanic corrosion caused by the presence of the Mg_xZn_y secondary phases [50].

Contrary to the T6-treated Mg-5Zn alloy, some researchers [65,66] concluded recently that fine precipitates with homogeneous distributions are a barrier to corrosion whereas coarse precipitates with random distributions act as micro-cathodes and thereby intensify the galvanic corrosion. TEM was used to investigate the secondary phases formed during the aging heat treatment of Mg-5.8Zn-0.5Zr-xYb alloys (with Yb content varying from 0 to 2%) [66]. The TEM micrographs of

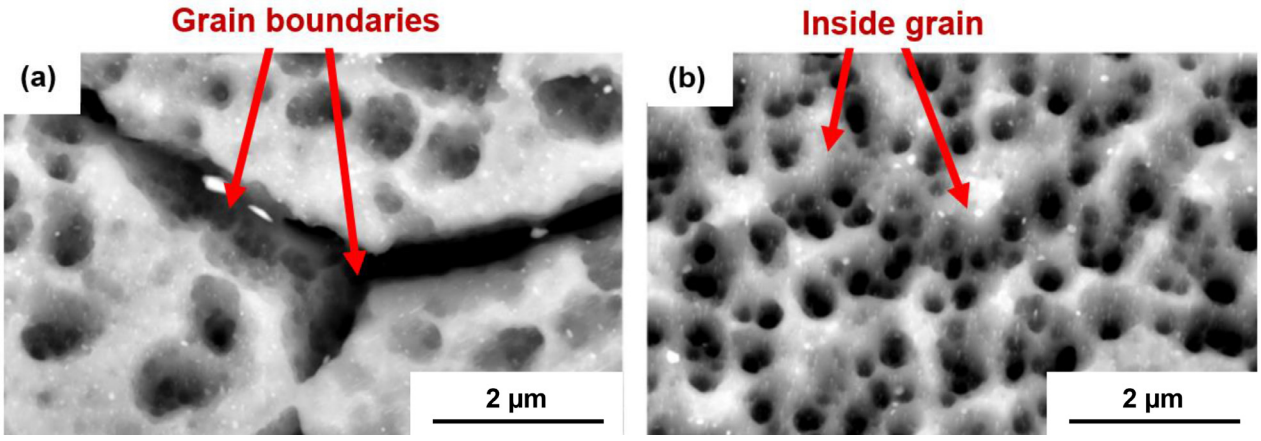

Fig. 9. After immersing the aged Mg-5Zn alloy in a 0.1 M NaCl solution for 30 min, the corrosion pits appear both at the grain boundaries (a), and within the grains (b). Reproduced from [50].

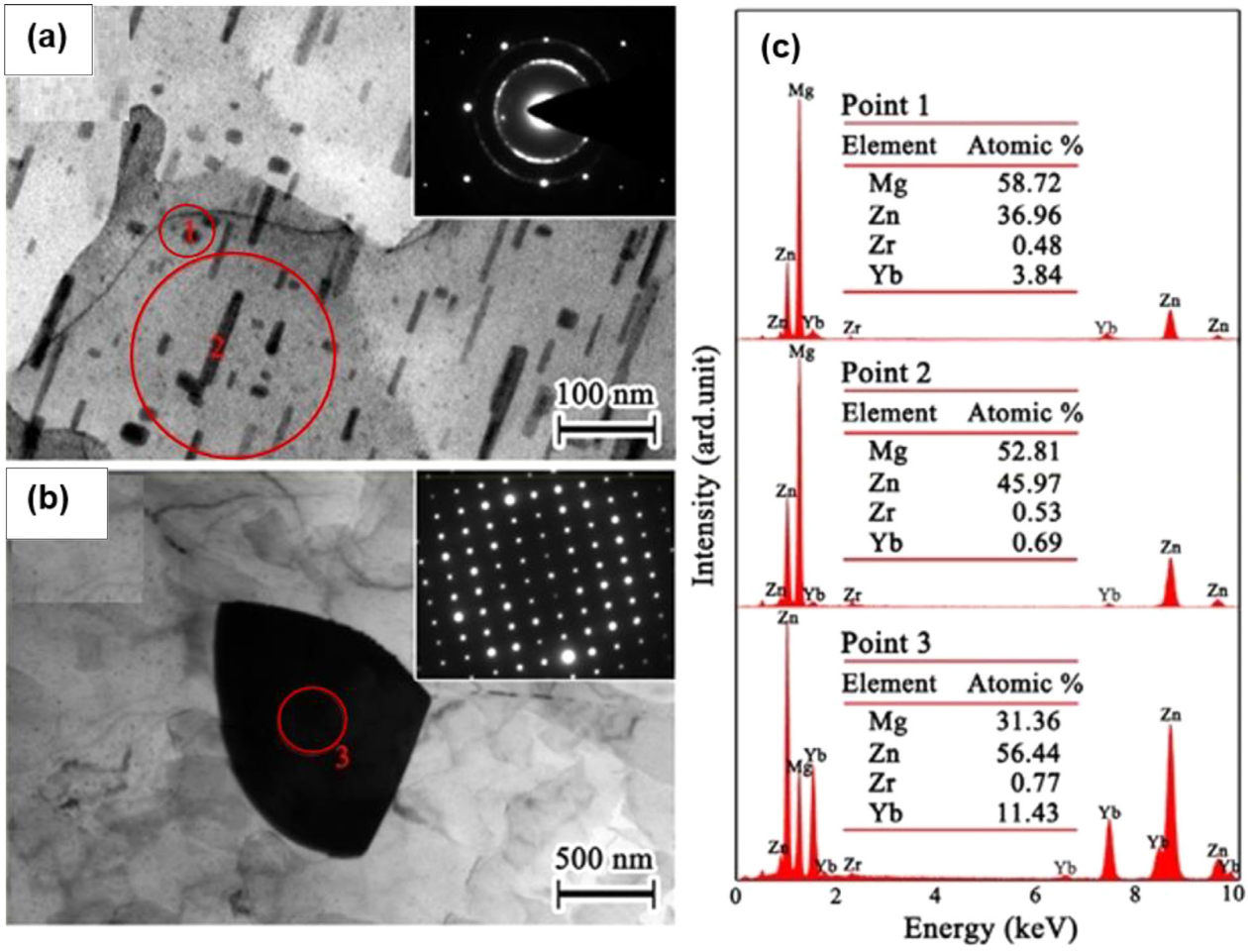

Fig. 10. TEM micrographs of the Mg-5.8Zn-0.5Zr-2Yb alloy after the T6 treatment (a,b), together with the corresponding TEM-EDS results of the corresponding precipitates (c). Reproduced from [66].

the Mg-5.8Zn-0.5Zr-2Yb alloy presented in Fig. 10 demonstrate the presence of three types of secondary phases; dot-shaped Mg-Zn-Yb particles (point 1), rod-shaped Mg-Zn particles (point 2) inside the grains and a small number of coarse blocky Mg-Zn-Yb phases (point 3) which were mostly located at the boundaries. These secondary phases with different sizes and distributions play different roles in the corrosion process for these alloys. The coarse blocky particles that were discontinuously located at the grain boundaries cause local corrosion due to the significant potential difference between the magne-

sium matrix and the relatively large intermetallic phase. In this study, the corroded surface did not experience severe pitting corrosion because these coarse particles were minimal. On the other hand, for the fine Mg-Zn-Yb and Mg-Zn particles distributed within the grains, an internal galvanic corrosion was observed to occur uniformly along the matrix, forming a passive film due to the very small sizes and the more uniform distribution. This passive film covered the entire surface and prevented further corrosion activity, thus creating an anti-corrosion barrier to protect the underlying magnesium surface [66].

With increasing aging time, it was observed that the size of the precipitates increased and the distribution of the precipitates became more inhomogeneous, where this can significantly influence the corrosion behavior of the Mg alloys. This was studied for an Mg-5.8Zn-2.0Yb-0.5Zr alloy [65]. Three kinds of samples were investigated, each aged for different times such that the under-aged sample (UA) was aged at 200 °C for 8 h, the peak-aged sample (PA) was aged at 200 °C for 16 h and the over-aged sample (OA) was aged at 200 °C for 24 h. It was concluded that the volume fraction and the distribution of the precipitates were noticeably different in these three samples (Fig. 11). The open circuit potential (OCP), dynamic polarization and immersion tests in Fig. 12 show that the PA sample exhibited a thermodynamically stable film and the best corrosion resistance, where the stable and compact film formed on the PA sample came directly from the uniform and fine nano-precipitates. The corrosion rates after the 240 h of immersion in an SBF solution at 37 °C showed that the corrosion rate of the OA sample was up to 26-fold higher than for the PA sample and multitudes of corrosion pits were observed on this sample (Fig. 12c and d).

A peak aging condition (aging at 200 °C for 10 h, after solutionizing at 510 °C for 3 h) in the Mg-1.2Zn-0.5Ca alloy with fine and uniformly dispersed precipitates was reported to improve the corrosion resistance and also the uniformity of the corrosion compared to the as-cast alloy and other aging conditions [69]. In this study, the as-cast alloy had the highest mass loss and degraded entirely after 28 days immersion in the modified SBF while the 10 h aged alloy possessed the lowest mass loss (Fig. 13). Therefore, the time and temperature of the aging treatment strongly affect the corrosion behavior of the Mg-Zn alloys depending on the composition of the alloy.

To provide an easier comparison, a summary of the effects of different heat treatments on the corrosion behavior of the biodegradable Mg-Zn alloys is presented in Table 1. In this tabulation, the chemical composition of the studied alloys is given in column 1, the processing condition is given in column 2, the corrosion media are presented in column 3, the Mg-Zn phases are presented in column 4, the condition to achieve the best corrosion resistance is given in column 5, some remarks are presented in column 6 and finally the corresponding references are given in the last column.

4.2. Mechanical behavior

4.2.1. The mechanical behavior of the Mg-Zn alloys after a T4 heat treatment

As already noted, the strength properties of the as-cast alloys after the solution treatment depend mainly on the two opposing factors of solid solution strengthening and the softening induced by the dissolution of the secondary phases. The former depends on some factors such as the severity of lattice distortion due to the atomic size difference and the latter depends mainly on the thermal stability of the secondary phases at the annealing temperature. It was reported that the ultimate shear strength of an as-cast Mg-2Zn-1Gd-1Ca alloy decreased up to 6% after solution treatment due to the dissolution of precipitates [24].

It has been reported [39] that a solution treatment at 400 °C for 2 h removed the deformation twins and defects and also homogenized the microstructure of the extruded ZK60 alloy. Such microstructural changes correspond to some softening which is reflected by the hardness reduction from 81.2 Hv in the extruded sample to 68.1 Hv in the solution-treated sample. More grain growth occurred by increasing the solution heat treatment temperature from 400 °C to 500 °C, where the grain size increased from 8.6 to 36 μm. This increase led to a further hardness reduction to 62.9 Hv.

In another study, the strength of an as-forged Mg-6.7Zn-1.3Y-0.6Zr alloy was compared with a T4-treated alloy [41] and it was found that the mechanical properties of the solution-treated alloy were influenced by two critical factors: (1) grain growth and the dissolution of the $MgZn_2$ precipitates and (2) the precipitation of nano-scale I-Mg_3Zn_6Y quasicrystals. While the first factor deteriorates the mechanical strength, the second factor has a strengthening effect. Overall, it was found that the mechanical properties of the alloy were degraded slightly by the solid solution heat treatment. There are also some reports of increasing the strength of the Mg-Zn alloys after the solution treatment. For example, it was reported that, by a solution heat treatment at 445 °C for 12 h, the ultimate tensile strength (UTS) of an as-cast Mg-Zn-Ca alloy was improved significantly as the result of an elimination of the casting defects, a homogenization of the microstructure and also solid solution hardening [40].

In addition to strength, the solution heat treatment can also affect the ductility of the Mg-Zn alloys. Thus, both a deterioration [63] and an improvement [49] of the ductility after the solution heat treatment were reported. It should be noted that two contrary factors control the ductility after the T4 treatment since severe grain growth decreases the ductility whereas the dissolution of the precipitates improves the ductility because of the easier dislocation movement. Accordingly, it may be concluded that a solution treatment at intermediate temperatures can improve the ductility while using very high temperatures may lead to some ductility reduction. This is confirmed in experiments where the elongation of an as-extruded Mg-2Zn-0.5Nd-0.5Zr alloy increased when the solution treatment temperature was below 500 °C [25]. However,

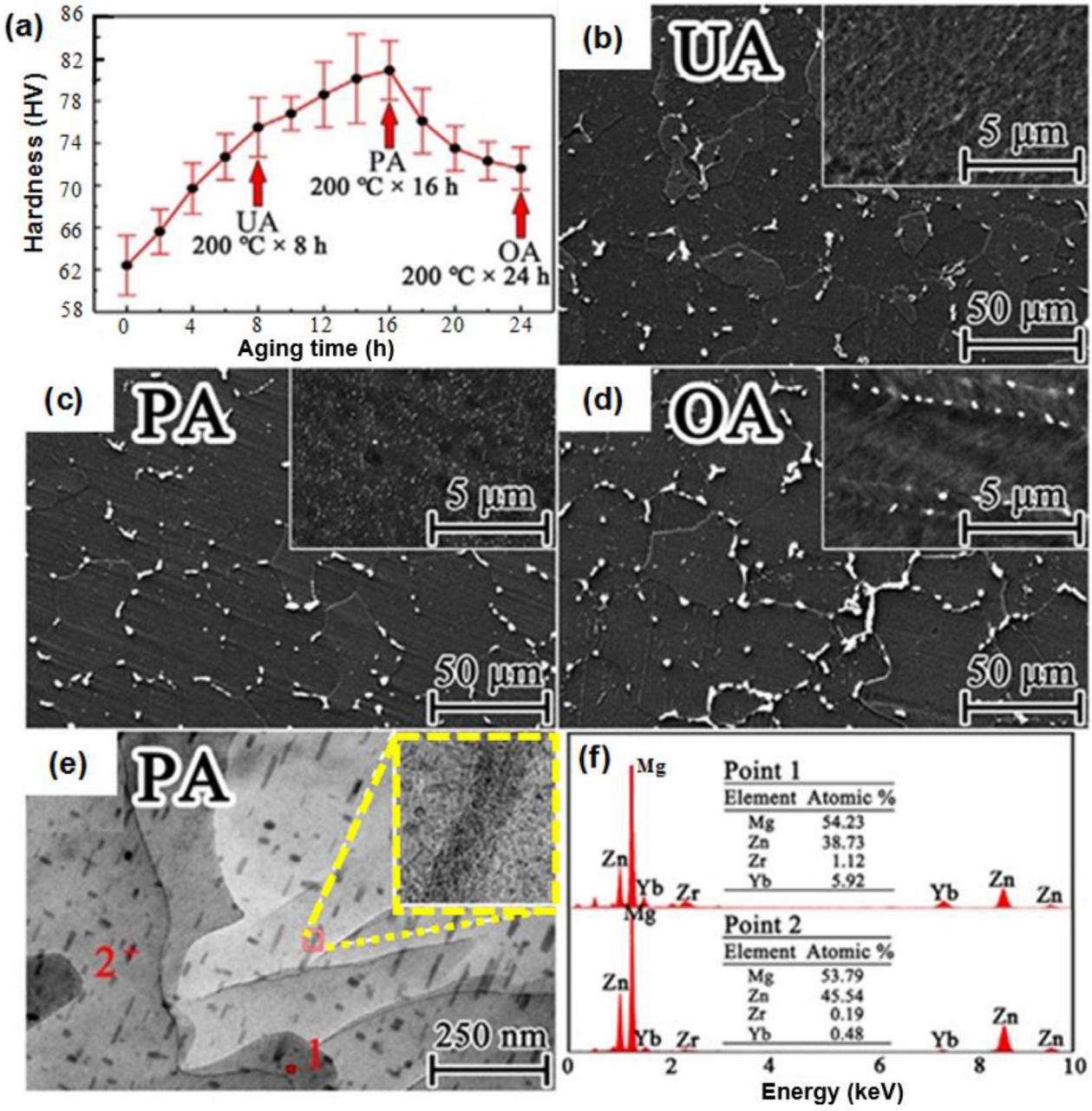

Fig. 11. (a) The micro-hardness evolution during aging, (b-d) SEM micrographs of the UA, PA, and OA samples, (e) the TEM micrograph of the PA sample, and (f) the EDS results of the precipitates in the PA sample, all for an Mg-5.8Zn-2.0Yb-0.5Zr alloy. Reproduced from [65].

when the solution temperature was higher, as at 550 °C, the grain coarsening phenomenon became more pronounced and this gave a decrease in the elongation. Fig. 14 shows the fracture surface of this alloy after different conditions. According to these SEM images, a cleavage fracture was observed on the fracture surface of the sample heat-treated at 550 °C.

4.2.2. The mechanical behavior of the Mg-Zn alloys after a T6 heat treatment

Generally, it is reasonable to anticipate that the aging treatment will result in some strengthening due to the precipitate strengthening effect and it is also common to lose some ductility after the aging treatment. During aging, some precipitates become thermodynamically stable and thus the solute atoms tend to diffuse and make clusters which gradually evolve to precipitates by a progressive diffusional process. Considering the mechanical strength, this is accompanied by gaining some precipitate strengthening at the expense of losing some solute strengthening. It was reported that there was a considerable increase in the critical resolved shear stress (CRSS) for basal slip in an Mg-4Zn alloy aged to peak aging condition (aging for 100 h at 149 °C) by comparison with the solution-treated sample 73. This was mainly attributed to the interaction of β_1' precipitates with the basal dislocations. In this case, these rod-shaped precipitates were elongated along the *c*-axis of the matrix and thus could effectively inhibit the

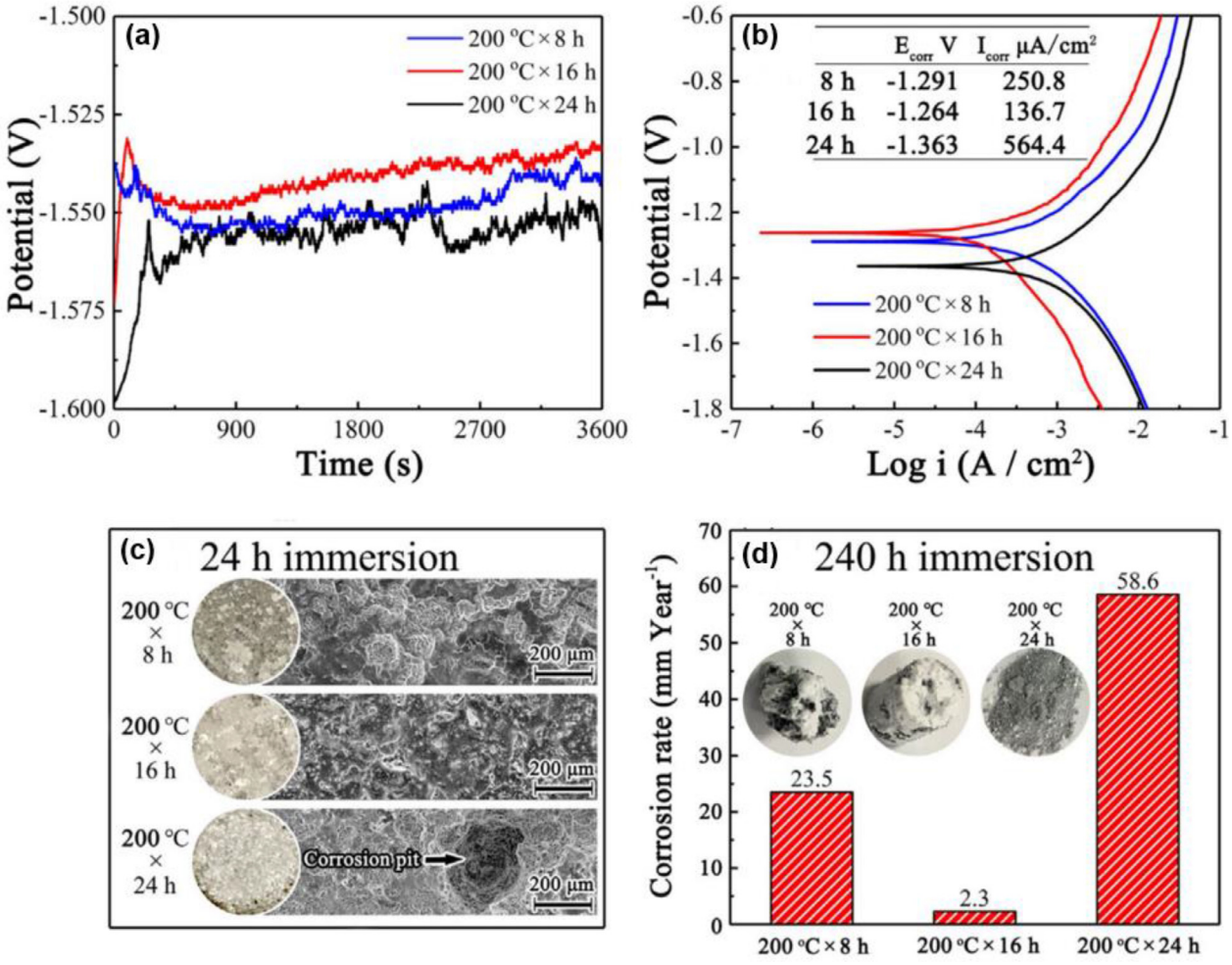

Fig. 12. (a) The OCP curves, (b) the dynamic potential polarization curves, (c) the corrosion morphology (both optical microscopy and SEM) after 24 h immersion and (d) the corrosion rates after 240 h immersion. The corrosion solution was SBF at 37 °C, and the studied material was an Mg-5.8Zn-2.0Yb-0.5Zr alloy. Reproduced from [65].

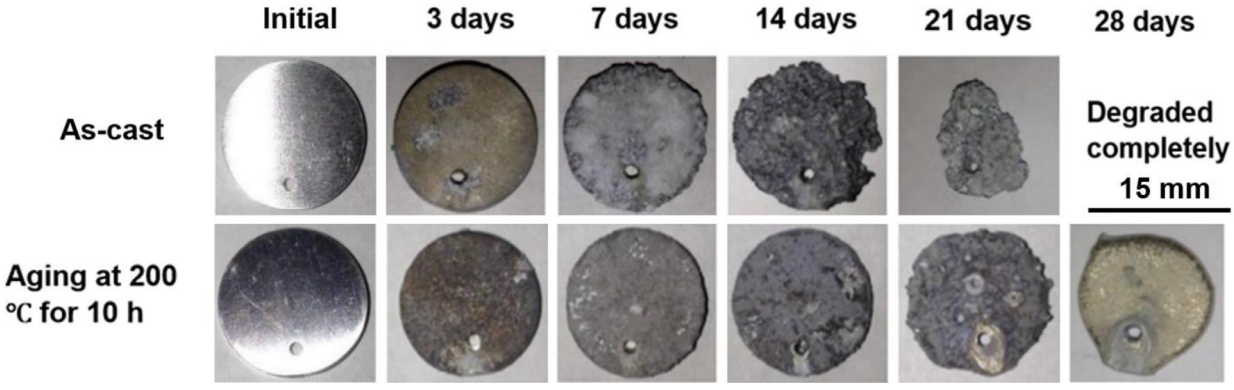

Fig. 13. Optical micrographs showing the initial and corroded surfaces of the Mg-1.2Zn-0.5Ca alloy in the as-cast (top row) and aged (bottom row) conditions. Samples were immersed in the SBF solution (with a pH range of 7.3-7.8) at 37 °C for 3, 7, 14, 21 and 28 days. Reproduced from [69].

motion of dislocations on the basal planes (Fig. 15). In another study, a considerable increase in creep resistance was reported in an aged Mg-4Zn alloy [43]. All of these reports indicate that the Mg-Zn precipitates can effectively strengthen the aged Mg-Zn alloys both at room temperature and at elevated temperatures.

The amount of strengthening obtained by the aging treatment depends strongly on the Zn content. In this regard, it was reported that by increasing the Zn content of Mg-Zn alloys both the yield stress and the ultimate tensile strength increase, where this was mainly attributed to the grain refining effect of Zn together with the increased solid solution and

Table 1
Effects of different heat treatments on the corrosion behavior of biodegradable Mg-Zn alloys in summary

Composition	Condition	Corrosion media	Containing phases	Best corrosion resistance	Remarks	Reference
Mg-2Zn-1Gd-0.5Zr	As-extruded & T4	Hanks' solution	W-phase $MgZn_2$	T4 at 510 °C for 5h	Enhanced corrosion resistance by the dissolution of the secondary phases into the matrix and uniform composition during the T4 treatment	[45]
Mg-2Zn-1Mn	As-extruded, T4 & T5	Ringer's solution	Mg_7Zn_3 Mg_xMn_y	T4 at 510 °C for 4 h	Corrosion resistance improvement due to the best film protection and lower defects in the T4 condition	[63]
Mg-3Zn-0.3Ca	As-cast & T4	Kokubo's SBF	$Ca_2Mg_6Zn_3$	T4 at 420 °C for 24 h	Lower corrosion rate was obtained as a result of a balance between the grain size and volume fraction of the secondary phases by properly adjusting the time and temperature of the T4 treatment	[44]
Mg-1.2Zn-0.5Ca	As-cast & T6	Modified SBF	$Ca_2Mg_6Zn_3$	T6: at 510 °C for 3 h with subsequent aging at 200 °C for 2 h	Reduction of the galvanic corrosion due to the homogenous distribution of the fine precipitates after the T6 treatment	[69]
Mg-9Zn	As-cast & T4	Kokubo's SBF	$Mg_{51}Zn_{20}$ $Mg_{12}Zn_{13}$	T4 at 340 °C for 18 h	Reduction of the micro-galvanic corrosion due to the dissolution of the secondary phases by the T4 treatment	[42]
Mg-5.8Zn-0.5Zr-*x*Yb	T4 & T6	SBF	Mg-Zn-Yb and Mg-Zn phases	T4 at 400 °C for 24 h	Corrosion resistance enhancement due to the stabilization of the Mg matrix by Yb addition in the T4 state	[66]
Mg-2Zn-0.5Nd-0.5Zr	As-extruded & T4	Hanks' solution	Mg-Zn $Mg_{12}Nd$	T4 at 500 °C for 5 h	Uniformity in composition, layer protection and less galvanic corrosion by the T4 treatment	[49]
Mg-4Zn-0.5Zr	As-cast & T4	DMEM + 10% FBS	Mg_7Zn_3	T4 at 300 °C for 1 h	Decrement of the secondary phases volume fraction and reduced micro-galvanic corrosion by the T4 treatment	[47]
Mg-3Zn-xAg	As-extruded & T4	SBF	$Mg_{51}Zn_{20}$ $Ag_{17}Mg_{54}$	T4 at 400 °C for 8 h	Improved corrosion resistance by the dissolution of secondary phases and segregation removal during the T4 treatment	[70]
Mg-5.2Zn-0.03Mn	As-extruded & T4	SBF & DMEM + 10% FBS	$MgZn_2$	T4 at 500 °C for 2 h	Minimizing the corrosion rate by the T4 treatment due to the twin-free microstructure and the uniform matrix	[71]
Mg-5.8Zn-2.0Yb-0.5Zr	T6 (UA, PA and OA)	SBF	Mg-Zn andMg-Zn-Yb phases	PA condition: at 400 °C for 48 with subsequent aging at 200 °C for 16 h	A tight and stable protective film by denser and more homogeneous nano-precipitates at the T6 (PA) condition	[65]
Mg-5Zn-xCa	As-cast & T4	Hank's solution	$Ca_2Mg_6Zn_3$ Mg_2Ca	T4 at 445 °C for 12 h	Reduction of the micro-galvanic corrosion by the dissolution of a large amount of the secondary phases and more homogenous microstructure in the T4 state	[72]

precipitation strengthening effects [29]. Moreover, the aging behavior strongly depends on other alloying elements added to Mg-Zn alloys. For example, it was reported that with the addition of 2% Yb to an Mg-Zn-Zr alloy a much higher density of nano-scaled precipitates was formed and this considerably improved the mechanical strength of the alloy [34]. By the addition of alloying elements, precipitates other than Mg-Zn phases can also contribute to the strengthening. The solid solution strengthening and precipitate strengthening by the $MgZn_2$, Mg_2Zn_3, and $Ca_2Mg_6Zn_3$ intermetallic compounds caused a substantial strengthening effect in a biodegradable Mg-2Zn-0.5Ca-1.0Mn alloy artificially aged at 175 °C for 8 h [74].

In addition to the as-cast alloys, the aging treatment was also performed on wrought alloys. Thus, a T6 heat treatment at 170 °C for 10 h was conducted on an as-extruded ZK60

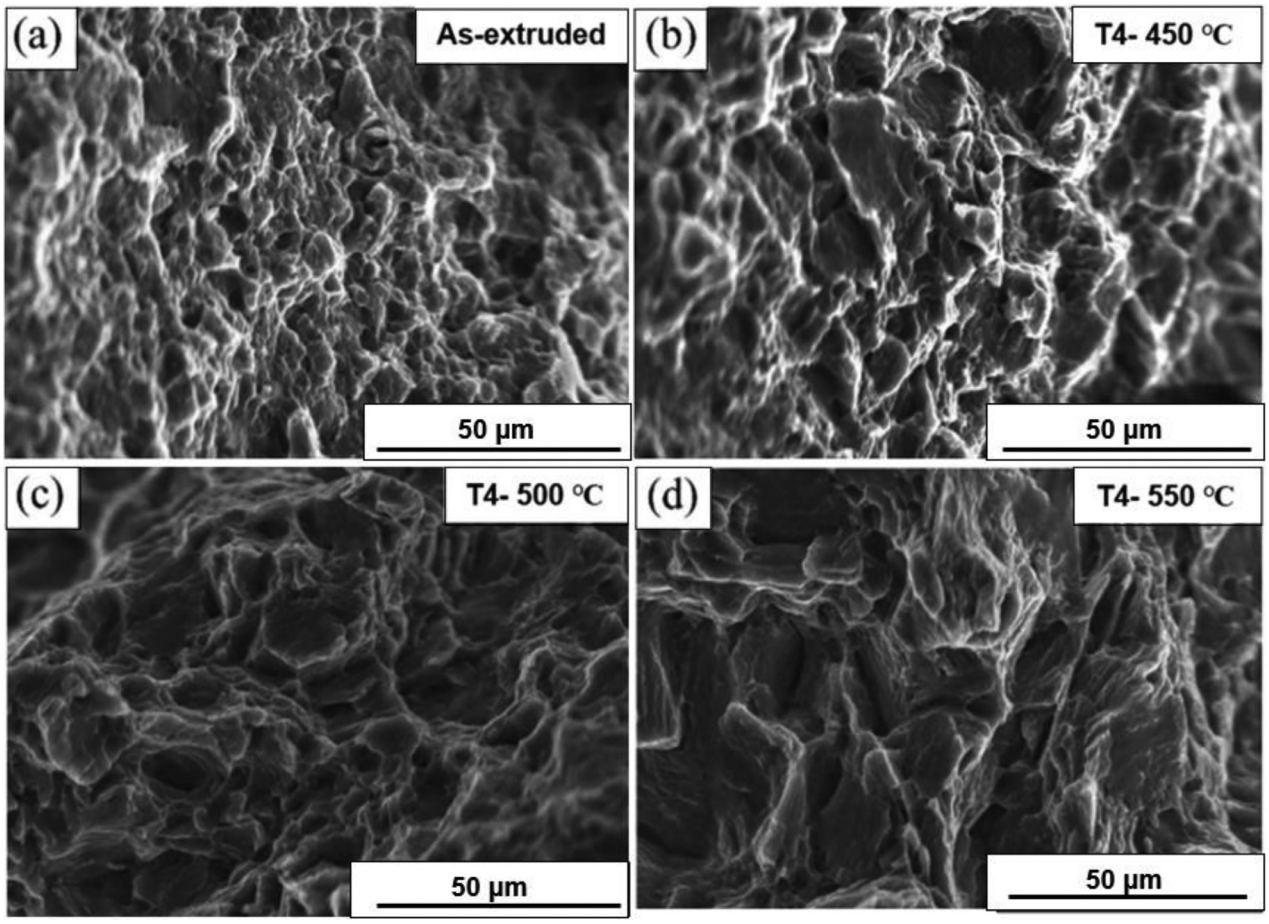

Fig. 14. SEM micrographs showing the fracture surfaces of the Mg-2Zn-0.5Nd-0.5Zr alloy in the as-extruded condition (a), and also after the T4-treatment at 450 °C (b), 500 °C (c) and 550 °C (d). Reproduced from [49].

alloy after a T4 treatment at 500 °C for 2 h. In this case, the high temperature of the solution treatment caused considerable grain growth and thus a coarse precipitation of MgZn secondary phases at the grain boundaries which led to a slight decrease in YS and UTS. Also, some ductility enhancement was achieved after the aging treatment due to the elimination of microstructural defects: for example, defects such as the work-hardening effects introduced during the extrusion process and the corresponding residual stresses and the thick and non-uniformly distributed secondary phases present in the microstructure of the extruded alloy [51].

Typically, the mechanical strength decreases after the peak aging condition which is attributed to a coarsening of the precipitates. Fig. 10 shows two types of precipitates in an Mg-Zn-Yb-Zr alloy in the peak-aged alloy: (1) rod-shaped Mg-Zn precipitates of 50-100 nm in length and (2) dot-like Mg-Zn-Yb precipitates with diameters of 20-50 nm. These precipitates are responsible for the microhardness increment in the early stages of the aging heat treatment, while extending the time of the process causes coarsening of the precipitates and this produces a microhardness decrement. In another report [69], the mechanical strength of an Mg-1.2Zn-0.5Ca alloy was improved by the aging heat treatment and reached a maximum level at 3-5 hours of aging (peak-age duration). Further increase in the aging time led to a lower number density of the $Ca_2Mg_6Zn_3$ fine precipitates, and therefore the mechanical strength of the alloy was decreased.

Table 2 is presented for an easier understanding and provides a comparison of different effects of heat treatments on the mechanical properties of biodegradable Mg-Zn alloys. In this table, the chemical composition of the studied alloy, the processing condition, the time and temperature of the best heat treatment condition, the mechanical properties of the heat-treated alloys (yield strength, ultimate tensile strength and elongation), and some remarks are presented in columns 1-7, respectively, and finally the corresponding references are given in the last column.

5. The effects of heat treatment on the Mg-rare earth alloys

Incorporation of biocompatible rare earth (RE) elements can substantially promote the bioperformance of biodegradable Mg alloys. In this section, the effects of heat treatment (T4 and T6) on the corrosion behavior and mechanical charac-

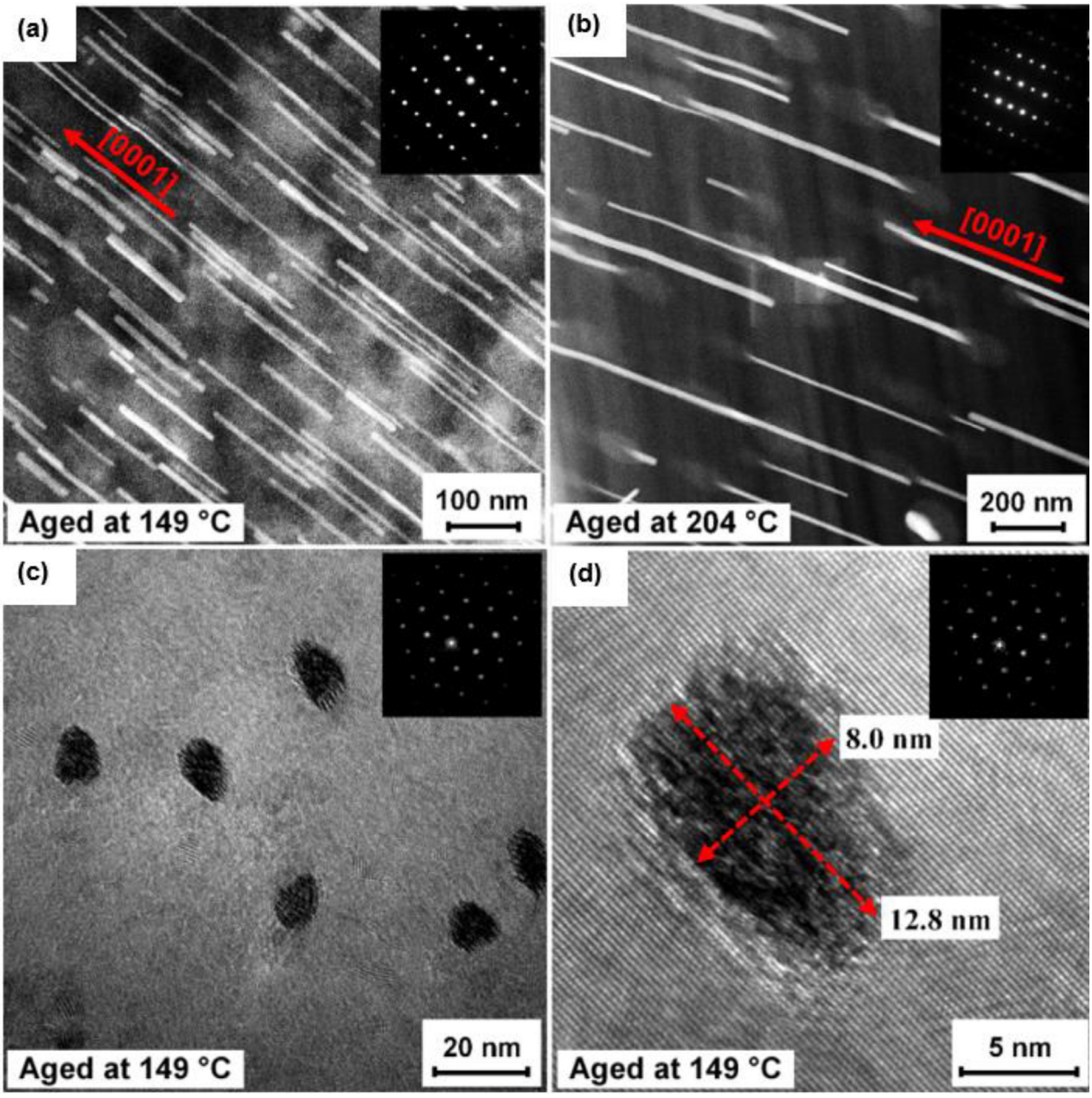

Fig. 15. Scanning transmission electron microscope (STEM) micrographs obtained from the planes perpendicular to the basal planes (a,b), and high-resolution transmission electron microscopy micrographs obtained from the planes parallel to the basal planes (c,d), showing the morphology of the β_1' precipitates in the aged Mg-4Zn alloy. The aging temperature is given at the left bottom corner of each image where the samples in (a, c and d) were aged at 149 °C for 100 h, and the sample in (b) was aged at 204 °C for 16 h. Reproduced from [73].

teristics of some well-known and heat-treatable Mg-rare earth alloys such as Mg-Gd, Mg-Y and Mg-Nd alloys are comprehensively discussed and reviewed.

5.1. Corrosion behavior

5.1.1. The corrosion behavior of the Mg-rare earth alloys in the as-cast condition

Gadolinium (Gd) is one of the common RE elements that has been widely used in the biodegradable Mg alloys with the intention of improving the mechanical properties, corrosion behavior, and biocompatibility [75]. The as-cast microstructure of the Mg-Gd alloys is mainly composed of primary α-Mg, dendrites and secondary phases which form a network structure. Gd has a high solid solution solubility in the α-Mg matrix which approaches the maximum solid solubility of 23.5 wt% at 548 °C. Therefore, the majority of Gd is concentrated in the α-Mg solid solution and thus the volume fraction of secondary phases is not significant, leading to lower galvanic corrosion in the as-cast condition of the biodegradable Mg-Gd alloys compared to other Mg-based alloys with less solid solution solubilities [76]. The addition

Table 2
Effects of different heat treatments on the mechanical properties of the biodegradable Mg-Zn alloys in summary

Composition	Condition	Time & temperature of heat treatment	Mechanical properties			Remarks	Reference
			YS	UTS	Elongation		
Mg-2Zn-1Gd-0.5Zr	EX + T4	At 400, 450, and 510 °C for 5 h	Decreased	Decreased	Decreased	Decrement in the mechanical properties due to the reduction in the second phase strengthening and also grain growth by the T4 treatment	[45]
Mg-4Zn-0.5Zr	As-cast + T4	At 300 °C for 1 h	Decreased	Decreased	Unchanged	A slight decrease in the YS and UTS of solution-treated alloy compared to as-cast alloy due to grain coarsening	[47]
Mg-5.8Zn-0.5Zr-xYb	As-cast + T6	At 565 °C for 24 h and at 300 °C for 20 h	Increased	Increased	Decreased	Improvement of the UTS and YS by the T6 treatment due to the formation of numerous fine precipitates	[66]
Mg-2Zn-1Mn	EX + T4	At 510 °C for 4 h	Decreased	Decreased	Decreased	Decreased mechanical properties of the T4-treated alloy due to grain growth	[63]
Mg-1.2Zn-0.5Ca	As-cast + T6	At 510 °C for 3 h with subsequent aging at 200 °C for 2 h	Increased	Increased	Increased	Elongation improvement and reduction in cracking tendency by a uniform distribution of the finely-dispersed precipitates in the T6 condition	[69]
Mg-2Zn-0.5Nd-0.5Zr	EX + T4	At 500 °C for 5 h	Decreased	Decreased	Increased	Elongation improvement due to the lower density of dislocations in the T4 condition	[49]
Mg-2Zn 0.5Ca-xMn	As-cast + T6	At 465 °C for 12 h with subsequent aging at 175 °C for 8 h	Increased	Increased	Decreased	Improvement of strength after the T6 treatment due to the effect of solution and dispersion strengthening	[74]
Mg-5Zn-xCa	As-cast + T4	At 445 °C for 12 h	Decreased	Increased	Increased	YS reduction due to the grain growth. UTS and elongation improvement due to reduction in defects as well as a more homogenous microstructure	[72]

of other alloying elements to Mg-Gd binary alloys significantly affects the properties of the as-cast Mg-Gd alloys by modifying the microstructure and mainly by increasing the volume fraction of the secondary phases. For example, it has been reported [77] that the high amount of the Mg_5Gd and Mg_2Ca secondary phases in the as-cast microstructure of the Mg-10Gd-1.2Ca-0.5Zr alloy, due to the addition of the alloying elements, accelerated the corrosion rate by promoting the galvanic corrosion.

The corrosion behavior of the magnesium alloys depends strongly on the protectiveness of the surface hydroxide-based corrosion products and, interestingly, it has been reported that Gd improves this protective film [78]. According to a report [76], the Gd boosted the magnesium hydroxide layer and the Gd^{3+} cations substituted the Mg^{2+} cations in a brucite lattice. The Gd^{3+} cations interacted with Cl^- anions, which mitigated the penetration of Cl^- anions in the hydroxide layer to the metallic substrate thereby producing a lower corrosion rate.

The Mg biodegradable alloys with long period stacking order (LPSO) structures have received significant attention in recent years due to their exceptional mechanical and corrosion properties. The LPSO phases are three-dimensional stacking and chemically ordered structures that have been reported in the Mg-M-RE systems (M: Al, Ni, Gd, Cu, and Zn, while RE: Y, Gd, Dy, Ho, Er, Tb and Tm). The LPSO phase has a considerable effect on the corrosion behavior of Mg-Gd biodegradable alloys and plays a dual role in tailoring the corrosion rate. They can either promote the filiform corrosion or act as a corrosion barrier [79]. It has been reported [80] that the LPSO structure in the as-cast Mg-3Gd-1Zn-0.4Zr alloy acted as a corrosion barrier between the matrix and the eutectic phase by forming at the outer edge of the matrix-grains, leading to a lower level of the micro-galvanic corrosion.

Yttrium (Y) is another interesting RE element to be utilized in biodegradable Mg implants which can induce many desirable properties. The Mg-Y alloys exhibit unique corrosion properties due to the equality of the standard electrochemical potential of Y with Mg (−2.37 V relative to the standard hydrogen electrode). The element Y shows no or relatively low signs of toxicity in the human body so that it is a common alloying element in the biodegradable Mg alloys [81,82]. The microstructure of the as-cast Mg-Y alloys mainly

consists of the α-Mg dendrites and the eutectic phases. The concentration of the solutes in the α-Mg is reported to be inhomogeneous and this inhomogeneity becomes more pronounced with a higher concentration of the alloying elements [83].

The incorporation of Y in the oxide film and also the precipitation of the Y-containing intermetallic compounds are the main two contributors in determining the corrosion behavior of the Mg-Y alloys. While the Mg-Y intermetallic compounds (e.g., $Mg_{24}Y_5$) may lead to micro-galvanic corrosion and thus accelerate the corrosion rate, Y can also become incorporated into the surface film and enhance the oxide film protection effect, thereby producing a corrosion resistance improvement [84,85]. According to [86], significantly improved corrosion resistance of the Mg-5.3Y-2.1Nd-0.9Gd-0.3Zr (WE54) alloy was attributed to the stabilization of the surface oxide layer by the Y and a scavenger effect of an RE addition. The impact of Y on the stabilization of the corrosion film is a distinguishing characteristic of this element which plays a determinant role in controlling the corrosion properties of the biodegradable Mg-Y alloys.

In addition to Gd and Y, Neodymium (Nd) is considered as another promising RE element to improve the mechanical properties and corrosion resistance of the biodegradable Mg alloys [87]. The biodegradable Mg-Nd-RE alloys with enhanced biocompatibility and antibacterial properties have been widely investigated [88–91]. The presence of Nd produces no cell toxicity making it a convenient alloying element for the Mg alloys in biomedical applications [92]. The maximum solid solubility of Nd in Mg is 3.6 at% at the eutectic temperature, but this is reduced sharply by decreasing temperature thereby indicating that the binary Mg-Nd alloy can be considered as a heat-treatable alloy. The dendritic structure, solute segregation, and inhomogeneous distribution of the secondary phases are the main microstructural characteristics of the as-cast Mg-Nd alloy [93]. The secondary phases play a dual role in affecting the corrosion behavior of the as-cast Mg-Nd alloys. These phases can act as a corrosion barrier and hinder any further corrosion propagation, while they can also act as the micro-cathodes and thus accelerate the micro-galvanic corrosion [94].

5.1.2. The corrosion behavior of the Mg-rare earth alloys after a T4 heat treatment

Substantial changes occur with the solid solution heat treatment in the microstructure of the Mg-RE biodegradable alloys. In the case of Mg-Gd alloys, the high solution treatment temperature leads to a decrease in the number of secondary phases and generates a supersaturated solid solution, resulting in the mitigation of the micro-galvanic corrosion and thus a lower corrosion rate. It was observed [95] that although the solution treatment of the Mg-15.24Gd-4.75Zn alloy at 540 °C for 4 h did not result in complete dissolution of the W-phase into the matrix, it limited the number of secondary phases and this resulted in a lower level of the micro-galvanic corrosion. On the other hand, as discussed earlier, grain growth is another notable phenomenon during the solution treatment. It has been reported [96] that the solution heat treatment of the Mg-10Gd at 525 °C for 24 h increased the grain size of the extruded alloy from 24 μm to 140 μm. As mentioned previously, the grain size and volume fraction of the secondary phases are two important factors that determine the overall corrosion rate of the biodegradable Mg alloys, and the best corrosion performance can be obtained with a balanced grain size and secondary phase volume fraction. In this regard, it was concluded [97] that the addition of Zn to the as-cast Mg-2Gd alloy decreased the grain size of the alloy and increased the volume fraction of the secondary phase. Subsequent solution treatment at 420 °C for 24 h balanced the secondary phase content and the grain size. In this study, the solution-treated Mg-2Gd-4Zn alloy exhibited the lowest corrosion rate (Fig. 16).

The formation of the protective film plays a vital role in the corrosion behavior of the biodegradable Mg-Gd alloys. The solid solution heat treatment generates a more homogenous microstructure with a more uniform distribution of the alloying elements existing in a supersaturated form, where this can help to form a better passivation layer that acts as a protective film. It has been reported [98] that the solution treatment of the Mg-7Gd-3Y-0.4Zn (GW73K) alloy at 520 °C for 8 h created a compact yellowish corrosion film. This tight corrosion film covered the surface and caused no localized corrosion on the surface of the alloy. Fig. 17 presents the results of the weight loss test after immersion in 5 wt% NaCl. According to these results, the T4 treatment remarkably decreased the corrosion rate by forming a tight corrosion film.

It is generally believed that the LPSO structure formation depends on the Gd content. The Gd atoms diffuse from the secondary phases and the LPSO structure to the α-Mg matrix throughout the solid solution heat treatment of the Mg-Gd alloys. Thus, the volume fraction of the LPSO structure varies during the heat treatment. A solid solution heat treatment was conducted on the as-cast Mg-6Gd-1.2Cu-1.2Zr alloy at four different temperatures (360, 390, 420, and 450 °C) for 12 h and, due to the composition and thermodynamic requirements of the LPSO structure formation, the volume fraction of the LPSO structure was the highest in the solution-treated alloy at 360 °C (T4-360) (Fig. 18b) 99. However, the LPSO structure disappeared at 450 °C due to the lack of Gd (Fig. 18e). According to mass loss and hydrogen evolution tests, the T4-360 alloy exhibited the best corrosion resistance, which was proof of the favorable effect of the LPSO on the corrosion properties. The LPSO structure acted as a barrier between the secondary phases and the α-Mg matrix, impeding the micro-galvanic corrosion. On the other hand, the T4-450 alloy suffered from severe galvanic corrosion due to lack of the LPSO structure, the large grain size and the dominant galvanic corrosion effect by the secondary phase, thereby exhibiting the weakest corrosion resistance.

The volume fraction of the secondary phase and its local potential in relation to the Mg matrix determine the overall severity of the micro-galvanic effect. It has been observed [100] that a new X phase with a 14H-type LPSO structure transformed during the solution treatment of the Mg-15Gd-

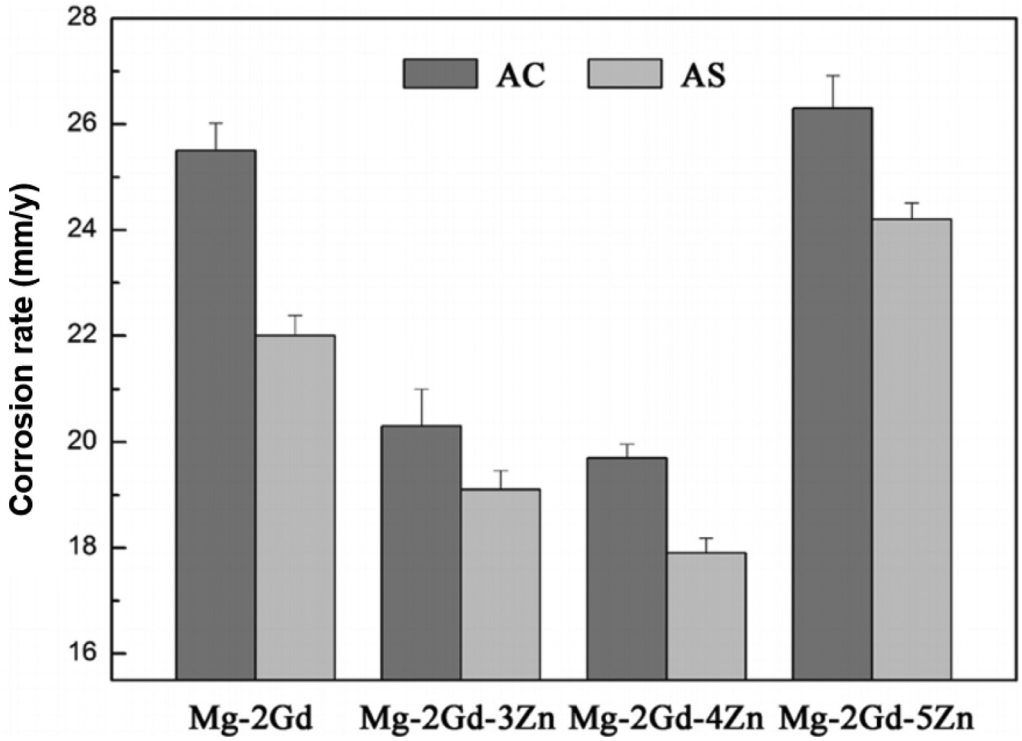

Fig. 16. The corrosion rate of the Mg-2Gd-xZn alloys in the as-cast (AC) and as-solution-treated (AS) conditions, after 9 days immersion in the SBF at 37.0 ± 0.5 °C. Reproduced from [97].

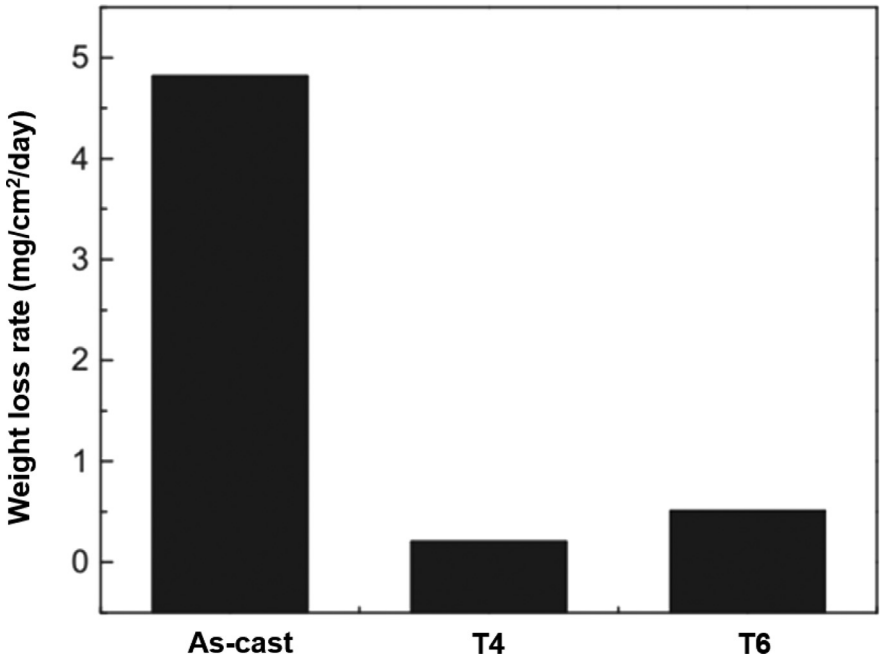

Fig. 17. The corrosion rates of the as-cast, T4-treated, and T6-treated GW73K alloy in the 5 wt% NaCl solution at 25 ± 2 °C for duration of 72 h. Reproduced from [98].

2Zn-0.39Zr alloy at 500 °C for 35 h. In this study, the as-cast alloy possessed the highest volume fraction of the secondary phases and a local potential difference of 290 mV, resulting in a high hydrogen evolution rate. The solution treatment caused a decrement in the volume fraction of the secondary phase from 42.8% to 27.0% and the generation of a new LPSO phase with a local potential difference of 243 mV. Therefore, the micro-galvanic corrosion was considerably mitigated by comparison with the as-cast alloy (Fig. 19). On the other hand, the solution treatment of the Mg-3Gd-1Zn-0.4Zr (GZ31K) alloy at 535°C for 12 h caused the dissolution of both the eutectic phase and the stacking faults

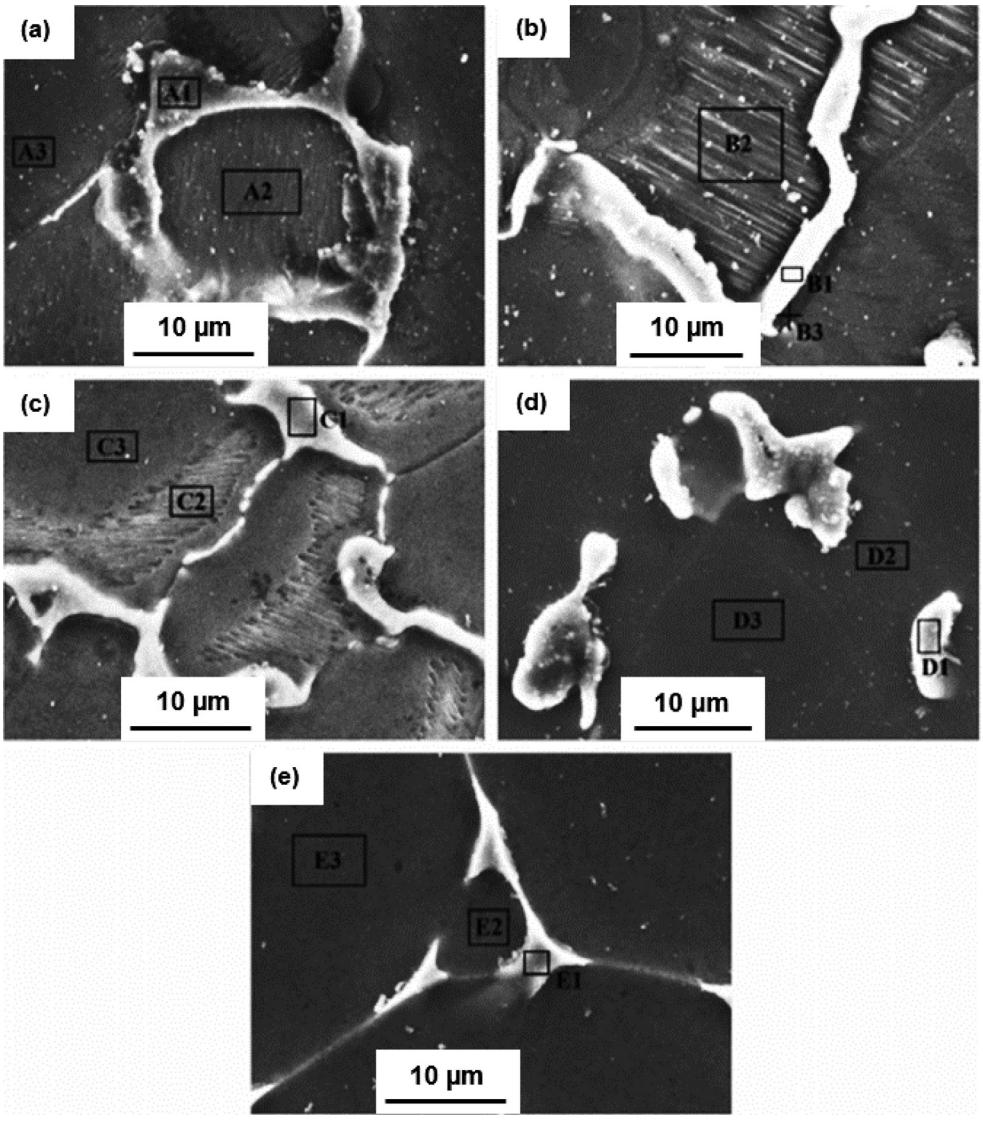

Fig. 18. The morphology of the LPSO structure in the Mg-6.0Gd-1.2Cu-1.2Zr alloy, in the as-cast (a), and also solution-treated states (b-e), where the solution temperature was 360 °C (b), 390 °C (c), 420 °C (d), and 450 °C (e). Reproduced from [99].

(SFs) and precipitation of abundant needle-like particles [80]. The SFs at the outer edge of the matrix grains played the same role as the LPSO structure and protected the grains against the corrosion propagation. Hence, the solid solution heat treatment in this study reduced the corrosion resistance. Fig. 20 depicts the corrosion process schematic diagram of the GZ31K alloy in the as-cast, T4, and as-extruded conditions in which the T4-treated alloy, with no stacking fault structures, in the later stages of the corrosion was severely damaged.

In another study [76], the formation of new Mg_5Gd particles during the solution treatment of an Mg-5Gd alloy at 500 °C for 30 h reduced the corrosion resistance of the alloy. It was observed that with the formation of the new Mg_5Gd particles, the α-Mg matrix was depleted from Gd, and the amount of Cu was increased to 0.4% in the new particles, which increased the nobility of the new phases, all of which resulted in a reduced corrosion resistance.

The implementation of T4 treatment on Mg-Y alloys has shown great promise. The solid solution heat treatment of the as-cast Mg-Y alloys reduces the residual casting stresses, decomposes and decreases the eutectic phases, increases the uniformity of the elemental distribution through the matrix and generates a supersaturated solid solution with the Y element [101]. All of these changes favor the corrosion resistance and effectively can decrease the corrosion rate [102]. Dissolution of the secondary phases during the solution treatment is one of the most important microstructural changes. According to 81, the solution treatment of the as-cast Mg-4Y-1Ag alloy at 525 °C for 3 h eliminated the coarse $Mg_{24}Y_5$ particles and reduced the corrosion rate by almost one-half compared with the primary as-cast alloy. At the same time, the solution treatment was practically ineffective in the case of

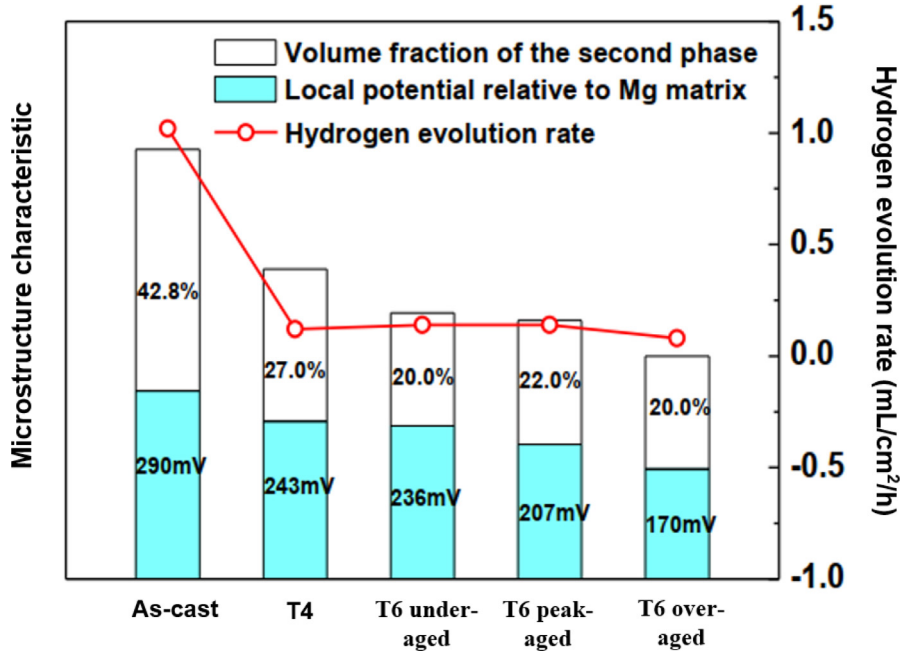

Fig. 19. The effects of two important microstructure characteristics (the volume fraction of the secondary phases and also local potential relative to the Mg matrix) on the hydrogen evolution rate of an Mg-15Gd-2Zn-0.39Zr alloy, in the as-cast, T4, T6-under aged, T6-peak aged and T6-over aged conditions. Reproduced from [100].

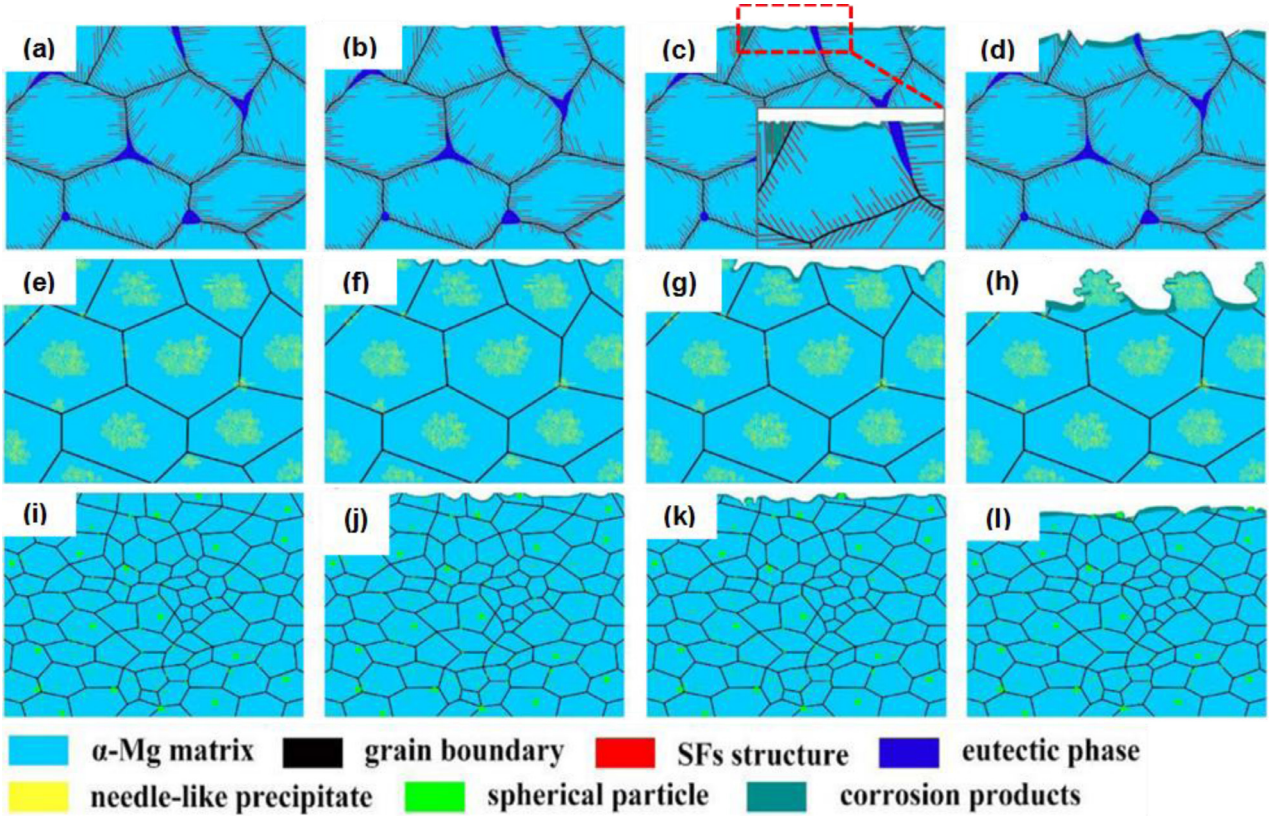

Fig. 20. Schematic representation of the corrosion process in the as-cast (a-d), solution-treated (e-h) and as-extruded (i-l) GZ31K alloy. Reproduced from [80].

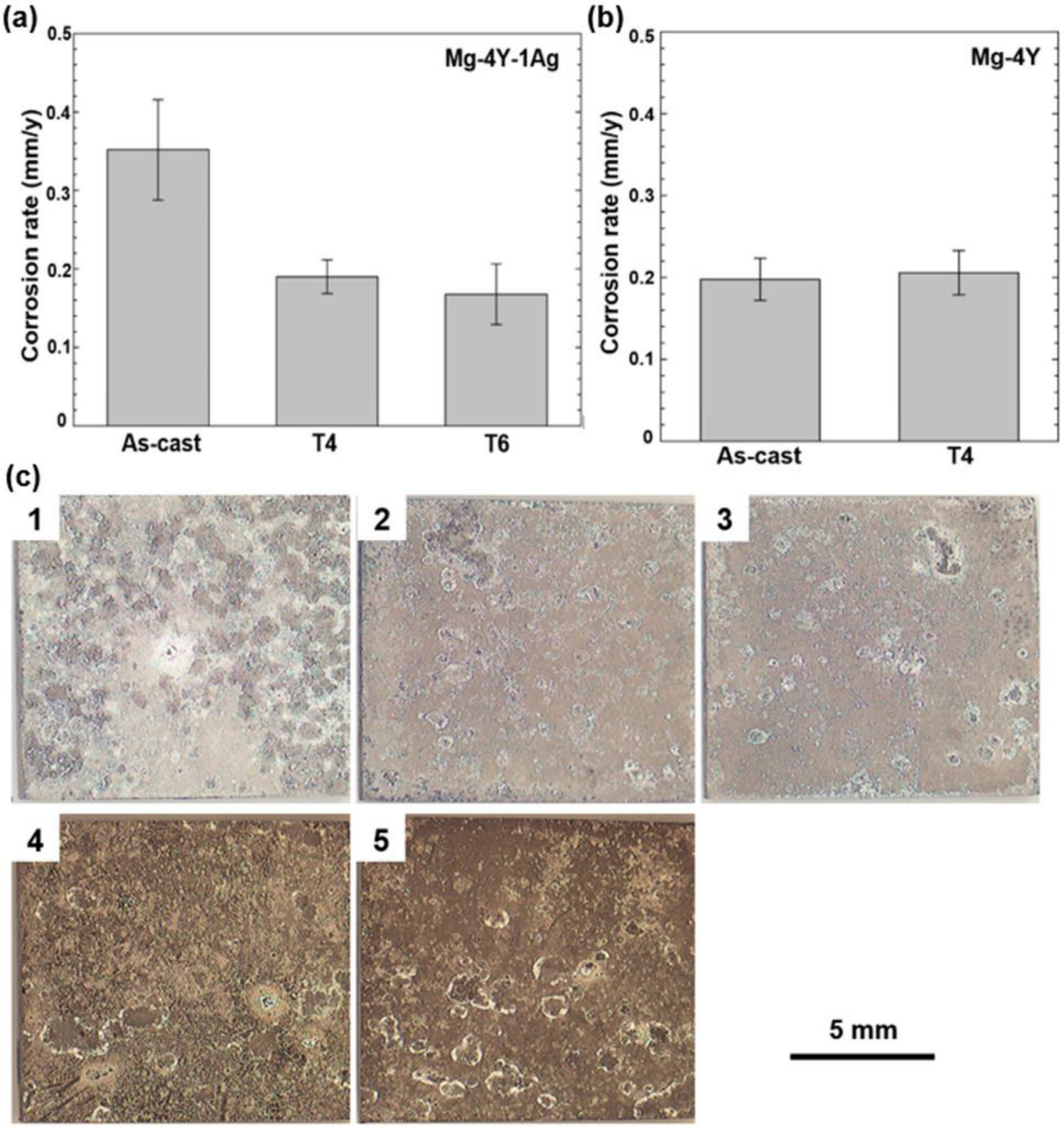

Fig. 21. The corrosion rate of the as-cast and heat-treated alloys, immersed in DMEM + 10% FBS for 7 days: (a) Mg-4Y-1Ag alloy, and (b) Mg-4Y alloy. The macrostructures of the as-cast and heat-treated alloys after the corrosion test are presented in (c), where: (1) as-cast Mg-4Y-1Ag, (2) T4-treated Mg-4Y-1Ag, (3) T6-treated Mg-4Y-1Ag, (4) as-cast Mg-4Y, and (5) T4-treated Mg-4Y. Reproduced from [81].

the Mg-4Y alloy due to its better microstructural homogeneity in the as-cast condition (Fig. 21). Therefore, the extent of microstructural changes, and thus the extent of change in the corrosion properties by the solution treatment, is strongly related to the concentration of the alloying elements in the as-cast conditions. Fig. 21c shows the macrostructures of the Mg-4Y and Mg-4Y-1Ag alloys in both the as-cast and T4-treated conditions, after immersion in Dulbecco's modified eagle medium (DMEM) with 10% Fetal Bovine Serum (FBS) for 168 h. The results indicate more severe corrosion pits on the as-cast Mg-4Y-1Ag alloy compared to the T4-treated alloy due to the improved homogeneity in the solution-treated conditions.

As discussed earlier, the element Y can be incorporated in the corrosion products as Y_2O_3 (and partly as $Y(OH)_3$) and thus enhance the protecting effect of the corrosion film. In addition, the dissolution of Y into the α-Mg matrix can improve the protective nature of the corrosion film and the film containing the Y element becomes more uniform [103]. Fig. 22 shows the corrosion morphologies of the as-cast and

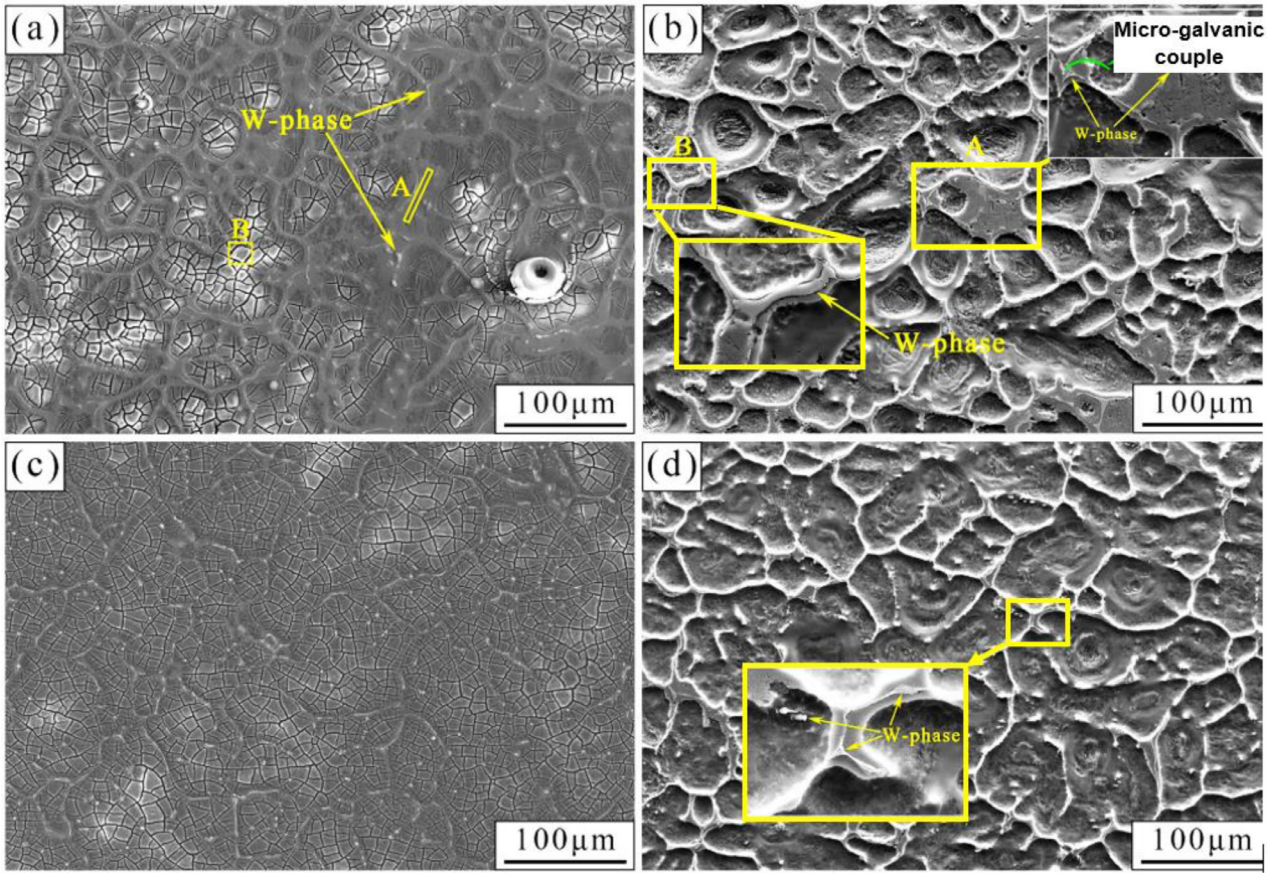

Fig. 22. SEM micrographs of the corroded samples of the Mg-2Y-1Zn-0.4Zn-0.3Sr alloy, both prior to (left) and after (right) removal of the corrosion products. The samples were immersed in the SBF solution (37 °C) for 45 min. The results are for the as-cast (a,b) and T4 (c,d) conditions. Reproduced from [104].

T4-treated Mg-2Y-1Zn-0.4Zn-0.3Sr alloy both prior to and after removal of the corrosion products from the samples immersed in the SBF [104]. As can be observed, the corrosion layer of the T4-treated alloy is relatively uniform and presents lower micro-galvanic corrosion couples compared to the as-cast alloy.

In another investigation [105], the influence of Y on the corrosion properties of the heat-treated Mg-Y alloys was studied. The corrosion rate was first decreased and then increased with increasing Y content (3-7 wt%) and the Mg-2Y alloy showed significantly different corrosion properties among the studied alloys. The single-phase solid solution and a lower number of Y-containing intermetallic compounds caused the Mg-2Y alloy to exhibit an extraordinary protective surface film (Fig. 23). By contrast, alloys with more Y concentrations suffered from severe filiform corrosion induced by a large amount of Y-containing intermetallic compounds. In conclusion, the presence of Y in the solid solution form improves the corrosion resistance by forming a protective surface film, while the Y-containing intermetallic compounds deteriorate the corrosion resistance by accelerating the micro-galvanic corrosion.

Remarkable modifications of corrosion features of Mg implants have been reported after the execution of T4 treatment on Nd incorporated Mg alloys. By solution treatment of the Mg-Nd alloys, the micro-segregation of the alloying elements and volume fraction of the secondary phases decrease and this seems to improve the corrosion resistance compared to the as-cast condition. However, some grain growth also occurs [76,106]. The as-cast Mg-Nd alloys possess a higher volume fraction of the secondary phases due to the lower solid solubility of the Nd in Mg at low temperatures compared to elements like Gd and Zn. Thus, the galvanic corrosion strongly affects the biodegradation behavior of the Mg-Nd alloys. For this reason, heat treatment is considered as a valuable tool for the modification of the microstructure to control the corrosion behavior, as well as mechanical properties of the biodegradable Mg-Nd alloys. In this regard, it has been reported [76] that the solid solution heat treating of the Mg-4Nd alloy at 520 °C for 20 h improved the corrosion resistance by partial dissolution of the eutectic $Mg_{12}Nd$ phase in the Mg matrix, and this led to a lower galvanic corrosion rate.

An investigation was conducted to determine the effect of 12 h solution treatments at different temperatures (500, 520, 540, and 560 °C) on the corrosion properties of the as-extruded biodegradable Mg-2.25Nd-0.11Zn-0.43Zr (NZ20K) alloy [88]. It was observed that grain growth and the decrease of the volume fraction of the precipitates significantly influenced the corrosion properties. The best corrosion resis-

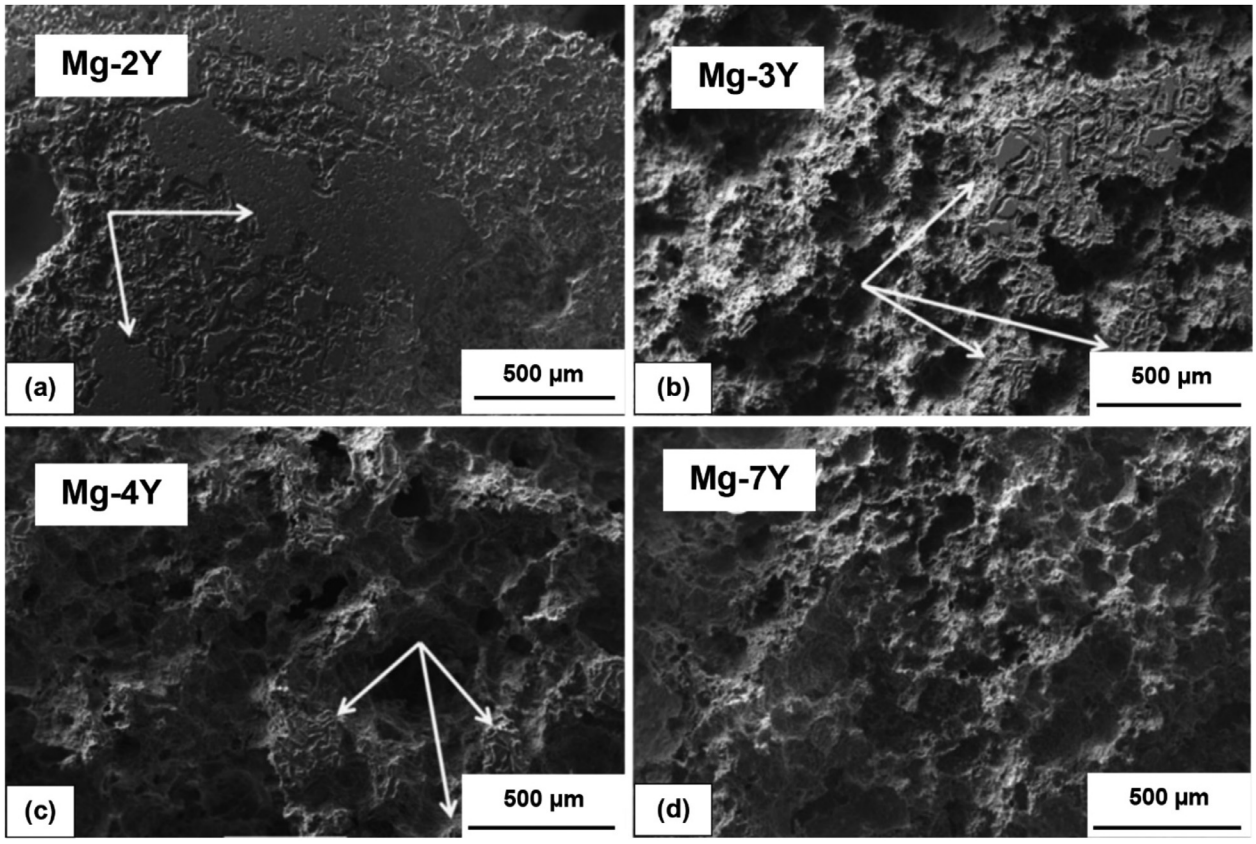

Fig. 23. SEM micrographs, showing the corroded surfaces of the Mg-xY (x = 2, 3, 4 and 7) alloys after immersion in the 0.1 M NaCl solution for 72 h. (a) Mg-2Y, (b) Mg-3Y, (c) Mg-4Y, and (d) Mg-7Y. Reproduced from [105].

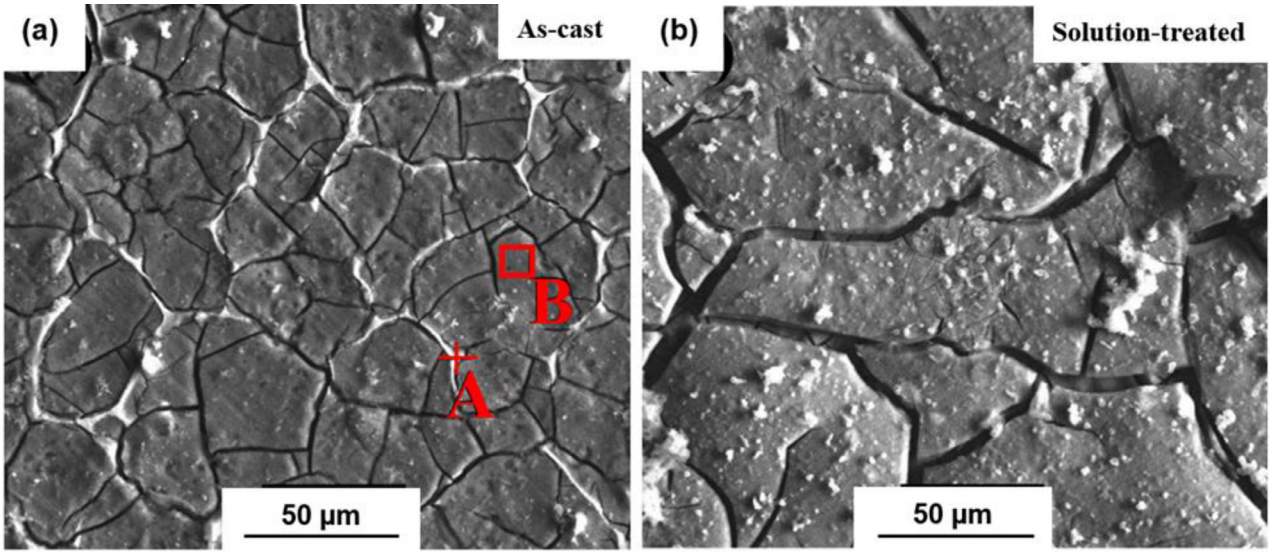

Fig. 24. The corrosion morphologies of the Mg-2.5Nd-0.3Zn-0.1Sr-0.4Zr alloy after immersion in SBF for 120 h: (a) the as-cast condition, and (b) the T4-treated condition. Reproduced from [93].

tance was achieved after the solution treatment at 540 °C due to a balance between the positive effect of the dissolution of the secondary phases and the negative impact of the grain growth. In this study, the solution-treated alloy at 560 °C suffered from irregular grain growth which was responsible for the 62% observed increase in the corrosion rate compared to the alloy solution-treated at 540 °C. In another investigation [107], a solution treatment of the Mg-2.7Nd-0.2Zn-0.4Zr alloy at 475 °C for 1 h, considered for a cardiovascular stent application, improved the corrosion resistance. A compromise

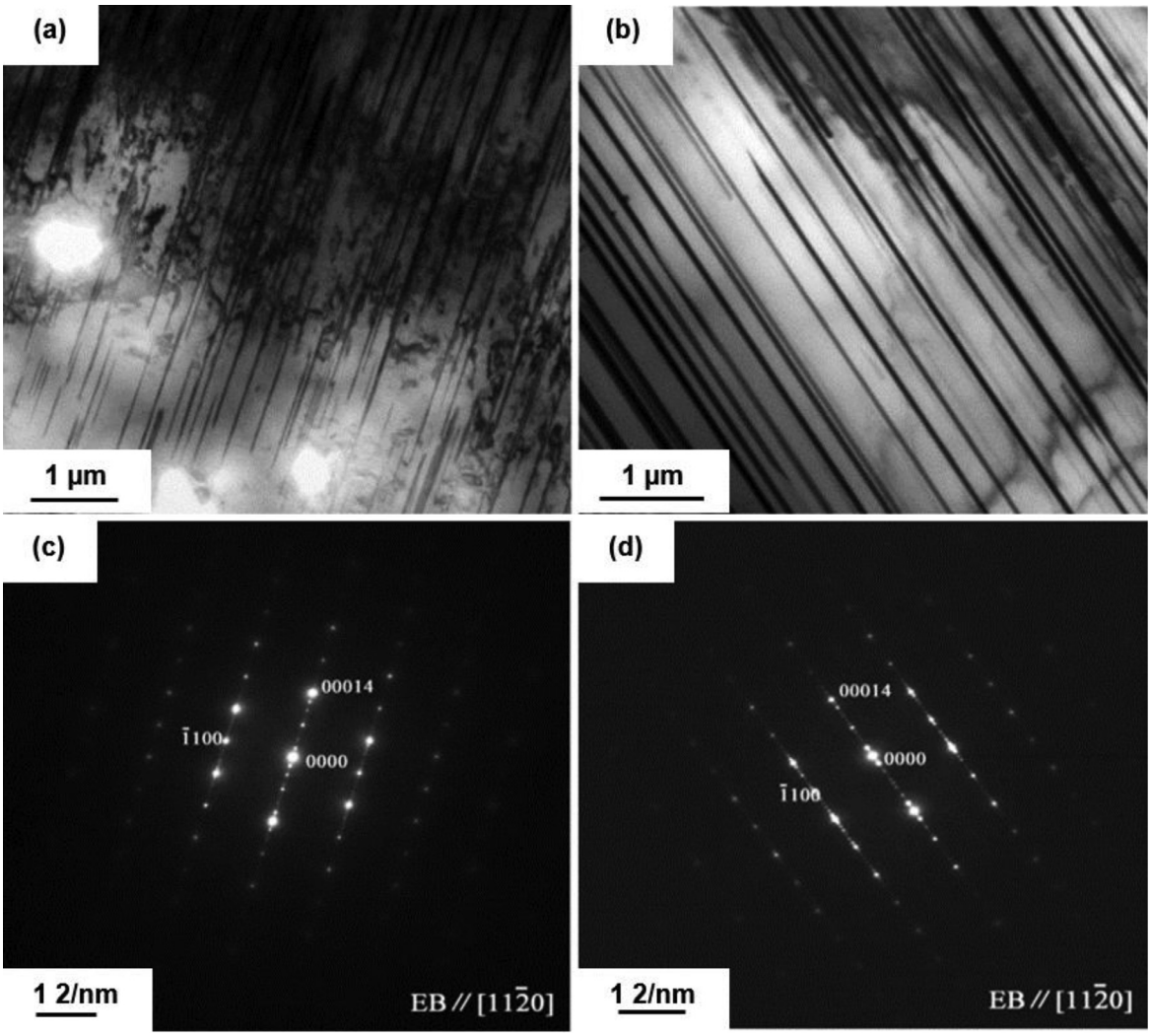

Fig. 25. TEM micrographs of the LPSO phase in the Mg-15.24Gd-4.75Zn alloy in different conditions: (a) T6-treated, and (b) T6F-treated. The corresponding SAED patterns of (a) and (b) are represented in (c) and (d), respectively. Reproduced from [95].

between the grain size and volume fraction of the secondary phase was obtained at 475 °C leading to a minimum corrosion rate.

It has been reported [108] that a solution treatment of the Mg-1.59Nd-2.91-Zn-0.05Zr-0.35Mn (NZKM) alloy at 480 °C for 10 h changed the continuous distribution of the β-$(MgNd)_4Zn_7$ phase (β-compounds) in the as-cast condition to discontinuous necklace-type distribution. The β-compounds acted as a cathode and accelerated the micro-galvanic corrosion in both the as-cast and T4-treated conditions. However, with the propagation of corrosion, the β-compounds in the solution-treated alloy piled off from the α-Mg matrix due to the lack of a stable attachment, resulting in a lower volume fraction of the cathodic phase and thus remarkably increased the corrosion resistance.

Contrary to the studies already described, it has also been reported [93] that a solution treatment decreased the corrosion resistance of the as-cast biodegradable Mg-2.5Nd-0.3Zn-0.1Sr-0.4Zr alloy. The deterioration of the corrosion resistance was mainly attributed to grain growth and the presence of a discontinuous intermetallic phase. The eutectic phase in the as-cast alloy was distributed relatively continuously, which wrapped the Mg matrix and acted as a corrosion barrier that could hinder the corrosion propagation. The solution treatment changed the continuous form of the eutectic phase into a discontinuous scattered form with a lower volume fraction, and thus the barrier effect was effectively diminished. Fig. 24 shows the corrosion morphology of the as-cast and T4-treated alloy after immersion in SBF for 120 h. The width of the micro-cracks on the corroded surface demonstrates the extent of the corrosion. The width of the micro-cracks was thicker in the T4-treated alloy than the as-cast alloy which shows that the solution-treated alloy possessed lower corrosion resistance.

5.1.3. The corrosion behavior of the Mg-rare earth alloys after a T6 heat treatment

Aging is another important heat treatment process which has significant impacts on the corrosion behavior of Mg-RE alloys. It is important to note that the size, distribution, mor-

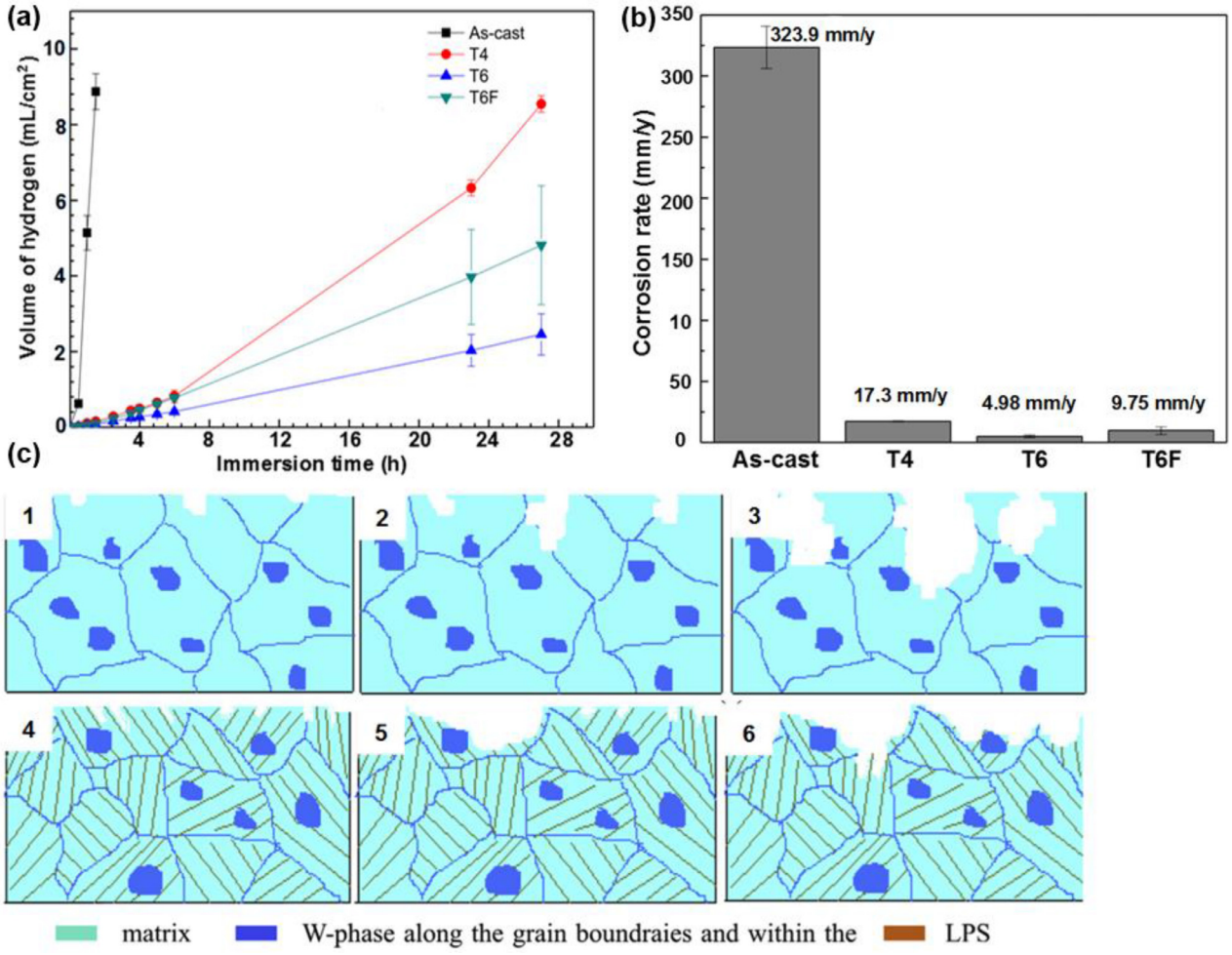

Fig. 26. The hydrogen evolution curves (a) and the corresponding calculated corrosion rates (b) of the Mg-15.24Gd-4.75Zn alloy in the as-cast, T4, T6 and T6F conditions. The corrosion process is schematically presented in (c), where the occurrence of the localized corrosion (1-3) and uniform corrosion (4-6) can be observed for the T4- and T6-treated samples, respectively. Reproduced from [95].

phology, and volume fraction of the precipitates after the T6 heat treatment dictate the corrosion behavior of the Mg-RE alloys. For instance, with the modification of microstructure and re-precipitation of new precipitates during the aging heat treatment, the micro-galvanic corrosion will be a decisive factor in determining the corrosion behavior of the Mg-Gd alloys. As discussed before and according to Eq. 1, the cathode to anode surface area ratio is an essential item in assessing the corrosion rate. It has been reported [98] that the size of the precipitates in the T6-treated Mg-7Gd-3Y-0.4Zr (GW73K) alloy was in the range of nanometers, while large particles in the range of micrometer were observed in the as-cast alloy. As a result, the galvanic corrosion was more severe in the as-cast alloy, and numerous corrosion pits having great depths were observed on these samples.

Another factor that affects the corrosion behavior of the aged Mg-Gd alloys is the LPSO structure. There is a report of a study on the effects of two different aging heat treatments on the microstructure and corrosion behavior of an as-cast Mg-15.24Gd-4.75Zn alloy 95. The first type of the heat treatment was solution treating at 540 °C for 4 h with subsequent aging at 450 °C for 10 h (T6) and the other type was s solution treatment at 540 °C for 4 h but this time the sample was furnace cooled (T6F). The LPSO structure, which was absent in the as-cast alloy, was formed within the aging process by the atomic diffusion. Fig. 25 shows the bright-field TEM images of the LPSO structure in the T6 and T6F samples. The LPSO structure in the T6 and T6F samples were discontinuous/dense and long/thick, respectively. The results of the hydrogen evolution tests revealed that the T6-treated alloy with dense distribution of the LPSO structure had the best corrosion resistance (Fig. 26a) and its corrosion rate reached the lowest 4.98 mm/y value (Fig. 26b). In this study, the LPSO structure in the T6-treated alloy occupied the whole of the α-Mg grains and reduced the exposed surface area to corrosion media, where this decreased the overall corrosion rate. The lamellar LPSO structure acted as an anode against the W-phase cathode during the micro-galvanic corrosion and obstructed the penetration of the corrosive ions. Fig. 26c depicts a schematic of the corrosion process of the T4-treated and T6-treated alloys and the influential role of the LPSO structure in enhancing the corrosion resistance.

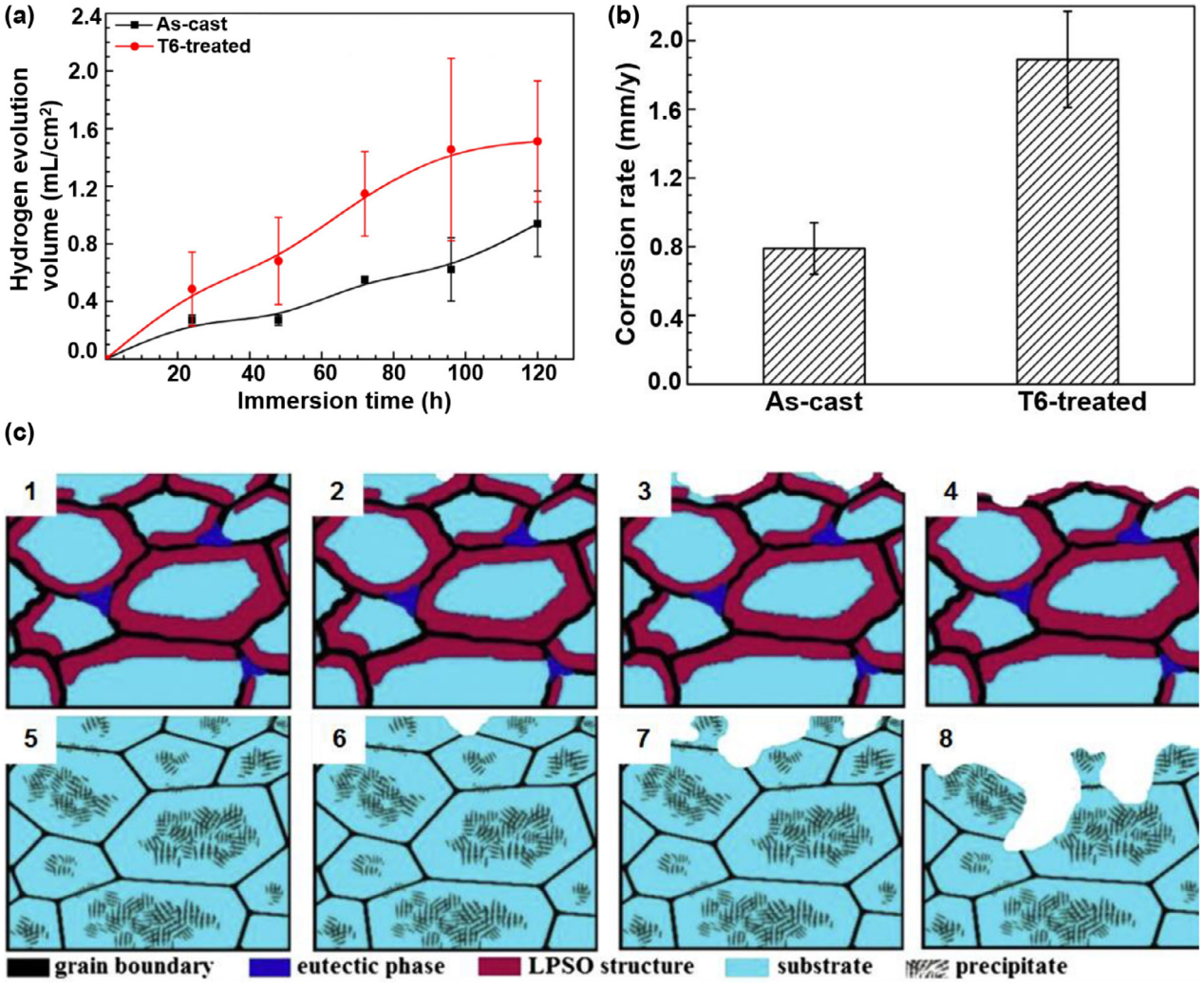

Fig. 27. The hydrogen evolution curves (a), and the corrosion rates calculated from the weight loss tests in SBF at 37 °C for 120 h (b), for the GZ51K alloy in the as-cast and T6 conditions. The corrosion process is schematically presented in (c), where the occurrence of the uniform (1-3) and localized corrosion (4-6) can be observed with increasing the immersion time for the as-cast (with the LPSO structure) and T6 (without the LPSO structure) samples, respectively. Reproduced from [75].

Contrary to the previous work, while the as-cast Mg-5Gd-1Zn-0.6Zr (GZ51) alloy contained the LPSO structure, aging at 120 °C for 12 h (after T4 treatment at 535 °C for 12 h) did not result in further LPSO formation and instead, the LPSO structure disappeared after this heat treatment [75]. In this study, after aging the eutectic phase and LPSO structure faded and new needle-like precipitates were formed. The immersion tests in SBF for 120 h disclosed numerous pits on the surface of the T6-treated alloy (without the LPSO structure) while the as-cast alloy (with the LPSO structure) exhibited a smooth and uniform surface. In this investigation, significantly improved corrosion resistance of the alloys with the LPSO structure was attributed to two main factors: (1) an enhanced passivation ability of the substrate material in forming a compact film on the surface by means of the LPSO structure and (2) the barrier role of the LPSO structure between the substrate and the eutectic phase. Fig. 27a and Fig. 27b show the results of the hydrogen evolution test and weight loss test after immersion in SBF. Fig. 27c demonstrates a schematic diagram of the corrosion processes of the as-cast and T6-treated GZ51K alloy with and without the LPSO structure in which the loss of the LPSO structure in the aged alloy caused severe corrosion damage.

The re-precipitation of the secondary phases during the aging treatment affects the corrosion properties of the Mg-Y alloys in many different ways. The precipitate would act as a cathode and accelerate the micro-galvanic corrosion. Also, the phases can contribute to forming a more pronounced passive layer which inhibits any further corrosion propagation and decreases the overall corrosion rate. It has been reported [83] that the solution treatment of the as-cast Mg-5Y-1.5Nd alloys at 535 °C for 20 h with subsequent aging at 225 °C for different times (6, 14, and 24 h) deteriorated the corrosion resistance by increasing the micro-galvanic couples. While the T6-24 h (overaged) alloy exhibited the highest amount of the bulky secondary phases and the highest corrosion rate, the

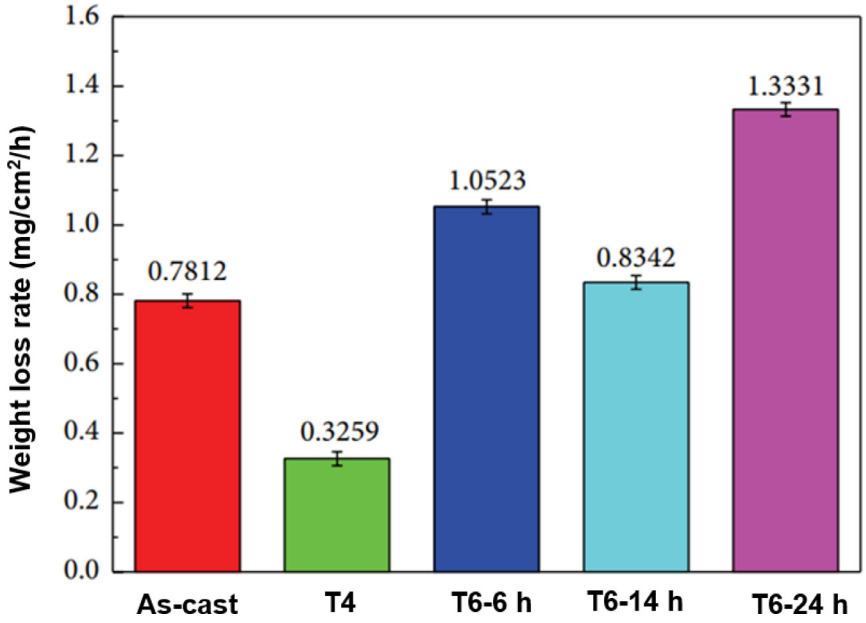

Fig. 28. The results of the weight loss test for the Mg-5Y-1.5Nd alloy in the as-cast, T4, T6 (6 h), T6 (14 h) and T6 (24 h) conditions. The samples were immersed in the 3.5% NaCl solution for 24 hours. Reproduced from [83].

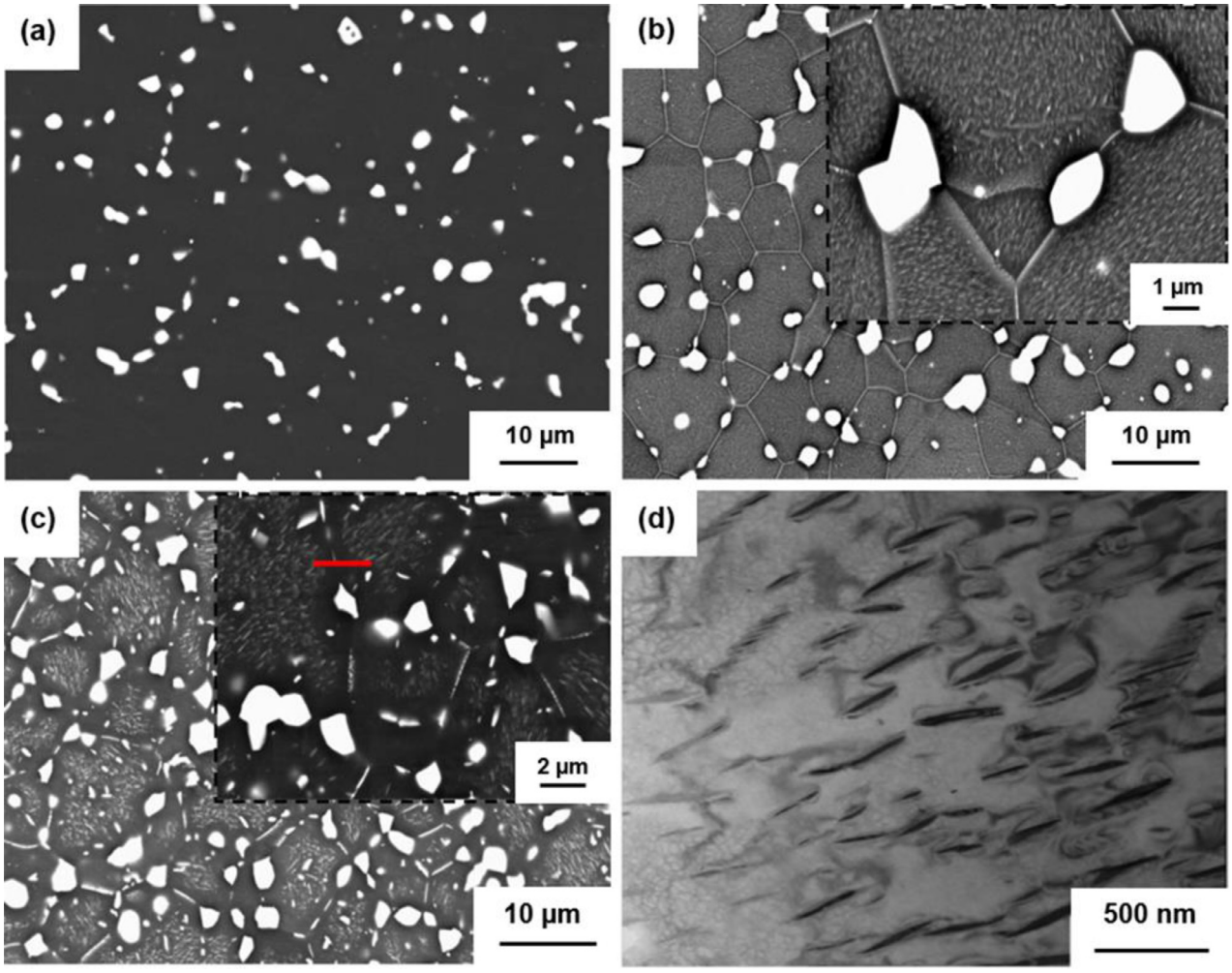

Fig. 29. SEM images of the extruded biodegradable Mg-5Nd alloy after different conditions: (a) T4 treatment, (b) T6 treatment at 200 °C, and (c) T6 treatment at 245 °C. TEM bright-field micrograph of the sample aged at 200 °C is shown in (d). Reproduced from [110].

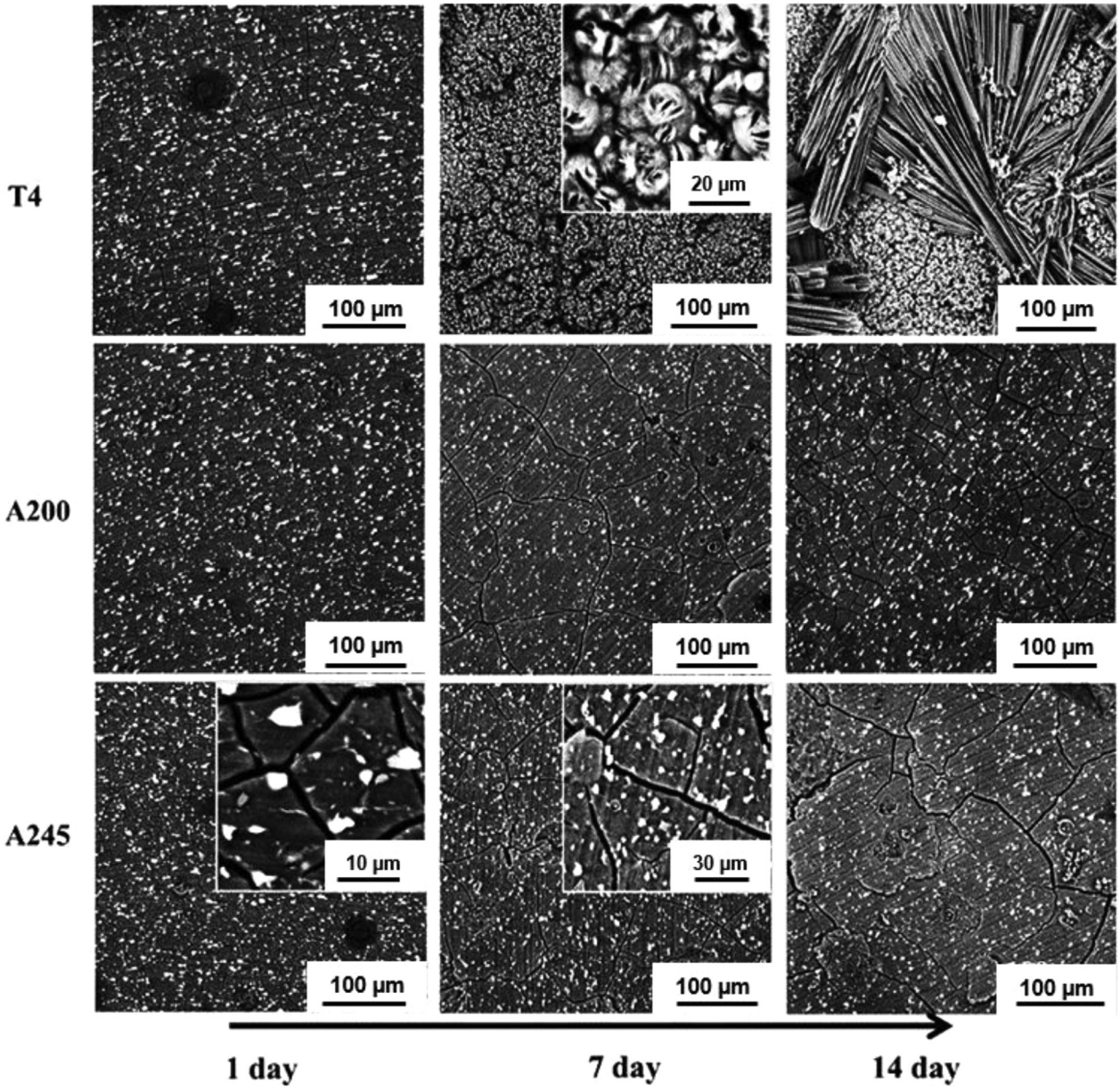

Fig. 30. SEM micrographs showing the morphology of the corrosion surfaces of the biodegradable Mg-5Nd alloy after immersion for 1, 7, and 14 days in DMEM + Glutamax solution. T4 refers to the sample solution treated at 530 °C for 24 h, A200 refers to the sample aged at 200 °C, and finally, A245 refers to the sample aged at 245 °C. Reproduced from [110].

T6-14h (peak-aged) alloy showed a more uniform distribution of the precipitates which formed a corrosion barrier and improved the corrosion resistance (Fig. 28).

According to [109], the aging treatment of the Mg-2.78Y-1.43Nd-0.43Gd-0.41Dy (WE32) and Mg-3.05Y-1.81Nd-0.50Gd-0.43Dy (WE33) alloys at 200 °C for 45 h remarkably decreased the corrosion rate. This improved corrosion behavior of the aged alloys was mainly attributed to the formation of a very noticeable passive layer, as a result of a sufficient amount of micro-galvanic couples between the α-Mg and precipitates at short distances. The results indicate that the T6-treated alloys corroded the least among the other mentioned conditions. In conclusion, the corrosion resistance of the Mg-Y alloys would be determined by the accelerated micro-galvanic corrosion by the precipitates or barrier effect of the Y-containing passive film and this can be significantly modified with heat treatment.

The Mg-Nd system is another biodegradable Mg-RE alloy, and it is demonstrated that aging treatment can remarkably influence its properties. Due to the low solid solubility of Nd in Mg (3.6 wt% at 549 °C), there are few investigations on the corrosion behavior of aged biodegradable Mg-Nd alloys. The distribution, volume fraction, and morphology of the precipitates significantly affect the corrosion behavior. It has been reported [110] that after the solution treatment of the Mg-5Nd alloy (at 530 °C for 24 h), some intermetallic compounds ($Mg_{41}Nd_5$) remained and failed to dissolve with these compounds distributed mainly at the grain bound-

Table 3
Effect of different heat treatments on the corrosion behavior of the biodegradable Mg-rare earth alloys in summary

Composition	Condition	Corrosion medium	Containing phases	Best corrosion resistance	Remarks	Reference
Mg-15Gd-5Zn	As-cast, T4 & T6	3.5% NaCl	Mg_5Gd LPSO	T6: aging at 450 °C for 10 h	Reduction of corrosion rate due to the covering whole of the Mg matrix grains by the LPSO structure, and also playing the role of anode against the W-phase cathode by the LPSO structure, formed during the T6 treatment	[95]
Mg-2Gd-1Ag	As-cast & T4	DMEM+ 10% FBS	-	At 510 °C for 48 h	Lower micro galvanic corrosion rate by the dissolution of the intermetallic phases by the T4 treatment	[111]
Mg-5Gd-1Zn-0.6Zr	As-cast & T6	SBF	LPSO	As-cast	The superior corrosion resistance of the as-cast alloy with the LPSO structure by playing a corrosion barrier role between the eutectic phase and substrate, enhancing the passivation ability of the substrate	[75]
Mg-5Gd	As-cast & T4	Aerated simulated physiological solution	Mg_5Gd	As-cast	More micro-galvanic corrosion after the T4 treatment due to the formation of the Mg_5Gd particles, and also decrease of the Gd-content in the surrounding α-Mg	[76]
Mg-15Gd-2Zn-0.39Zr	As-cast, T4 & T6	3.5% NaCl	LPSO $(Mg, Zn)_3Gd$	T6: aging at 200 °C for 300 h	Reduction in the micro-galvanic corrosion due to the decrement of the local potential difference and the volume fraction of the secondary phase by forming the LPSO structure during the T4 and T6 heat treatments	[100]
Mg-10Gd-1Eu-1Zn-0.2Zr	As-cast, T4 & T6	1% NaCl	-	T6: aging at 250 °C for 6 h	Improving the corrosion resistance by enhanced passivation ability of the alloy by the T6 treatment	[112]
Mg-6.0Gd-1.2Cu-1.2Zr	As-cast & T4	SBF	LPSO	At 360 °C for 12 h	The beneficial effect of the LPSO structure by acting as a corrosion barrier and reducing the micro-galvanic corrosion in the T4 condition	[99]
Mg-10Gd-1.2Ca-0.5Zr	As-cast, T4, & T6	DMEM+ 10% FBS	Mg_5Gd	T4 at 495 °C for 16 h	Boosting the passivation film by the Gd in the supersaturated state, and dissolution of the secondary phases by the T4 treatment, leading to a lower corrosion rate	[77]
Mg-4Y-1Ag	As-cast & T4	DMEM+ 10% FBS	$Mg_{24}Y_5$	T4 at 525 °C for 3 h	Lower galvanic corrosion by reducing the volume fraction of the coarse $Mg_{24}Y_5$ phase and increasing the homogeneity of the microstructure during the T4 treatment	[81]
Mg-3.05Y-1.81Nd-0.50Gd-0.43Dy	As-extruded, T4 & T6	Ringer's acetate solution	Mg_5(Gd, Y, Dy, Nd)	T6: Aging at 200 °C for 48 h	Forming a pronounced Y-containing passive film during the T6 treatment	[109]
Mg-5Y-1.5Nd	As-cast, T4 & T6	3.5% NaCl	Mg_3(Y, Nd) Mg_{12}(Y, Nd)	At 535 °C for 20 h	Formation of a single-phase microstructure and thus, reduced micro-galvanic corrosion by the T4 treatment	[83]
Mg-2Y-1Zn-0.4Zr-0.3Sr	As-cast, T4 & as-extruded	SBF	$Mg_3Y_2Zn_3$ (W-phase)	At 500 °C for 25 h	Corrosion resistance was improved as a result of the dissolution of the secondary phases and distribution of Y in matrix, resulting in an improved protective nature of the corrosion film by the T4 treatment	[104]

(*continued on next page*)

Table 3 (*continued*)

Composition	Condition	Corrosion medium	Containing phases	Best corrosion resistance	Remarks	Reference
Mg-15Y	As-cast & T4	3.5% NaCl	$Mg_{24}Y_5$	At 340 °C for 18 h	Dissolution of the $Mg_{24}Y_5$ precipitates, resulting in lower micro-galvanic corrosion and enhanced corrosion film protection with the presence of Y during the T4 treatment	[102]
Mg-Y-2.1Nd-0.9Ag	As-cast & T4	Ringer-Lactate	-	At 525 °C for 24 h	Improvement of the corrosion resistance due to the formation of the corrosion products in the form of a passive layer (Y_2O_3) in the T4-treated samples	[103]
Mg-4Y-0.6Ca-0.4Zr	As-cast & T4	DMEM+ 10% FBS	Y-rich intermetallic particle	-	Unaffected corrosion rate due to a compromise between the dissolution of the secondary phases (reducing micro-galvanic corrosion) and increasing the grain size (retarding the passivation kinetics)	[113]
Mg-4Nd	As-cast & T4	Aerated simulated physiological solution	$Mg_{12}Nd$	At 520 °C for 20 h	Reduction of the eutectic $Mg_{12}Nd$ phase by the T4-treatment, which gives a lower galvanic corrosion	[76]
Mg-2.25Nd-0.11Zn-0.43Zr	As-extruded & T4	SBF	$Mg_{12}Nd$	At 540 °C for 12 h	A balance between the positive effect of the dissolution of the secondary phase and the negative impact of the grain growth can be achieved by the T4 treatment at 540 °C	[114]
Mg-2.7Nd-0.2Zn-0.4Zr	As-extruded & T4	SBF	-	At 475 °C for 1 h	A compromise between the grain size and the volume fraction of the secondary phase during the T4 treatment at 475 °C, leading to a minimum corrosion rate	[107]
Mg-2.5Nd-0.3Zn-0.1Sr-0.4Zr	As-cast & T4	SBF	$Mg_{41}Nd_5$	As-cast	Deterioration of the corrosion resistance mainly by the grain growth, discontinuous intermetallic phase and precipitates during the T4 treatment	[93]
Mg-5Nd	T4 & T6	DMEM+ Glutamax+ 10% FBS	$Mg_{12}Nd$ $Mg_{41}Nd_5$	T6: at 530 °C for 24 h with subsequent aging at 245 °C for 528 h	Corrosion resistance improvement by the nano-scale precipitations formed during the T6 treatment due to their dense and uniform distribution, resisting the corrosion propagation	[110]

aries. With subsequent aging at 200 °C, new fine precipitates ($Mg_{12}Nd$) were formed both at the grain boundaries and inside the grains, shown in Figs. 33c and d. With increasing the aging temperature to 245 °C, fine $Mg_{41}Nd_5$ precipitates formed, while the number of the $Mg_{12}Nd$ particles was reduced. Accordingly, the large $Mg_{41}Nd_5$ particles (at the grain boundaries), fine $Mg_{41}Nd_5$ precipitates, and possibly some $Mg_{12}Nd$ precipitates were present in the microstructure of the Mg-5Nd alloy aged at 245 °C. The microstructure of the Mg-5Nd alloy after different heat treatment conditions mentioned above is shown in Fig. 29 (a-d). The effects of such microstructural differences would be reflected in the corrosion resistance of the alloys, as shown in Fig. 30. In this figure, the corrosion surfaces of the Mg-5Nd alloy in the T4, T6-200 °C (A200), and T6-245 °C (A245) conditions are shown after immersion in the DMEM + Glutamax + 10% FBS solution for three different numbers of days (1, 7, and 14). The SEM images indicated that the thickness of the corrosion layer was the thickest for the T4-treated alloy. This is in accordance with the corrosion results, which showed that the lowest corrosion resistance among the studied heat treatments was achieved for the sample heat-treated by the T4 treatment where the microstructure contained no nano-sized particles. By contrast, the corrosion layer of the T6-treated alloy with nano-sized $Mg_{12}Nd$ precipitations was much thinner, thereby implying exceptional corrosion resistance. Fine nano-scale precipitates formed during the aging treatment and no corrosion products were observed around them at the initial stage of corrosion indicating that no corrosion occurred inside the grains. However, they played an essential role in the propagation of the corrosion. Thus, fine nano-scale precipitates enhanced the corrosion resistance due to their

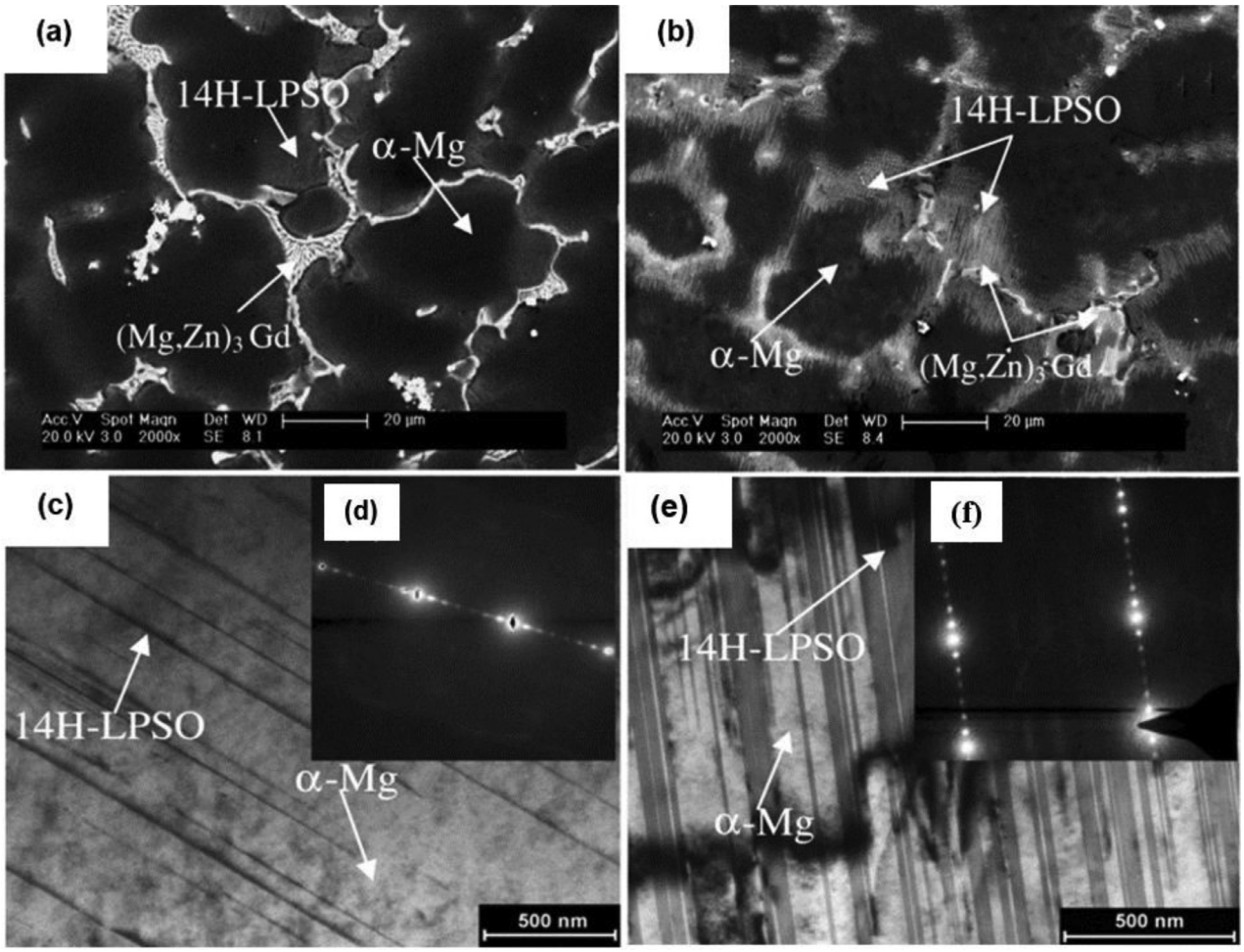

Fig. 31. Microstructure of the Mg-11Gd-1Zn alloy, showing the morphology of the precipitates and the LPSO structures: (a) SEM image of the as-cast specimen, (b) SEM image of the annealed specimen, (c,d) TEM image and the corresponding SAED pattern of the as-cast alloy, and (e,f) TEM image and the corresponding SAED pattern of the as-annealed alloy. Reproduced from [117].

dense and homogenous distribution that resisted the corrosion propagation.

Table 3 summarizes the effects of different heat treatments on the corrosion behavior of the biodegradable Mg-RE alloys. In this table, the chemical composition of the studied alloy, the processing condition, the corrosion media, Mg-Nd phases, the condition to achieve the best corrosion resistance, and some remarks are presented in columns 1-6, respectively, and finally the corresponding references are given in the last column.

5.2. Mechanical behavior

5.2.1. The mechanical behavior of the Mg-rare earth alloys after a T4 heat treatment

A T4 treatment can remarkably modify the mechanical behavior of biodegradable Mg-RE alloys. According to the phase diagram of the Mg-Gd alloying system, by proper heat treatment and subsequent quenching, a single-phase solid solution can be formed [43]. In this state, solid solution strengthening is the main strengthening mechanism in Mg-Gd alloys due to the notable atomic size difference between the Gd and Mg atoms (12.5%) which generates a strong lattice distortion [115].

Grain growth can considerably deteriorate the mechanical properties of the solution-treated alloys. The Mg-Gd alloys with more content of alloying elements experience less grain growth [116]. In this respect, it was reported [96] that the addition of La and Nd to the Mg-Gd alloys restricted the grain boundary mobility and hence decreased the grain growth rate. In addition, La and Nd caused the formation of some precipitates which did not dissolve completely during the solution treatment and thus could improve the mechanical strength of the solution-treated alloy. In this study, the weakest alloy from the viewpoint of the mechanical properties was the binary Mg-10Gd alloy which suffered from significant grain growth and also the dissolution of the Mg-Gd precipitates, while the quaternary Mg-10Gd-1Nd-1La alloy possessed the highest hardness after the solution treatment.

As discussed earlier, the LPSO structure may be formed while the precipitates tend to be dissolved during the solution treatment. For example, solution treatment of the Mg-11Gd-1Zn alloy at 500 °C for 8 h increased the amount of the LPSO structure and decreased the volume fraction of the

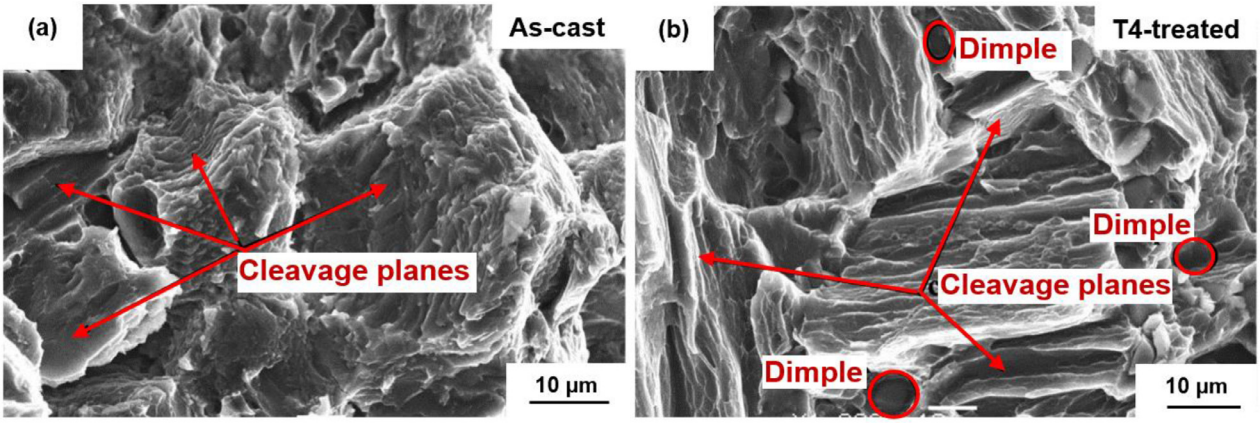

Fig. 32. The fracture surfaces of the biodegradable Mg-2.5Nd-0.3Zn-0.1Sr-0.4Zr alloy in the: (a) as-cast condition, and (b) T4condition. Reproduced from [93].

secondary phases (Fig. 31) [117]. Tensile testing revealed a significant increase in the yield strength and ultimate tensile strength after such solution treatment. This study achieved 103 MPa and 22 MPa enhancement in UTS and YS of the as-cast alloy, respectively, by the T4 treatment. In another study [118], extruding the Mg-5Gd-1Zn-0.6Zr alloy after the solution treatment generated the LPSO structure in the microstructure and improved the mechanical strength. This improvement is related to the interaction of dislocations with the LPSO structure and also the grain refinement achieved during the extrusion process.

As well as Mg-Gd alloys, the mechanical properties of the T4-treated Mg-Y alloys can be altered greatly by the T4 treatment. A dissolution of the secondary phases because of the high solid solubility of Y in Mg, a reduction of the dislocation density due to the recovery processes and grain growth phenomenon are three important processes during the T4 treatment at elevated temperatures which significantly affect the mechanical properties [119]. It has been reported [113] that the dissolution of the secondary phases and the larger grain size of the solution-treated biodegradable Mg-4Y-0.6Ca-0.4Zr alloy reduce the compressive strength and also ductility of this alloy. In another study [120], a significantly reduced mechanical strength of the solution-treated WE32 alloy (at 525 °C for 8 h) was attributed to the dissolution of the majority of the intermetallic compounds and an increase in the grain size from 15 μm to 102 μm.

In the Mg-Nd system, the T4 treatment of the as-cast Mg-4Nd alloy led to some softening due to the dissolution of the hard eutectic $Mg_{12}Nd$ phase in the Mg matrix [76]. The weak solid solution strengthening effect was attributed to the low solid solubility of Nd in Mg in this alloy. In another study, it was reported [107] that the solution treatment at 500 °C for 1 h reduced the yield strength of the as-extruded Mg-2.7Nd-0.2Zn-0.4Zr alloy from 291 MPa to 163 MPa due to the growth of the grains and also a reduction of the volume fraction of the secondary phases. On the contrary, the solution treatment remarkably improved the yield strength and ultimate tensile strength of an as-cast Mg-2.5Nd-0.3Zn-0.1Sr-0.4Zr alloy [93]. In this case, enhancement of the mechanical properties was mainly attributed to the positive effect of the solution strengthening effect which overcame the negative impact of the grain growth. In another investigation [121], a T4 treatment of the as-cast Mg-1.59Nd-2.91Zn-0.05Zr-0.35Mn alloy increased the UTS value from 169 MPa to 230 MPa. After the solution treatment, the network eutectic compounds were dissolved partially and a discontinuous pattern of the particles was formed. Such a discontinuous pattern of the eutectic compounds could improve the mechanical properties. In another investigation [122], the eutectic phase with coarse morphology in the as-cast Mg-2.49Nd-1.82Gd-0.19Zn-0.4Zr alloy induced local stress concentrations and this led to weaker mechanical properties. In this case, the solution treatment reduced the eutectic phases and thus the stress concentrations which substantially enhanced the UTS.

In addition to strength, the ductility of the as-cast biodegradable Mg-Nd alloys can also be improved by a solution treatment. In this regard, numerous dimples were observed on the fracture surface of the T4-treated biodegradable Mg-2.5Nd-0.3Zn-0.1Sr-0.4Zr alloy which indicates a ductile mode of fraction in this condition. On the other hand, the as-cast alloy presented a cleavage fracture (Fig. 32) [93]. According to [121], the solution treatment decreased the volume fraction of the eutectic phase. A reduction of the hard and brittle eutectic compounds, which can act as crack sources during the plastic deformation, enhanced the elongation by 63% compared to the as-cast alloy.

5.2.2. The mechanical behavior of the Mg-rare earth alloys after a T6 heat treatment

The aging behavior of the biodegradable Mg-RE alloys has been widely studied. In the Mg-Gd system, the maximum solubility of the Gd element in Mg is 23.49 wt% at 548 °C, which significantly reduces to 3.82 wt% at 200 °C, thereby implying a significant aging response. According to some reports [123], the addition of alloying elements to the Mg-Gd alloys can enhance the aging response, resulting in a greater hardness. For example, adding 1% Zn to the Mg-10Gd-3Y-0.5Zr alloy was reported to improve the mechanical

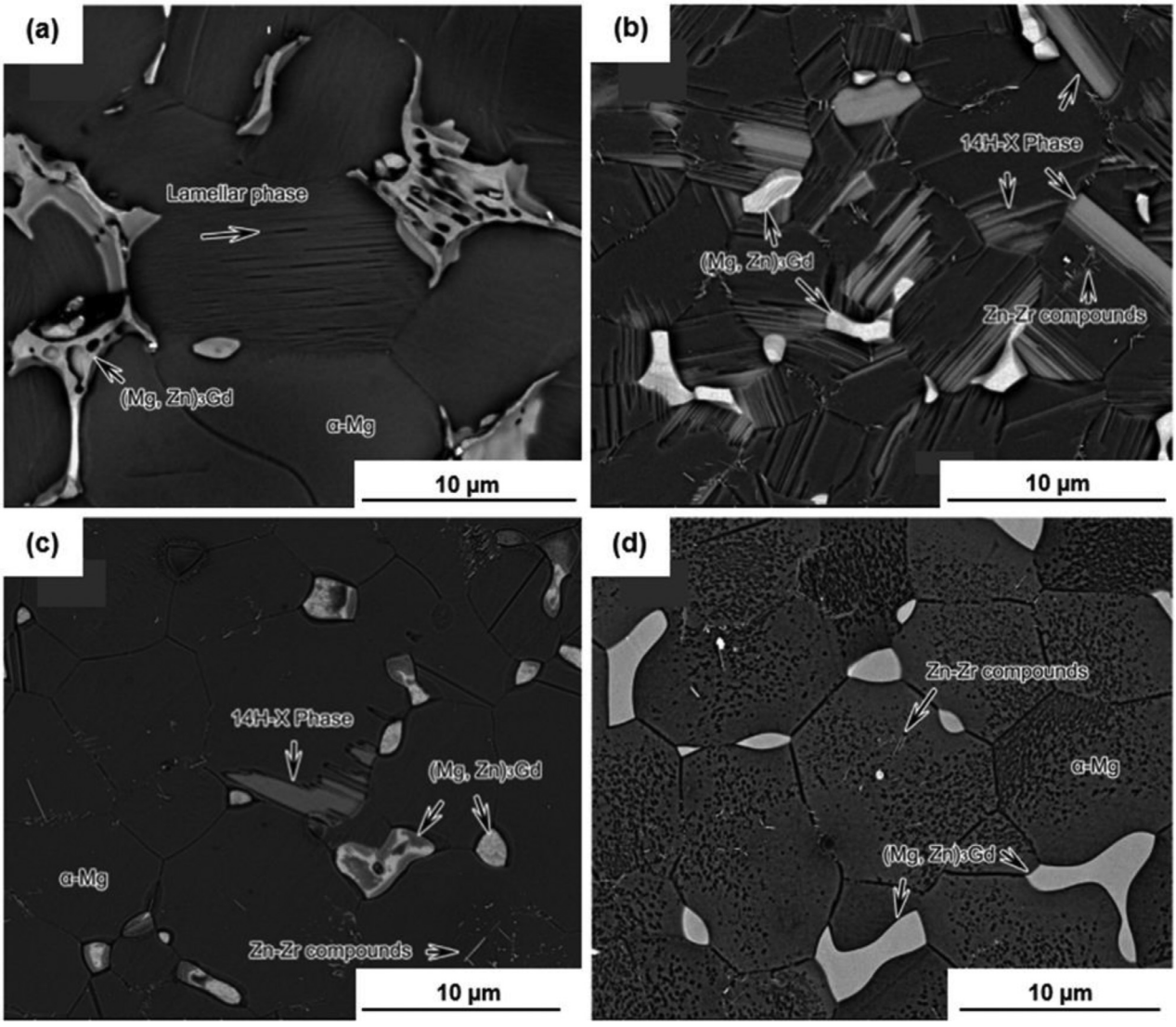

Fig. 33. SEM backscattered electron images of the Mg-14.33Gd-2.09Zn-0.51Zr alloy in the as-cast (a), T4-treated at 480 °C for 12 h (b), T4-treated at 500 °C for 10 h (c), and T4-treated at 520 °C for 12 h (d) conditions. Reproduced from [125].

properties of the aged alloy due to the larger number of precipitates by the addition of Zn.

The precipitation sequence of the Mg-Gd-RE alloys has been described as the decomposition of the α-Mg supersaturated solid solution $\rightarrow$ $\beta''(D0_{19})$ $\rightarrow$ β' (cbco) $\rightarrow$ β_1 (fcc)$\rightarrow$ β (fcc). The precipitation strengthening in the peak-aged alloys is mainly attributed to the β' phase due to the significant resistance of these precipitates to the shearing forces exerted by the dislocations [77,115]. According to [115], the addition of 1.8 wt% Ag to the Mg-9.8Gd-2.7Y-0.4Zr alloy refined the β' precipitates and increased the density of the nano-scale plate-like precipitates, resulting in improvements in the mechanical strength.

In addition to affecting the corrosion properties, the LPSO structure also plays an important role in strengthening the aged Mg-Gd and Mg-Gd-RE alloys. In this regard, there is a comparison of the mechanical properties of the as-cast, as-extruded, T4-treated, T5-treated, and T6-treated Mg-11Gd-1Zn alloy [59]. The 14H-LPSO plates and the β' precipitates exist in the T6-treated alloy and the volume fraction of the LPSO structure was the highest compared to the other mentioned conditions resulting in a higher strength and ductility for the T6-treated alloy. In another study [124], the LPSO structure in the T6-treated Mg-10Gd-3Y-1.2Zn-0.5Zr alloy behaved as a barrier for crack propagation and also plastic deformation, leading to superior shear properties. The mechanical properties of the T6-treated Mg-Gd-RE alloys strongly depend on two main factors: (1) the strengthening effect of the LPSO structure, and (2) a reduction in the precipitation strengthening effect due to consumption of the solute content by the formation of the LPSO structure. Depending on how much each factor is dominant, the overall effect of the LPSO structure on the mechanical properties of the T6-treated alloy would be determined. It was reported [125] that different

temperatures of the solid solution heat treatment lead to a significant difference in the volume fractions of the LPSO structure and secondary phase of an Mg-14.33Gd-2.09Zn-0.51Zr alloy. Fig. 33 demonstrates the microstructure of this alloy at different solution temperatures with different amounts of the LPSO structure and the secondary phase. In this regard, a high solution temperature led to a lower amount of the LPSO structure and more solution content of the Gd and Zn atoms in the supersaturated state, resulting in a more significant aging response. In this investigation, the presence of Gd and Zn atoms as precipitates led to a better strengthening effect than in the form of the LPSO structure. Therefore, the solution-treated alloy at 520 °C (the highest solution temperature) for 12 h with a subsequent aging at 200 °C for 64 h exhibited the best mechanical strength.

Similarly, the mechanical properties of the Mg-Y alloys can also be widely adjusted by proper aging treatment for biomedical applications as well. The success in strengthening by the aging treatment is strongly dependent on the ability of the precipitates in hindering the movement of dislocations. In this regard, the number density, distribution, size, and nature of the precipitates would also affect the mechanical properties of the T6-treated alloys [126].

The β′ phase is known to be one of the most effective precipitates in Mg-RE alloys from the viewpoint of strengthening. It has been reported [127] that the β′ and β" phases formed during the T6 treatment of the Mg-4Y-3Nd-1Gd-0.2Zn-0.5Zr alloy at 250 °C for 10 h were coherent with the α-Mg and generated a strong stress field. A high density with high volume fraction of the fine β′ and β" precipitates in the T6-treated alloy resulted in a beneficial combination of strength and ductility (YS of 198 MPa, UTS of 276 MPa, and 7.6% elongation at failure). In another study [126], the β′ and β" phases in the peak-aged condition of the T6-treated Mg-3.2Y-2.5Nd-0.5Zr alloy (aged at 225 °C) increased the YS from 135 MPa in the as-cast alloy to 202 MPa. In this investigation, increasing the aging temperature to 250 °C led to a decrease in the volume fraction and number density of the fine β′ phase, leading to a decrease in strength by comparison with the alloy aged at 225 °C.

Grain growth during the aging treatment has also been reported to decrease the ductility of the Mg-Y alloys as larger grains are not capable of effectively coordinating the plastic deformation [119]. According to [120], despite a hardness and tensile yield strength improvement in the Mg-2.78Y-1.49Nd-0.43Gd-0.4Dy (WE43) alloy by the T6 treatment, the ductility decreased by 80% compared to the primary extruded alloy due to the effect of grain growth.

Besides the Mg-Gd and Mg-Y systems, it has been pointed out that a T6 treatment has a pronounced impact on the mechanical strength of Mg-Nd alloys. In these alloys, the precipitation sequence in the T6-treated Mg-Nd alloys follows the route (SSS) $\rightarrow$ β'' (Mg_3Nd) $\rightarrow$ β' (Mg_7Nd) $\rightarrow$ β ($Mg_{12}Nd$) [128]. The β'' precipitates form at the early stages of the aging process and with an increment of time/temperature of the aging treatment the β' phase forms as the expense of the β'' phase. It was reported [122] that the precipitation of the β'' and β' particles within the α-Mg matrix during the aging treatment was capable of impeding dislocation slip. The dense β' phase had a greater strengthening effect on the dislocation glide as compared to the β'' phase. In this investigation, the aging treatment (at 205 °C for 18 h) of the as-cast Mg-2.49Nd-1.82Gd-0.19Zn-0.4Zr alloy significantly improved the UTS from 184 MPa to 287 MPa. In another study [129], the precipitation of the fine nano-scale β'' phase at the peak-aged condition (at 200 °C for 12 h) of the Mg-2.7Nd-0.6Zn-0.5Zr alloy profoundly enhanced the mechanical properties. The strengthening by the β'' phase increased the UTS and YS by 110 MPa and 83 MPa, respectively, where a 1.4% improvement in ductility was also obtained.

Table 4 is presented for an easier understanding of the effects of different heat treatments on the mechanical properties of the biodegradable Mg-RE alloys. In this table, the chemical composition of the alloy, the processing condition, the time and temperature of the best heat treatment condition, the mechanical properties of heat-treated alloys (yield strength, ultimate tensile strength, and elongation) and some remarks are presented in columns 1-7, respectively, and finally the corresponding references are given in the last column.

6. The effects of heat treatment on the Mg-Al alloys

6.1. The corrosion behavior

6.1.1. The corrosion behavior of the Mg-Al alloys in the as-cast condition

The application of aluminum (Al) as an abundant element in the earth's crust and the biological system is widespread. Unique features of Al have made it one of the promising candidates in the biomedical applications [131–135]. The neurotoxicity and associated diseases (Alzheimer's and dementia) have been reported as side effects of Al usage in the human body [132]. However, these side effects could be avoided by exactly controlling the Al concentration [136]. The human body uses 9-14 mg of Al daily and indeed it is widely used as an antacid [132,137]. In this part, the modification of the biodegradable Mg-Al alloys by heat treatment will be discussed.

The general microstructure of the as-cast biodegradable Mg-Al alloys is commonly composed of three constituents: the α-Mg phase, the β-$Mg_{17}Al_{12}$ phase and the eutectic structure (alternating layers of α and β phases) [133]. The β-$Mg_{17}Al_{12}$ phase has been shown to be a very critical and determining factor in controlling the corrosion performance of the biodegradable Mg-Al alloys. The concentration of Al in the β-$Mg_{17}Al_{12}$ phase is much more by comparison with the α-Mg phase, which makes the β-$Mg_{17}Al_{12}$ phase a robust cathode to cause micro-galvanic corrosion [134]. According to [138], the difference in Al concentration between the α-Mg and β-$Mg_{17}Al_{12}$ phases was measured as around 31% in an Mg-9.1Al-0.17Mn-0.04Zn (AZ91D) alloy, and this resulted in severe micro-galvanic corrosion. It was also observed that the corrosion was mainly initiated in the α-Mg grains with less than 8% Al content. The β-$Mg_{17}Al_{12}$ phase, like the LPSO

Table 4
Effects of different heat treatments on the mechanical properties of the biodegradable Mg-rare earth alloys in summary

Composition	Condition	Time & temperature of heat treatment	Mechanical properties			Remarks	Reference
			YS (MPa)	UTS (MPa)	Elongation (%)		
Mg-8.5Gd-2.3Y-1.8Ag-0.4Zr	As-cast, T4 & T6	Aging at 200 °C for 32 h	268	403	4.2	Mechanical enhancement by the precipitation strengthening by the β' phase and the plate-like precipitate, formed during the T6 treatment	[115]
Mg-10Gd-3Y-1.0Zn-0.5Zr	As-cast & T6	Aging at 225 °C	253	364	2	Significant aging response with the addition of 1% Zn	[123]
Mg-11Gd-1Zn	As-cast & T6	Aging at 250 °C	235	416	7.2	Superior mechanical properties of the T6-treated alloy due to the higher volume fraction of the 14H-LPSO phase	[117]
Mg-14.33Gd-2.09Zn-0.51Zr	As-cast & T6	Aging at 200 °C for 64 h	291.7	404.7	5.3	Higher solution temperature led to a higher amount of the precipitates and lower amount of the LPSO structure, and the best mechanical properties by the T6 treatment	[125]
Mg-10Gd	As-cast & T4	At 525 °C for 24 h	81.47	222.7	-	Dissolution of the precipitates and grain growth were mainly responsible for the observed softening after the T4 treatment	[130]
Mg-10Gd-1.2Ca-0.5Zr	As-cast & T6	Aging at 200 °C for 72 h	217.4	282.7	0.7	Significant resistance to dislocation motion provided by the β' precipitates led to a mechanical strength improvement in the T6-treated alloy	[77]
Mg-9.02Y-2.95MM-0.58Z	As-extruded & T6	At 490 °C for 2 h with subsequent aging at 200 °C	325	364	3	Mechanical strength improvement due to hindrance effect of the β' phase formed during the T6 treatment and elongation decrement due to the grain growth	[119]
Mg-3Y-1.5Nd-0.4Gd-0.4Dy	As-cast & T6	At 525 °C for 8 h with subsequent aging at 250 °C for 8 h	133	235	15.4	Hindrance of dislocation slip by the presence of precipitates in the T6-treated alloy	[120]
Mg-3.5Y-2.5Nd-0.5Zr	As-cast & T6	At 525 °C for 4 h with subsequent aging at 225 °C for 34 h	202	301	6.9	Excellent mechanical strength due to precipitate strengthening by the β' and β" phases in the T6-treated alloy	[126]
Mg-4Y-3Nd-1Gd-0.2Zn-0.5Zr	As-cast & T6	At 525 °C for 6 h with subsequent aging at 250 °C for 10 h	198	276	7.6	A desirable combination of strength and ductility due to the high density and strong stress field of the β' and β" phases in the T6 condition	[127]
Mg-2.7Nd-0.2Zn-0.4Zr	As-cast & T4	At 500 °C for 1 h	163	287	25.1	Reduction of the mechanical strength by the T4 treatment due to grain growth and reduction of the secondary phase	[107]
Mg-1.59Nd-2.91Zn-0.05Zr-0.35Mn	As-cast & T4	At 480 °C for 10 h	103	230	20.5	Enhancement of the mechanical properties by the discontinuous eutectic compounds behaving like reinforcement phases, formed during the T4 treatment	[121]
Mg-2.49Nd-1.82Gd-0.19Zn-0.4Zr	As-cast & T6	At 515 °C for 18 h with subsequent aging at 205 °C for 18 h	206	287	4.5	Mechanical strength enhancement due to the impeding effect of the β'' and β' precipitates within the α-Mg matrix which formed during the T6 treatment	[122]
Mg-2.49Nd-1.82Gd-0.19Zn-0.4Zr	As-cast & T4	At 515 °C for 18 h	123	248	11	Decreased stress concentration as a result of dissolution of the eutectic phase during the T4 treatment, leading to mechanical properties enhancement, especially ductility improvement	[122]

(continued on next page)

Table 4 (*continued*)

Composition	Condition	Time & temperature of heat treatment	Mechanical properties			Remarks	Reference
			YS (MPa)	UTS (MPa)	Elongation (%)		
Mg-4Nd	As-cast & T4	At 520 °C for 20 h	-	-	-	Deterioration of the mechanical strength by the solution treatment due to the dissolution of the hard eutectic $Mg_{12}Nd$ phase in the Mg matrix	[76]
Mg-2.7Nd-0.6Zn-0.5Zr	As-cast & T6	At 525 °C for 12 h with subsequent aging at 200 °C for 12 h	191	258	4.2	Precipitation strengthening by the precipitation of fine nano-scale β'' phase at the peak-aged condition	[129]
Mg-2.5Nd-0.3Zn-0.1Sr-0.4Zr	As-cast & T4	At 545 °C for 12 h	-	-	-	Mechanical properties improvement due to the more pronounced positive effect of the solution strengthening by comparison with the negative impact of grain growth during the T4 treatment	[93]

structure discussed previously in the section on Mg-Gd, plays a dual role in the corrosion behavior of the Mg-Al alloys. This phase can act as a corrosion barrier and inhibit the corrosion propagation, while it can also act as a cathode and accelerate the micro-galvanic corrosion. The volume fraction and distribution of the β-$Mg_{17}Al_{12}$ phase are two important parameters in determining its role in the corrosion process. In this regard, heat treatment can modify the distribution, volume fraction, size and configuration of the β-$Mg_{17}Al_{12}$ phase and thus, enhance the corrosion resistance.

6.1.2. The corrosion behavior of the Mg-Al alloys after a T4 heat treatment

The solid solution heat treatment would homogenize the distribution of the alloying elements, create supersaturated solid solutions, and decrease the volume fraction of the secondary phases (the β-$Mg_{17}Al_{12}$ phase in particular). However, according to the time/temperature of the solution treatment, some undissolved Al-rich phases may continue to remain in the microstructure [134,139].

The nature of the corrosion film in the solution-treated Mg-Al alloys is relatively weak and would fail during the corrosion process [133,135]. In this regard, it has been reported [134] that the corrosion film was mainly formed on the α-Mg grains with high Al concentrations in a solution-treated AZ91D alloy (at 445 °C for 24 h). Accordingly, the corrosion rate was the lowest in the initial stages of corrosion, and prolonging the exposure time led to the breakdown of the weak corrosion film. Thus, the corrosion rate was significantly increased, where the variations of the corrosion rate with the immersion time are shown in Fig. 34a. Failure of the corrosion film and thus deterioration of the corrosion resistance was related to the accelerated corrosion due to the localized corrosion of the residual β-$Mg_{17}Al_{12}$ particles. It was reported that the same behavior occurred in the Mg-5Al-1Zn-1Sn alloy solution treated at 400 °C for 20 h [102]. It was also reported there was increased corrosion resistance in the early stages of the immersion because of the uniform distribution of the alloying elements and the partial dissolution of the secondary phases. Again, at longer immersion times the breakdown of the oxide film and the local corrosion on the residual secondary phases notably increases the corrosion rate.

The amount of the lattice distortions and the grain size are other factors affecting the corrosion behavior of the solution-treated biodegradable Mg alloys. It was reported [140] that the distortion of the supersaturated α-Mg grains by the solution treatment (at 410 °C for 12 h) had an effect on decreasing the corrosion resistance of the Mg-8.6Al-0.85Zn (AZ91) alloy. In fact, in this investigation, the negative impact of distortion overcame the positive effect of the reduced micro-galvanic corrosion (due to the dissolution of the β-$Mg_{17}Al_{12}$ phase). In another study [141], the T4 treatment at 500 °C for 3 h reduced the density of the grain boundaries which could act as a physical barrier to corrosion, and this produced a deterioration of the corrosion resistance of the Mg-2.95Al-1.07Zn-0.39Mn (AZ31B) alloy. It was also reported [142] that the solution treatment of the AZ91 and Mg-2.75Al-0.91Zn (AZ31) alloys for 6 h at 410 °C and 340 °C, respectively, mitigated the galvanic corrosion and enhanced the corrosion resistance compared to the as-cast condition.

6.1.3. The corrosion behavior of the Mg-Al alloys after a T6 heat treatment

As discussed earlier, the volume fraction, size, and distribution of the β-$Mg_{17}Al_{12}$ precipitates significantly affect the corrosion behavior of the Mg-Al alloys. All of these parameters change during the T6 treatment. The microstructure of the biodegradable Mg-Al alloys would be more homogenous with the re-distribution of Al atoms and re-precipitation of the secondary phases during the aging treatment. By increasing the aging time, the distribution of the β-$Mg_{17}Al_{12}$ phase becomes more in the form of a continuous network. This continuity of the precipitations is highly dependent on the Al concentration such that the higher the Al content so the lower the aging times that are required to form a continuous distribution [139].

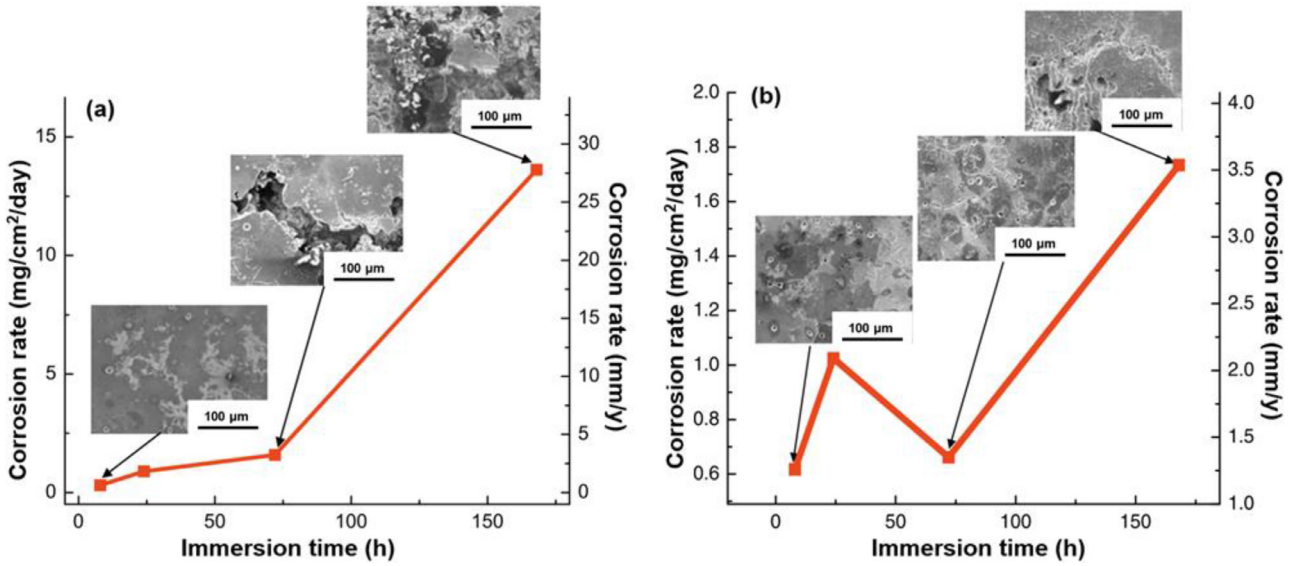

Fig. 34. The corrosion rate of the T4-treated (a) and T6-treated (b) AZ91D alloy, as a function of immersion time in the SBF solution. Reproduced from [134].

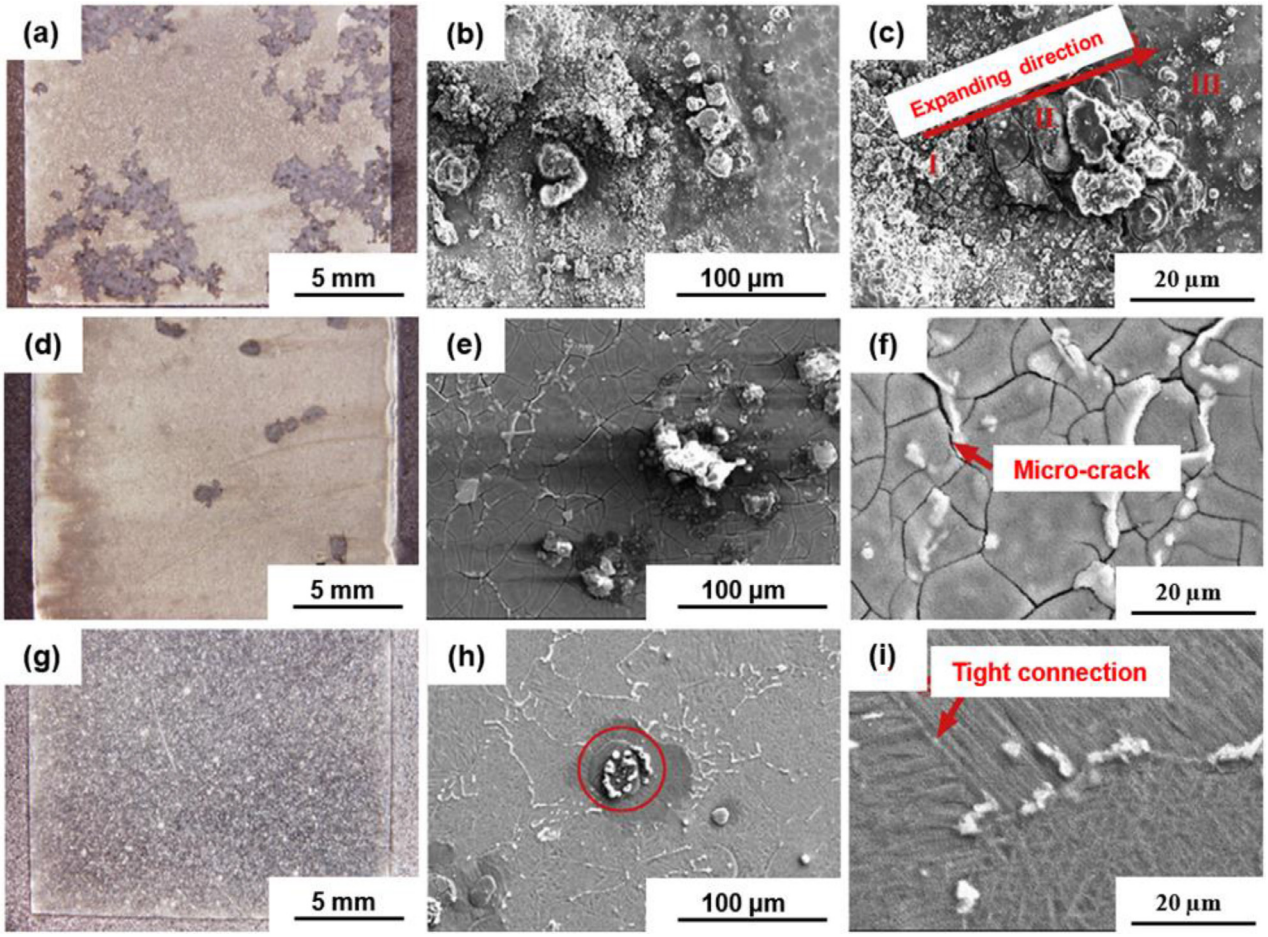

Fig. 35. The OM (a,d,g) and SEM (b,c,e,f,h,i) micrographs showing the corroded surfaces of the $Mg_{91.5}Al_{3.5}Gd_5$ (at%) alloy in the as-cast (a–c), T4 (d–f), and T6 (g–i) conditions. These micrographs were taken from the samples immersed for 12 h in the 1.0 wt% NaCl solution. Reproduced from [135].

The oxide film on the surface of the T6-treated Mg-Al alloys is reported to be more uniform and compact compared to the as-cast and T4 conditions due to the more homogenous microstructure with uniform distribution of Al and this leads to a higher corrosion resistance [133–135]. According to [133], a stable oxide film was formed on the aged AZ63 alloy and led to an increase in the free corrosion potential during immersion in SBF, demonstrating the influential barrier role of the oxide film. However, the micro-galvanic corrosion between the α-Mg and β-$Mg_{17}Al_{12}$ phases is inevitable, and the aged alloy is seriously susceptible to pitting corrosion. Due to the relatively small size of the β-$Mg_{17}Al_{12}$ precipitates, the cathode to anode surface area ratio (Eq. 1) is not sufficiently large to provoke severe corrosion damage [134]. Fig. 34b presents the corrosion extent of the T6-treated AZ91D alloy. Compared to the T4-treated alloy (Fig. 34a), the T6-treated alloy experienced minor corrosion attacks due to the tight film formation so that there are only a few shallow corrosion pits observed on this sample due to the weak micro-galvanic corrosion.

An interesting comparison of the corrosion behavior of an $Mg_{91.5}Al_{3.5}Gd_5$ (at%) alloy in the as-cast, T4-treated and T6-treated conditions was made in another investigation [135]. It was reported that in the as-cast state the extensive network area with inhomogeneous distribution resulted in severe pitting corrosion whereas micro-galvanic corrosion occurred in the vicinity of the secondary phases and spread from region I to region III (Fig. 35c). Diffusion of Al and Gd atoms from the secondary phases into the matrix during the T4 treatment (at 565 °C for 24 h) led to the formation of a dense oxide film. As a result of the T4 treatment, the grain boundaries developed a much more negative potential and thus the micro-galvanic corrosion between the matrix as the cathode and the grain boundaries as the anode increased the corrosion rate leading to micro-crack formation. Contrary to the solution-treated and as-cast conditions, the T6 treatment (subsequent aging of the T4-treated alloy at 300 °C for 20 h) caused the formation of a uniform and compact oxide film which covered the whole surface (Fig. 35). Fig. 36 depicts a schematic representation of the corrosion processes and the mechanisms in the as-cast, T4, and T6 conditions. It is worth noting that the self-remediation ability of the oxide film in the T6-treated alloy significantly boosts the barrier effect of the corrosion film. Thus, the oxide film becomes more compact and thicker with prolonged time, leading to the best corrosion performance among the studied conditions.

6.2. The mechanical behavior of the Mg-Al alloys after T4 and T6 heat treatments

The formation of the supersaturated solid solutions, the dissolution of the secondary phases and grain growth are three determining phenomena during the solution treatment that affect the mechanical properties of the biodegradable Mg-Al alloys. The final performance of the T4-treated alloy is determined according to which specific phenomenon dominates [140,142]. It has been reported [140] that the solution treatment of the AZ91 alloy resulted in a slight increase in hardness due to the solid solution strengthening effect which was more pronounced than the detrimental effects of the dissolution of the secondary phases and grain growth. In another study [142], the solution treatment decreased the amount of hard and brittle β-$Mg_{17}Al_{12}$ phase and increased the grain size of the AZ31 and AZ91 alloys, leading to lower hardness values by comparison with the as-cast condition.

According to [143], the morphology, distribution, and volume fraction of the newly formed β-$Mg_{17}Al_{12}$ phase from the supersaturated grains influence the mechanical properties of the T6-treated Mg-Al alloys. In this study, hardness increased as a function of the volume fraction of the β-$Mg_{17}Al_{12}$ phase. The β-$Mg_{17}Al_{12}$ phase is reported as an effective barrier against dislocation movement.

Although the mechanical properties of the heat-treated Mg-Al alloys have been extensively studied, this research is not fully related to the alloys used for biomedical applications. Thus, the mechanical properties of biodegradable Mg-Al alloys after T4 and T6 treatment have not been widely discussed and more investigations are needed to achieve a better understanding.

7. The effects of heat treatment on the Mg-Ag alloys

7.1. The corrosion behavior

7.1.1. The corrosion behavior of the Mg-Ag alloys in the as-cast condition

Implant-associated infections are serious obstacles in the healing process of a damaged tissue, which would cause a biofilm formation in the surgery site with subsequent failure of implantation [36,144,64,145]. In this regard, incorporation of an Ag element in biodegradable Mg alloys and the development of Mg-Ag implants seems to be a promising approach, since the well-established antibacterial activities of Ag can treat and hinder infections, leading to a facilitated healing process [146]. Also, addition of Ag can improve the mechanical properties of the Mg matrix by the formation of hard Ag-containing intermetallic phases. However, the dendritic microstructure, grain boundaries saturated with silver segregation and Ag-rich precipitates make the Mg-Ag alloys susceptible to micro-galvanic corrosion [147]. Therefore, their corrosion behavior requires further improvement.

7.1.2. The corrosion behavior of the Mg-Ag alloys after a T4 heat treatment

As discussed previously, the as-cast Mg-Ag alloys, with antibacterial activities, mostly suffer from severe galvanic corrosion between the α-Mg matrix and the Ag-rich precipitates. A volume fraction reduction of Ag-rich precipitates with the implementation of solution treatment would be an appropriate approach to tackle this problem and achieve the desired antibacterial and corrosion properties simultaneously. Bryla *et al.* [147] investigated the effect of T4 treatment (at

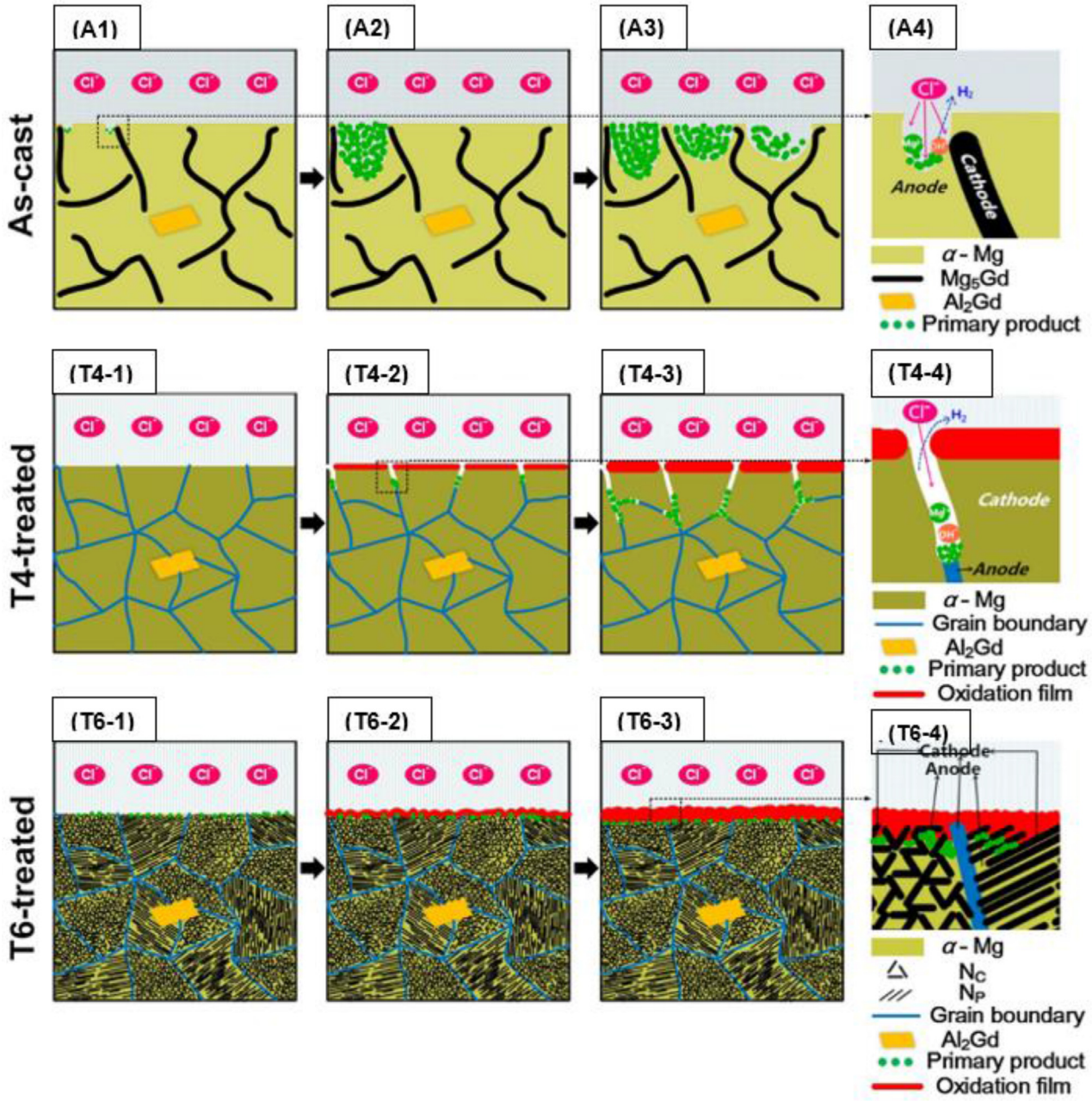

Fig. 36. Schematic illustration of the corrosion process in the as-cast (A1–A4), T4-treated (T4-1–T4-4), and T6-treated (T6-1–T6-4) $Mg_{91.5}Al_{3.5}Gd_5$ (at%) alloy. Reproduced from [135].

440 °C for 16 h) on the corrosion behavior of biodegradable Mg-4Ag alloy. They realized that the dissolution of $Mg_{54}Ag_{17}$ precipitates, as well as the homogenization of the dendritic structure, decreased the corrosion rate by mitigating galvanic corrosion. In another report [148], a uniform distribution of Ag-rich precipitates caused the formation of a dense and uninterrupted surface film after solution treatment and this would prevent the localized corrosion attack. In this study, the corrosion rate of the as-cast Mg-6Ag alloy decreased from 1.4 mm/year to 0.5 mm/year by the T4 treatment.

Liu *et al.* [36] investigated the effects of T4 treatment and extrusion on biodegradability of Mg-xAg (x = 6 and 8 wt%) alloys and the results are presented in Fig. 37. They realized that the existence of large $Mg_{54}Ag_{17}$ precipitates in the extruded alloys, as presented in the XRD pattern (Fig. 37k), induced micro-galvanic corrosion. On the other hand, this effect was prevented due to the elimination of secondary phases during solution treatment (at 430 °C for 16 h). The corrosion surface of the alloys after an immersion test are presented in Fig. 37a-j. Aggregated Ag, loose corrosion product and severe degradation are evident in extruded Mg-Ag alloys, while only cracks, which were formed by the dehydration of corrosion layer, are presented on the surface of pure Mg and T4-treated Mg-Ag alloys, indicating the positive role of the

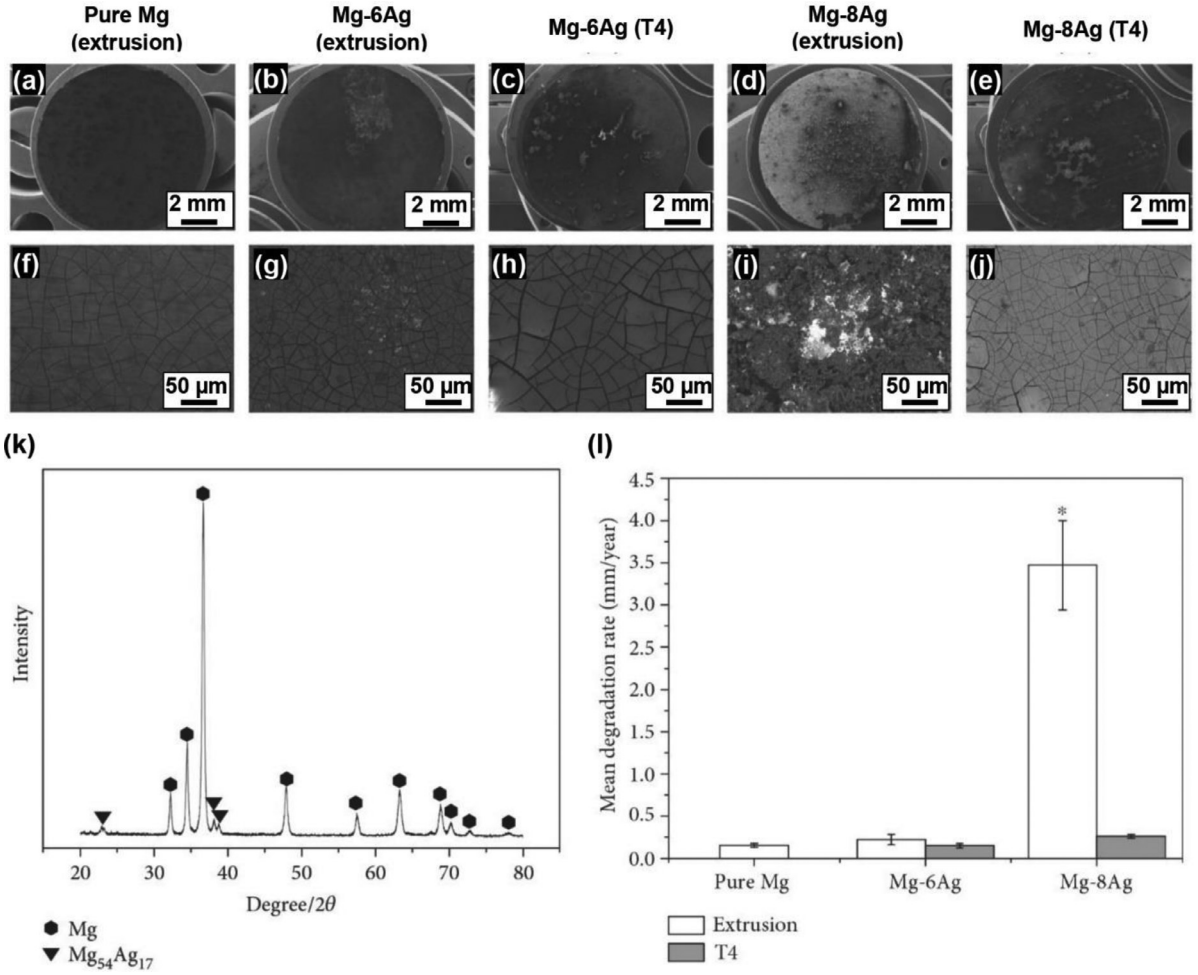

Fig. 37. Corroded surface of pure Mg and Mg-Ag alloys after immersion in cell culture medium (CCM) + DMEM + GlutaMAX + 10% FBS for 168 h: (a-e) low magnification and (f-j) higher magnification SEM micrographs. (k) XRD pattern of extruded Mg-8Ag alloy, and (l) the mean degradation rate of the studied alloys. Reproduced from [36].

heat treatment in promoting the corrosion behavior. The corrosion rates were 3.44 mm/year and lower than 0.5 mm/year for the extruded and T4-treated Mg-8Ag alloys, respectively (Fig. 37 l). Accordingly, it can be pointed out that an appropriate heat treatment is crucial for developing biodegradable Mg-Ag alloys.

Table 5 is presented to give better insight into the heat treatment effects on the corrosion behavior of the biodegradable Mg-Al and Mg-Ag alloys. In this table, the chemical composition of the alloy, the processing condition, the corrosion media, the secondary phases, the condition to achieve the best corrosion resistance and some remarks are presented in columns 1-6, respectively, and finally the corresponding references are given in the last column.

7.2. The mechanical behavior of the Mg-Ag alloys after T4 and T6 heat treatments

Considerable solid solution strengthening has been obtained in Mg-Ag alloys after a T4 treatment due to the high solid solubility of Ag in Mg (15.02 wt% at 472 °C). For instance, the generated solution strengthening by a T4 treatment of as-cast Mg-4Ag alloy caused 11% and 31% improvement in hardness and ultimate compressive strength, respectively [147]. In this report, the mechanical characteristics and corrosion behavior were significantly enhanced with the execution of solid solution heat treatment. It has been also reported [148] that the reprecipitation of the Mg_4Ag phase by an aging treatment of the Mg-6Ag alloy increased the hardness from 35.9 Hv for the as-cast alloy to 43.3 Hv.

8. Analyzing and interpreting results

This review has mainly concentrated on collecting and summarizing the results found in the literature describing the effect of the T4 and T6 heat treatments on the mechanical and corrosion properties of some important heat-treatable biodegradable Mg alloys, including the Mg-Zn, Mg-Gd, Mg-Y, Mg-Nd, Mg-Al and Mg-Ag systems. While there are many consistent aspects, it is now readily apparent that different alloying systems may respond very differently to similar heat treatments. Accordingly, it is shown that by precise control of

Table 5
The effects of different heat treatments on the corrosion behavior of the biodegradable Mg-Al and Mg-Ag alloys in summary

Composition	Condition	Corrosion media	Containing phases	Best corrosion resistance	Remarks	Reference
Mg-5.9Al-3.5Zn-0.18Mn	As-cast & T6	SBF	β-$Mg_{17}Al_{12}$	T6: at 413 °C for 24 h with subsequent aging at 216 °C for 12 h	Corrosion resistance improvement by the formation of tight corrosion film on the surface of the T6-treated sample, inhibiting the corrosion propagation	[133]
Mg-9.1Al-0.17Mn-0.04Zn	As-cast & T6	SBF	β-$Mg_{17}Al_{12}$	T6: at 445 °C for 24 h with subsequent aging at 200 °C for 16 h	Better corrosion resistance in the T6-treated alloy due to the more homogeneous distribution of the β-$Mg_{17}Al_{12}$ precipitates as well as the aluminum content	[134]
$Mg_{91.5}Al_{3.5}Gd_5$ (at%)	As-cast & T6	1 wt% NaCl	Mg_5Gd, $Mg_{12}ZnY$-type, and Al_2Gd	T6: at 565 °C for 24 h with subsequent aging at 300 °C for 20 h	Best corrosion resistance due to the formation of the uniform and compact oxide film, covering the whole surface in the T6-treated alloy	[135]
Mg-5Al-1Zn-1Sn	As-cast & T6	3.5 wt% NaCl	β-$Mg_{17}Al_{12}$ Al_8Mn_4Y	T6: at 400 °C for 20 h with subsequent aging at 260 °C for 4 h	Enhanced corrosion resistance due to the small corrosion driving force in each pitting corrosion area in the T6-treated alloy	[139]
Mg-8.6Al-0.85Zn	As-cast & T4	3.5 wt% NaCl	β-$Mg_{17}Al_{12}$	As-cast	Corrosion resistance deterioration due to the lattice distortion in the supersaturated grains during the T4 treatment	[140]
Mg-2.75Al-0.91Zn	As-cast & T4	3.5 wt% NaCl	β-$Mg_{17}Al_{12}$	At 340 °C for 6 h	Stress relieving and dissolution of the secondary phase lead to a lower corrosion rate in the T4-treated alloy	[142]
Mg-xAg (x = 0, 6 and 8 wt%)	Extruded and T4	DMEM + 10% FBS	$Mg_{54}Ag_{17}$	At 430 °C for 16 h	Significantly enhanced corrosion resistance due to the mitigation of micro-galvanic corrosion after T4 treatment	[36]
Mg-4Ag	As-cast & T4	SBF	$Mg_{54}Ag_{17}$	At 440 °C for 16 h	Significantly enhanced corrosion rate by decrement of Ag-rich precipitates after solution treatment	[147]
Mg-xAg (x = 0, 2, 4 and 6 wt%)	As-cast, T4 & T6	DMEM + 10% FBS	$Mg_{54}Ag_{17}$ Mg_4Ag	At 440 °C for 16 h	Uniform distribution of corrosion potential on the surface after T4 treatment led to a better corrosion resistance	[148]

the heat treatment parameters (e.g., time and temperature), it is possible to achieve remarkable improvements in each alloy.

A comparative summary of the mechanical strength (yield strength and ultimate tensile strength) of some heat-treatable Mg alloys in the as-cast, T4 and T6 conditions is presented in Fig. 38. As can be observed in Fig. 38, significant changes in the mechanical strength of the as-cast biodegradable Mg alloys have not been reported after a T4 treatment. As a result of the solution treatment, the final strength of the solution-treated alloys is a compromise between the solid solution strengthening and the inherent softening mechanisms of grain growth, precipitate dissolution and the reduction of defects. Solution strengthening is not similar in different alloying systems. Several mechanisms are involved in solid solution hardening such as: (1) elastic interactions caused by shear modulus and size misfits, (2) chemical interactions, and (3) electrical interactions [149].

The size misfits of Zn, Gd, Y, Nd, Al and Ag solutes with Mg are presented in Table 6 together with their maximum solid solubility. As can be observed in Fig. 38, among the reviewed biodegradable Mg-based alloy systems in this study, Mg-Gd and Mg-Y can provide higher solution strengthening effects due to their substantial size misfits with the Mg matrix, while this effect is not significant in Mg-Nd alloys due to the low solid solubility of Nd in Mg. In addition, the electron state between the atoms or electrical interactions have been reported to have a remarkable impact. In this regard, the high efficiency of Y and Gd (compared to other alloying elements like Al) to promote the solid solution strengthening has been attributed to the strong bond energy of Gd and Y with Mg [43].

As can be observed in Fig. 38, the T6 treatment can significantly improve the mechanical strength of the biodegradable Mg alloys. A precipitation strengthening effect by the fine and dense precipitates is the major contributor to the observed mechanical strength enhancement. In this regard, the precise control of temperature and time of heat treatment plays an important role in obtaining dense and nano-sized pre-

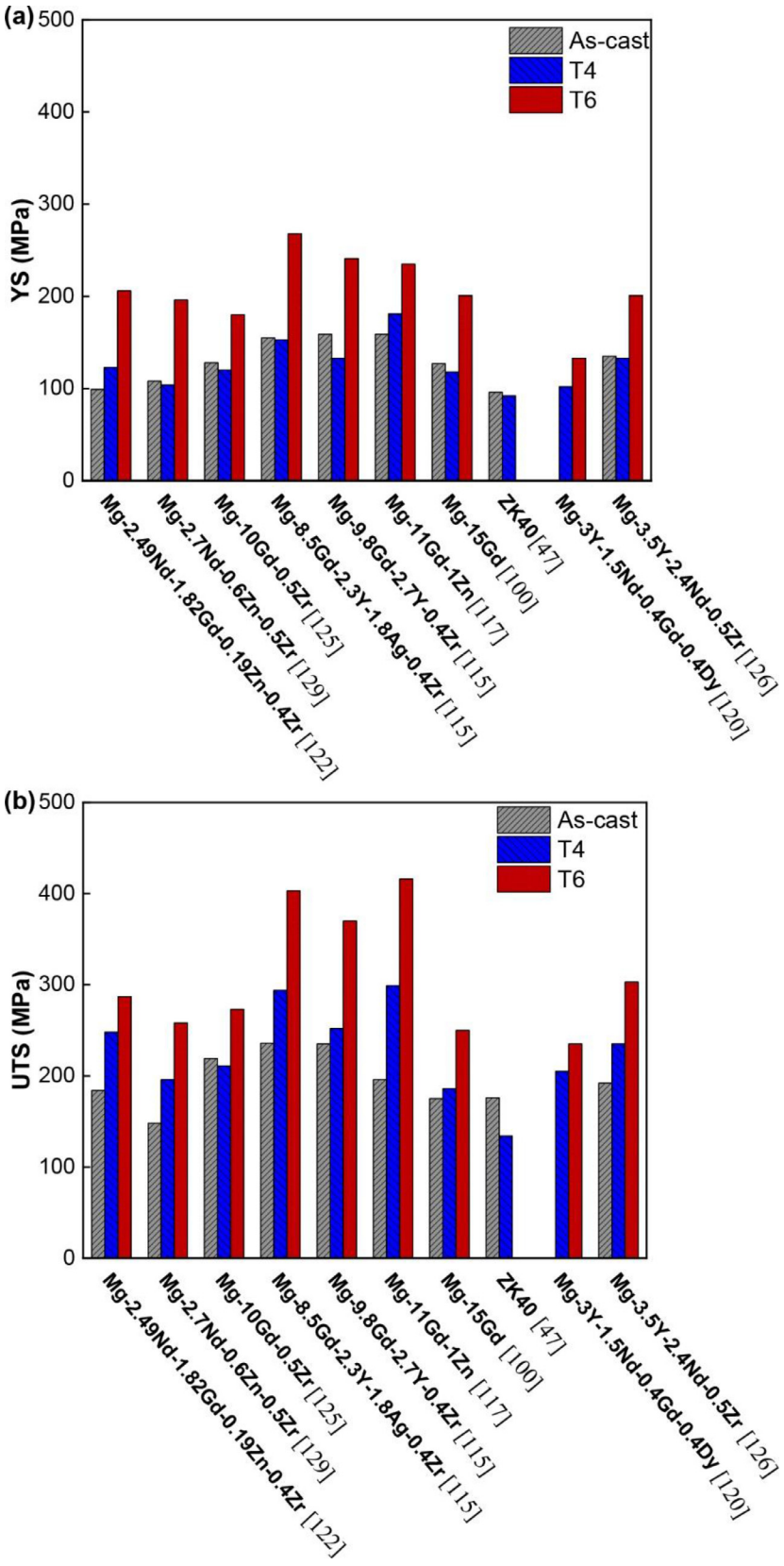

Fig. 38. A summary of the YS (a) and UTS (b) values of some biodegradable Mg alloys in as-cast, T4, and T6 conditions.

Table 6
Maximum solid solubility, atomic radius, and the size misfits of Zn, Gd, Y, Nd, Al and Ag elements with Mg (the atomic radius for Mg is 0.172 nm)

Solute element	Maximum solid solubility (wt%) and corresponding temperature (°C)	Atomic radius (nm)	Size misfit	References
Zn	6.2% at 340 °C	0.153	–0.11	[150]
Gd	23.5% at 548 °C	0.254	0.477	[76,150]
Y	11.4% at 572 °C	0.227	0.32	[150,151]
Nd	3.6% at 549 °C	0.229	0.33	[152]
Al	12.6% at 436 °C	0.182	0.058	[150]
Ag	15.02% at 472 °C	0.175	0.017	[153,154]

cipitates, which would be robust obstacles for the dislocation motion.

As discussed earlier, an LPSO structure can be beneficial for the mechanical strength of biodegradable Mg alloys as the result of its effective interaction with dislocations. Interestingly, the amount of LPSO structure can be increased during a T4 treatment in alloys like Mg-Gd and Mg-Y. Therefore, monitoring the LPSO structure evolution during heat treatment can lead to enhanced mechanical properties.

Regarding the corrosion properties, it is not feasible to plot comparative diagrams similar to Fig. 38 for the mechanical properties because of the several different parameters used in the corrosion tests including different solutions, temperatures and time durations, etc. All of these factors mean that it is difficult to make a simple comparison. However, some general conclusions can be made:

1) The T4 treatment may homogenize the microstructure, reduce the density of the crystal defects (e.g., dislocations) and decrease the volume fraction of the secondary phases. This can be of special interest and importance from the corrosion point of view, especially since micro-galvanic corrosion would be avoided.
2) Grain growth, reduction of precipitates volume fraction, and reduction of the defects density are the main factors controlling the corrosion behavior of as-extruded Mg alloys after being subjected to a heat treatment process. In this regard, suitable selection of time and temperature of heat treatment, where the occurrence of insignificant grain growth with a noticeable reduction in volume fraction of precipitates and defects, can be beneficial for improving the corrosion resistance.
3) The protectiveness of the formed corrosion film can be boosted by the T4 treatment as a result of a more uniform distribution of the alloying elements. This effect is more noticeable in Mg-Gd and Mg-Y alloys.
4) Heat treatment significantly affects the corrosion properties of LPSO structure-containing alloys such as the Mg-Gd system. This structure can hinder corrosion propagation and effectively decrease the corrosion rate. Regarding the adjustable amount of LPSO structure in microstructure, its volume fraction can be tailored by time and temperature of heat treatment, implying the importance of performing a suitable heat treatment process to maximize the corrosion resistance.
5) The re-distribution of the secondary phases and the alloying elements in the microstructure of the aged alloys considerably affects the extent of the galvanic corrosion and also the protectiveness of the corrosion film. While the dense and fine nano-scale precipitates are considered to improve the corrosion resistance by helping to form a more compact protective film or acting as corrosion barriers, the coarse, blocky, and discontinuous precipitates deteriorate the corrosion resistance due to their high cathode to anode surface area ratio which accelerates the micro-galvanic corrosion. This is schematically shown in Fig. 39 for the aged Mg-5.8Zn-2.0Yb-0.5Zr alloy where the relevant data to plot such figure was taken from published reports [65,66].

In Mg-Zn alloys, the optimum properties can be obtained by appropriate T6 treatment with the establishment of homogenous, fine and dense Zn-rich precipitates that can act as a strong barrier for corrosion propagation and also dislocation motion, leading to excellent corrosion and mechanical properties. Likewise, nano-sized precipitates in Mg-Nd alloys are favorable, since they would not provoke severe galvanic corrosion and can promote their properties. Contrarily, the established solution strengthening effect in Mg-Ag alloys, as well as the dissolution of Ag-rich precipitates (which are strong cathode), have made the T4 treatment a suitable choice for achieving optimal features in this system. A T4 treatment is also promising for Mg-Y alloys due to the formed distinctive Y-incorporated corrosion protective film after solution treatment. In the Mg-Gd system, the optimum properties induced by heat treatment depend on the amount of LPSO structure in the primary condition of the alloy, which would be changed concerning the time and temperature of heat treatment. However, both T4 and T6 can significantly enhance their bioperformance.

9. Future research directions

As was thoroughly discussed, the corrosion behavior and mechanical properties of biodegradable Mg alloys can be improved with the implementation of an appropriate heat treatment. However, there remain many challenges and uncertain

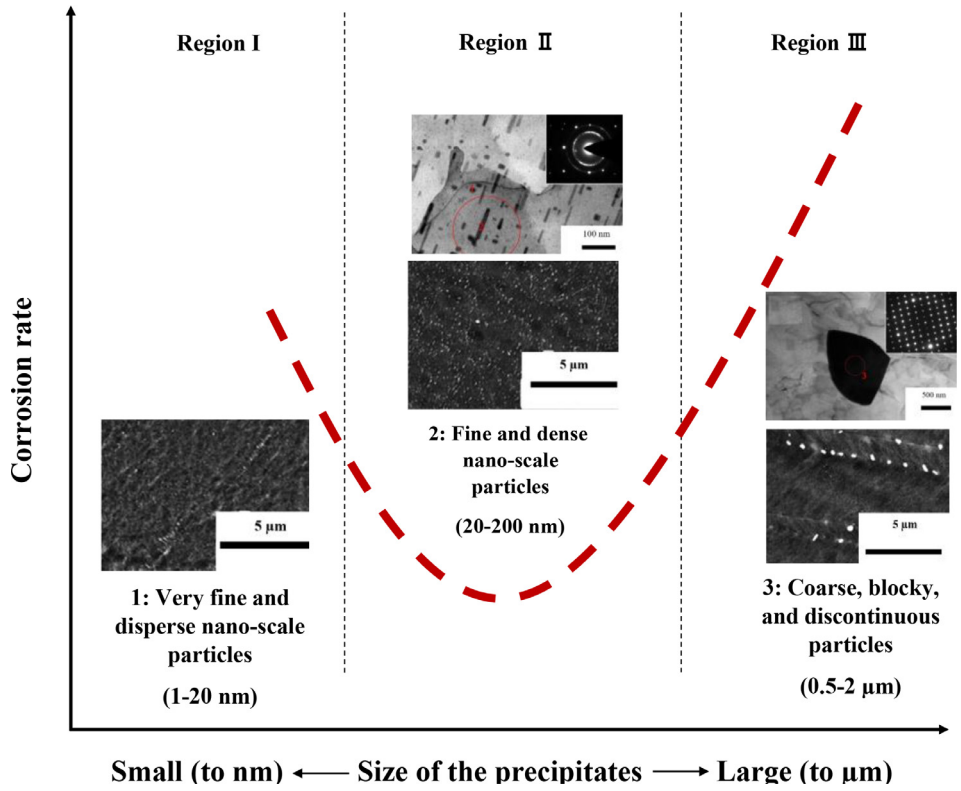

Fig. 39. A schematic representation of the effects of the precipitate size and distribution on the corrosion behavior of the biodegradable Mg-5.8Zn-2.0Yb-0.5Zr alloy during the T6 treatment. Data collected from [65,66].

aspects which need more investigations. For example, the effect of the distribution of the nano-scale precipitates on the corrosion film formation and the corresponding protectiveness, and also the extent of the nano-galvanic corrosion, should be further clarified. In addition, the role of the large micron-size precipitates in forming corrosion barriers needs further attention in different alloying systems, similar to the trend observed in Mg-Al alloys, where it was found that the large β-$Mg_{17}Al_{12}$ phase with continuous morphology could inhibit the corrosion propagation.

Although simulation models have been proposed to predict the microstructure evolution of some Mg-based systems like Mg-Al and Mg-Zn during an aging treatment, more investigations are required to more precisely determine the optimum time and temperature of heat treatment in different biodegradable Mg alloys to obtain the best possible corrosion and mechanical properties.

The formation and composition of the surface corrosion film on Mg-based alloys have been widely examined [155–157]. Nonetheless, there is a lack of systematic reports on investigating the effect of alloying elements and their concentration as well as heat treatment on the protectivity and stability of corrosion film. Therefore, a future study should provide a path to developing a surface film with the highest integrity, which can prevent localized corrosion attacks with the help of heat treatment.

Mg biodegradable composites in which the reinforcement phases are mainly based on hydroxyapatite (HAP), calcium polyphosphate (CPP), β-tricalcium phosphate (β-TCP) particles and hybrid HAP + β-TCP particles can provide a combination of unique characteristics including adjustable mechanical properties (i.e. tensile strength, elastic modulus, ductility) as well as corrosion resistance and biocompatibility [158]. In such materials, which can be suitably fabricated by powder metallurgy techniques [159], if heat treatable magnesium alloys are chosen as the matrix, then the same principles reported for the alloys can be applied for the Mg matrix and thus heat treatment can effectively be utilized to further improve the properties of such composites. However, there are few studies reporting the effects of heat treatment on the characteristics of Mg-based composite biomaterials and this is an interesting research topic for future investigations.

Additively manufactured biodegradable Mg implants, which are gaining considerable attention in recent years, also suffer from the same problems of high degradation rate and insufficient mechanical properties [160,161]. In this regard, using heat-treatable Mg alloys for additive manufacturing can be of great practical interest and needs further investigation [162]. Furthermore, computer simulation has proved to be a useful tool to optimize the microstructure and thus the corrosion and mechanical properties [163,164]. In this regard, more investigations are required to correlate the microstructural features with the heat treatment parameters in different alloying systems. The above-mentioned topics would provide important support for the future processing and design of biodegradable Mg-based implants, where heat treatment can

play a critical role in addition to the other parameters used to optimize the properties.

10. Conclusions

This review has mainly concentrated on collecting and summarizing the results describing the effect of the T4 and T6 heat treatments on the mechanical and corrosion properties of some important heat-treatable biodegradable Mg alloys, including the Mg-Zn, Mg-Gd, Mg-Y, Mg-Nd, Mg-Al and Mg-Ag systems. While there are many consistent aspects, it is now readily apparent that different alloying systems may respond very differently to similar heat treatments. In general, a T4 treatment can cause a lower degree of galvanic corrosion by the dissolution of secondary phases, enhanced corrosion protection film by microstructural homogeneity as well as a uniformly distributed alloying element and solid solution strengthening effect. It is also believed that the T6 treatment in most cases can significantly improve the mechanical properties by re-precipitation of new secondary phases. However, the size, morphology and distribution of precipitates are critical factors that determine the ability of the alloy to resist corrosion propagation as well as dislocation motion, which would be modified by heat treatment. Accordingly, it is shown that by precise control of the heat treatment parameters of time and temperature it is possible to attain remarkable improvements in each alloy. Furthermore, employing the discussed future perspectives in conjunction with heat treatment can be a promising approach in the development of Mg alloys for biomedical applications.

Acknowledgement

The work of one of us was supported by the European Research Council under Grant Agreement No. 267464-SPDMETALS (TGL).

References

[1] Y. Chen, Z. Xu, C. Smith, J. Sankar, Acta Biomater 10 (2014) 4561–4573, doi:10.1016/j.actbio.2014.07.005.
[2] A.S. Mao, D.J. Mooney, Proc. Natl. Acad. Sci. U. S. A. 112 (2015) 14452–14459, doi:10.1073/pnas.1508520112.
[3] K. Kumar, R.S. Gill, U. Batra, Mater. Technol. 33 (2018) 153–172, doi:10.1080/10667857.2017.1377973.
[4] M. Moravej, D. Mantovani, Int. J. Mol. Sci. 12 (2011) 4250–4270, doi:10.3390/ijms12074250.
[5] Q. Chen, G.A. Thouas, Mater. Sci. Eng. R Reports. 87 (2015) 1–57, doi:10.1016/j.mser.2014.10.001.
[6] M.P. Staiger, A.M. Pietak, J. Huadmai, G. Dias, Biomaterials 27 (2006) 1728–1734, doi:10.1016/j.biomaterials.2005.10.003.
[7] M. Mohammadi Zerankeshi, S. Mofakhami, E. Salahinejad, Ceram. Int. (2022), doi:10.1016/J.CERAMINT.2022.05.103.
[8] M. Mohammadi Zerankeshi, R. Bakhshi, R. Alizadeh, Bioprinting 25 (2022) e00191, doi:10.1016/J.BPRINT.2022.E00191.
[9] E. Gerashi, R. Alizadeh, T.G. Langdon, J. Magnes. Alloy. 10 (2) (2022) 313–325, doi:10.1016/J.JMA.2021.09.009.
[10] Z. Wang, N. Li, R. Li, Y. Li, L. Ruan, Prog. Nat. Sci. Mater. Int. 24 (2014) 423–432, doi:10.1016/j.pnsc.2014.08.008.
[11] D.R. Lopes, C.L.P. Silva, R.B. Soares, P.H.R. Pereira, A.C. Oliveira, R.B. Figueiredo, T.G. Langdon, V.F.C. Lins, Adv. Eng. Mater. 21 (2019) 1900391, doi:10.1002/adem.201900391.
[12] N. Zirak, A. Bolandparvaz Jahromi, E. Salahinejad, Ceram. Int. 46 (2020) 508–512, doi:10.1016/j.ceramint.2019.08.290.
[13] M.S. Song, R.C. Zeng, Y.F. Ding, R.W. Li, M. Easton, I. Cole, N. Birbilis, X.B. Chen, J. Mater. Sci. Technol. 35 (2019) 535–544, doi:10.1016/j.jmst.2018.10.008.
[14] J. Chen, L. Tan, X. Yu, I.P. Etim, M. Ibrahim, K. Yang, J. Mech. Behav. Biomed. Mater. 87 (2018) 68–79, doi:10.1016/j.jmbbm.2018.07.022.
[15] Y. Chen, J. Yan, Z. Wang, S. Yu, X. Wang, Z. Yuan, X. Zhang, C. Zhao, Q. Zheng, Mater. Sci. Eng. C. 42 (2014) 116–123, doi:10.1016/j.msec.2014.05.014.
[16] C. Liu, X. Fu, H. Pan, P. Wan, L. Wang, L. Tan, K. Wang, Y. Zhao, K. Yang, P.K. Chu, Sci. Rep. 6 (2016) 27374, doi:10.1038/srep27374.
[17] M. Li, L. Ren, L.H. Li, P. He, G.B. Lan, Y. Zhang, K. Yang, J. Mater. Sci. Technol. 30 (2014) 888–893, doi:10.1016/j.jmst.2014.04.010.
[18] A. Mazur, J.A.M. Maier, E. Rock, E. Gueux, W. Nowacki, Y. Rayssiguier, Arch. Biochem. Biophys. 458 (2007) 48–56, doi:10.1016/j.abb.2006.03.031.
[19] F. Abdiyan, R. Mahmudi, H.M. Ghasemi, Mater. Chem. Phys. 271 (2021) 124878, doi:10.1016/j.matchemphys.2021.124878.
[20] Y. Koo, Y. Jang, Y. Yun, Mater. Sci. Eng. B Solid-State Mater. Adv. Technol. 219 (2017) 45–54, doi:10.1016/j.mseb.2017.02.009.
[21] M.S. Uddin, C. Hall, P. Murphy, Sci. Technol. Adv. Mater. 16 (2015) 053501, doi:10.1088/1468-6996/16/5/053501.
[22] L.Y. Li, L.Y. Cui, R.C. Zeng, S.Q. Li, X.B. Chen, Y. Zheng, M.B. Kannan, Acta Biomater 79 (2018) 23–36, doi:10.1016/J.ACTBIO.2018.08.030.
[23] W. Weng, A. Biesiekierski, Y. Li, M. Dargusch, C. Wen, Acta Biomater 130 (2021) 80–97, doi:10.1016/J.ACTBIO.2021.06.004.
[24] Y. Ding, C. Wen, P. Hodgson, Y. Li, J. Mater. Chem. B. 2 (2014) 1912–1933, doi:10.1039/C3TB21746A.
[25] E.C. Huse, Chicago Med J Exam 172 (1878) 11.
[26] F. Witte, Acta Biomater 6 (2010) 1680–1692, doi:10.1016/j.actbio.2010.02.028.
[27] B. Heublein, R. Rohde, V. Kaese, M. Niemeyer, W. Hartung, A. Haverich, Heart 89 (2003) 651, doi:10.1136/HEART.89.6.651.
[28] B. Schaller, N. Saulacic, S. Beck, T. Imwinkelried, B.T. Goh, K. Nakahara, W. Hofstetter, T. Iizuka, Mater. Sci. Eng. C. Mater. Biol. Appl. 69 (2016) 247–254, doi:10.1016/J.MSEC.2016.06.085.
[29] U. Riaz, I. Shabib, W. Haider, J. Biomed. Mater. Res. - Part B Appl. Biomater. 107 (2019) 1970–1996, doi:10.1002/jbm.b.34290.
[30] C. Liu, Z. Ren, Y. Xu, S. Pang, X. Zhao, Y. Zhao, Scanning 2018 (2018) 9216314, doi:10.1155/2018/9216314.
[31] D. Persaud-Sharma, A. Mcgoron, J. Biomim. Biomater. Tissue Eng. 12 (2012) 25, doi:10.4028/WWW.SCIENTIFIC.NET/JBBTE.12.25.
[32] N. Eliaz, Materials (Basel) 12 (3) (2019) 407, doi:10.3390/MA12030407.
[33] G. Eddy Jai Poinern, S. Brundavanam, D. Fawcett, Am. J. Biomed. Eng. 2 (2013) 218–240, doi:10.5923/j.ajbe.20120206.02.
[34] M. Erinc, W.H. Sillekens, R.G.T.M. Mannens, R.J. Werkhoven, Magnes. Technol. (2009) 209–214.
[35] J. Fischer, D. Pröfrock, N. Hort, R. Willumeit, F. Feyerabend, Mater. Sci. Eng. B. 176 (2011) 830–834, doi:10.1016/J.MSEB.2011.04.008.
[36] Z. Liu, R. Schade, B. Luthringer, N. Hort, H. Rothe, S. Müller, K. Liefeith, R. Willumeit-Römer, F. Feyerabend, Oxid. Med. Cell. Longev. 2017 (2017) 8091265, doi:10.1155/2017/8091265.
[37] J. Zhang, C. Xu, Y. Jing, S. Lv, S. Liu, D. Fang, J. Zhuang, M. Zhang, R. Wu, Sci. Reports 51 (5) (2015) 13933 2015, doi:10.1038/srep13933.
[38] D. Bairagi, S. Mandal, J. Magnes. Alloy. 10 (2021) 627–669, doi:10.1016/J.JMA.2021.09.005.
[39] M.R. Norton, G.W. Kay, M.C. Brown, D.L. Cochran, Int. J. Adhes. Adhes. 102 (2020) 102647, doi:10.1016/J.IJADHADH.2020.102647.
[40] C.E. Baker, S.N. Moore-Lotridge, A.A. Hysong, S.L. Posey, J.P. Robinette, D.M. Blum, M.A. Benvenuti, H.A. Cole, S. Egawa, A. Okawa, M. Saito, J.R. McCarthy, J.S. Nyman, M. Yuasa, J.G. Schoenecker,

Clin. Rev. Bone Miner. Metab. 16 (2018) 142–158, doi:10.1007/S12018-018-9256-X/FIGURES/9.
[41] Y. Kang, B. Du, Y. Li, B. Wang, L. Sheng, L. Shao, Y. Zheng, T. Xi, J. Mater. Sci. Technol. 35 (2019) 6–18, doi:10.1016/J.JMST.2018.09.020.
[42] A.F. Lotfabadi, H.R. Bakhsheshi-Rad, M.H. Idris, E. Hamzah, M. Kasiri-Asgarani, Can. Metall. Q. 55 (2016) 53–64, doi:10.1179/1879139515Y.0000000031.
[43] L. Gao, R.S. Chen, E.H. Han, J. Alloys Compd. 481 (2009) 379–384, doi:10.1016/j.jallcom.2009.02.131.
[44] Y. Lu, A.R. Bradshaw, Y.L. Chiu, I.P. Jones, Mater. Sci. Eng. C. 48 (2015) 480–486, doi:10.1016/j.msec.2014.12.049.
[45] J.X. Chen, M. Gao, L.L. Tan, K. Yang, Rare Met 38 (2019) 532–542, doi:10.1007/s12598-019-01213-6.
[46] S.M.G. Shahri, M.H. Idris, H. Jafari, B. Gholampour, M. Assadian, Trans. Nonferrous Met. Soc. China. 25 (2015) 1490–1499, doi:10.1016/S1003-6326(15)63750-5.
[47] D. Hong, P. Saha, D.T. Chou, B. Lee, B.E. Collins, Z. Tan, Z. Dong, P.N. Kumta, Acta Biomater 9 (2013) 8534–8547, doi:10.1016/j.actbio.2013.07.001.
[48] M. Janbozorgi, K. Karimi Taheri, A. Karimi Taheri, J. Magnes. Alloy. 7 (2019) 80–89, doi:10.1016/j.jma.2018.11.002.
[49] J. Chen, S. Wei, L. Tan, K. Yang, Mater. Technol. 34 (2019) 592–601, doi:10.1080/10667857.2019.1603657.
[50] Y. Song, E.H. Han, D. Shan, C.D. Yim, B.S. You, Corros. Sci. 60 (2012) 238–245, doi:10.1016/j.corsci.2012.03.030.
[51] J. Chen, L. Tan, K. Yang, Bioact. Mater. 2 (2017) 19–26, doi:10.1016/j.bioactmat.2016.12.002.
[52] G. Xu, L. Zhang, L. Liu, Y. Du, F. Zhang, K. Xu, S. Liu, M. Tan, Z. Jin, J. Magnes. Alloy. 4 (2016) 249–264, doi:10.1016/J.JMA.2016.11.004.
[53] M. Vlček, F. Lukáč, H. Kudrnová, B. Smola, I. Stulíková, M. Luczak, G. Szakács, N. Hort, R. Willumeit-Römer, Mater 10 (2017) 55 2017Page1055, doi:10.3390/ma10010055.
[54] M. Paliwal, I.H. Jung, Calphad 64 (2019) 196–204, doi:10.1016/J.CALPHAD.2018.12.006.
[55] M. Paliwal, D.H. Kang, E. Essadiqi, I.H. Jung, Metall. Mater. Trans. A 458 (45) (2014) 3596–3608 2014, doi:10.1007/S11661-014-2288-Z.
[56] S. Celotto, Acta Mater 48 (2000) 1775–1787, doi:10.1016/S1359-6454(00)00004-5.
[57] W. Zhao, J. Wang, J. Weiyang, B. Qiao, Y. Wang, Y. Li, D. Jiang, J. Magnes. Alloy. 8 (2020) 374–386, doi:10.1016/J.JMA.2020.02.008.
[58] J. Kubásek, D. Vojtěch, J. Mater. Sci. Mater. Med. 24 (2013) 1615–1626, doi:10.1007/s10856-013-4916-3.
[59] S. Cai, T. Lei, N. Li, F. Feng, Mater. Sci. Eng. C. 32 (2012) 2570–2577, doi:10.1016/j.msec.2012.07.042.
[60] H.R. Bakhsheshi-Rad, E. Hamzah, A. Fereidouni-Lotfabadi, M. Daroonparvar, M.A.M. Yajid, M. Mezbahul-Islam, M. Kasiri-Asgarani, M. Medraj, Mater. Corros. 65 (2014) 1178–1187, doi:10.1002/maco.201307588.
[61] D.N. Pham, S. Hiromoto, E. Kobayashi, Corrosion 77 (2021) 323–338, doi:10.5006/3672.
[62] H.S. Brar, J. Wong, M.V. Manuel, J. Mech. Behav. Biomed. Mater. 7 (2012) 87–95, doi:10.1016/j.jmbbm.2011.07.018.
[63] D. Jiang, Y. Dai, Y. Zhang, Y. Yan, J. Ma, D. Li, K. Yu, J. Mater. Eng. Perform. 28 (2019) 33–43, doi:10.1007/s11665-018-3781-0.
[64] M. Mohammadi Zerankeshi, R. Alizadeh, Materialia 23 (2022) 101445, doi:10.1016/J.MTLA.2022.101445.
[65] L. Li, T. Wang, M. Hou, P. Xue, H. Lv, C. Huang, Mater. Lett. 282 (2021) 128682, doi:10.1016/j.matlet.2020.128682.
[66] L. Li, T. Wang, Y. Wang, C. cai Zhang, H. Lv, H. Lin, W. bin Yu, C. jie Huang, J. Magnes. Alloy. 8 (2020) 499–509, doi:10.1016/j.jma.2019.11.013.
[67] X. Bin Liu, D.Y. Shan, Y.W. Song, E.H. Han, Trans. Nonferrous Met. Soc. China (English Ed. 20 (2010) 1345–1350, doi:10.1016/S1003-6326(09)60302-2.
[68] D. Liu, T. Zhou, Z. Liu, B. Guo, J. Appl. Biomater. Funct. Mater. 18 (2020), doi:10.1177/22808000019887906.
[69] H. Ibrahim, A.D. Klarner, B. Poorganji, D. Dean, A.A. Luo, M. Elahinia, J. Mech. Behav. Biomed. Mater. 69 (2017) 203–212, doi:10.1016/j.jmbbm.2017.01.005.
[70] L. qing WANG, G. wu QIN, S. neng SUN, Y. ping REN, S. LI, Trans. Nonferrous Met. Soc. China (English Ed. 27 (2017) 2607–2612, doi:10.1016/S1003-6326(17)60288-7.
[71] D.J. Lin, F.Y. Hung, M.L. Yeh, T.S. Lui, J. Mater. Sci. Mater. Med. 26 (2015) 248, doi:10.1007/s10856-015-5572-6.
[72] X.N. Ly, S. Yang, Y. Qin, IOP Conf. Ser. Mater. Sci. Eng. 182 (2017) 012054, doi:10.1088/1757-899X/182/1/012054.
[73] R. Alizadeh, J. LLorca, Acta Mater 186 (2020) 475–486, doi:10.1016/j.actamat.2020.01.028.
[74] Y. Yandong, K. Shuzhen, P. Teng, L. Jie, L. Caixia, Metallogr. Microstruct. Anal. 4 (2015) 381–391, doi:10.1007/s13632-015-0224-2.
[75] X. Zhang, Z. Ba, Q. Wang, Y. Wu, Z. Wang, Q. Wang, Corros. Sci. 88 (2014) 1–5, doi:10.1016/j.corsci.2014.07.004.
[76] J. Kubásek, D. Vojtěch, Trans. Nonferrous Met. Soc. China (English Ed. 23 (2013) 1215–1225, doi:10.1016/S1003-6326(13)62586-8.
[77] L. ling Shi, Y. Huang, L. Yang, F. Feyerabend, C. Mendis, R. Willumeit, K. Ulrich Kainer, N. Hort, J. Mech. Behav. Biomed. Mater. 47 (2015) 38–48, doi:10.1016/j.jmbbm.2015.03.003.
[78] M. Sabbaghian, R. Mahmudi, K.S. Shin, Metall. Mater. Trans. A 524 (52) (2021) 1269–1281 2021, doi:10.1007/S11661-021-06160-5.
[79] D. Xu, E.H. Han, Y. Xu, Prog. Nat. Sci. Mater. Int. 26 (2016) 117–128, doi:10.1016/j.pnsc.2016.03.006.
[80] X. Zhang, J. Dai, R. Zhang, Z. Ba, N. Birbilis, J. Magnes. Alloy. 7 (2019) 240–248, doi:10.1016/j.jma.2019.02.009.
[81] M. Vlček, F. Lukáč, H. Kudrnová, B. Smola, I. Stulíková, M. Luczak, G. Szakács, N. Hort, R. Willumeit-Römer, Materials (Basel) 10 (2017) 55, doi:10.3390/ma10010055.
[82] A.C. Hänzi, P. Gunde, M. Schinhammer, P.J. Uggowitzer, Acta Biomater 5 (2009) 162–171, doi:10.1016/J.ACTBIO.2008.07.034.
[83] X. Ma, Q. Jiang, Y. Li, B. Hou, Int. J. Electrochem. 2016 (2016) 7097589, doi:10.1155/2016/7097589.
[84] M.I. Jamesh, G. Wu, Y. Zhao, D.R. McKenzie, M.M.M. Bilek, P.K. Chu, Corros. Sci. 91 (2015) 160–184, doi:10.1016/J.CORSCI.2014.11.015.
[85] A.C. Hänzi, I. Gerber, M. Schinhammer, J.F. Löffler, P.J. Uggowitzer, Acta Biomater 6 (2010) 1824–1833, doi:10.1016/J.ACTBIO.2009.10.008.
[86] B. Smola, L. Joska, V. Březina, I. Stulíková, F. Hnilica, Mater. Sci. Eng. C. 32 (2012) 659–664, doi:10.1016/j.msec.2012.01.003.
[87] X. Zhang, G. Yuan, L. Mao, J. Niu, P. Fu, W. Ding, J. Mech. Behav. Biomed. Mater. 7 (2012) 77–86, doi:10.1016/j.jmbbm.2011.05.026.
[88] Y. Wang, Z. Zhu, Y. He, Y. Jiang, J. Zhang, J. Niu, L. Mao, G. Yuan, Int. J. Mol. Med. 29 (2012) 178–184, doi:10.3892/ijmm.2011.815.
[89] L. Mao, G. Yuan, J. Niu, Y. Zong, W. Ding, Mater. Sci. Eng. C. 33 (2013) 242–250, doi:10.1016/j.msec.2012.08.036.
[90] H. Qin, Y. Zhao, Z. An, M. Cheng, Q. Wang, T. Cheng, Q. Wang, J. Wang, Y. Jiang, X. Zhang, G. Yuan, Biomaterials 53 (2015) 211–220, doi:10.1016/j.biomaterials.2015.02.096.
[91] J. Niu, G. Yuan, Y. Liao, L. Mao, J. Zhang, Y. Wang, F. Huang, Y. Jiang, Y. He, W. Ding, Mater. Sci. Eng. C. 33 (2013) 4833–4841, doi:10.1016/j.msec.2013.08.008.
[92] K. Xie, L. Wang, Y. Guo, S. Zhao, Y. Yang, D. Dong, W. Ding, K. Dai, W. Gong, G. Yuan, Y. Hao, J. Orthop. Transl. 27 (2021) 96–100, doi:10.1016/J.JOT.2020.11.007.
[93] X.B. Zhang, Y. Zhang, K. Chen, Z.X. Ba, Z.Z. Wang, Q. Wang, Mater. Sci. Technol. (United Kingdom). 31 (2015) 866–873, doi:10.1179/1743284714Y.0000000661.
[94] J. Zhang, B. Jiang, Q. Yang, D. Huang, A. Tang, F. Pan, Q. Han, J. Alloys Compd. 849 (2020) 156619, doi:10.1016/j.jallcom.2020.156619.
[95] J. Wang, W. Jiang, Y. Ma, Y. Li, S. Huang, Mater. Chem. Phys. 203 (2018) 352–361, doi:10.1016/j.matchemphys.2017.09.035.

[96] P. Maier, M. Bechly, C.L. Mendis, N. Hort, Metals (Basel) 8 (2018) 640, doi:10.3390/met8080640.
[97] M. Zhang, W.L. Deng, X.N. Yang, Y.K. Wang, X.Y. Zhang, R.Q. Hang, K.K. Deng, X.B. Huang, Rare Met 38 (2019) 620–628, doi:10.1007/s12598-019-01220-7.
[98] S. Liang, D. Guan, X. Tan, Mater. Des. 32 (2011) 1194–1199, doi:10.1016/j.matdes.2010.10.022.
[99] J. Dai, X. Zhang, Z. Wang, Mater. Technol. 33 (2018) 301–310, doi:10.1080/10667857.2018.1438154.
[100] J. Liu, L. Yang, C. Zhang, B. Zhang, T. Zhang, Y. Li, K. Wu, F. Wang, J. Mater. Sci. Technol. 35 (2019) 1644–1654, doi:10.1016/j.jmst.2019.03.027.
[101] M. Mohammadi Zerankeshi, R. Alizadeh, S. Labbaf, SSRN Electron. J. (2022), doi:10.2139/SSRN.4037190.
[102] H. Xu, X. Deng, X. Zhang, K. Zhang, Y. Liu, S. Li, J. Wuhan Univ. Technol. Mater. Sci. Ed. 30 (2015) 796–803, doi:10.1007/s11595-015-1230-6.
[103] V. Kodetová, B. Smola, I. Stulíková, H. Kudrnová, M. Vlach, V. Neubert, J. Therm. Anal. Calorim. 138 (2019) 2167–2174, doi:10.1007/s10973-019-08782-9.
[104] T. Huang, L. Yang, C. Xu, J. Zhang, Z. Song, C. Xu, Q. Zhang, F. Li, Q. Jia, J. Kuan, Z. Zhang, X. Wu, Z. Wang, Materwiss. Werksttech. 51 (2020) 1543–1560, doi:10.1002/mawe.202000045.
[105] M. Liu, P. Schmutz, P.J. Uggowitzer, G. Song, A. Atrens, Corros. Sci. 52 (2010) 3687–3701, doi:10.1016/j.corsci.2010.07.019.
[106] X.B. Zhang, Y.J. Xue, Z.Z. Wang, Trans. Nonferrous Met. Soc. China (English Ed. 22 (2012) 2343–2350, doi:10.1016/S1003-6326(11)61469-6.
[107] X.B. Zhang, G.Y. Yuan, X.X. Fang, Z.Z. Wang, T. Zhang, Mater. Technol. 28 (2013) 155–158, doi:10.1179/1753555712Y.0000000048.
[108] Z. Gui, Z. Kang, Y. Zhou, J. Zhang, Adv. Eng. Mater. 23 (2021) 2000752, doi:10.1002/ADEM.202000752.
[109] P. Maier, N. Lauth, C.L. Mendis, M. Bechly, N. Hort, Jom 71 (2019) 1426–1435, doi:10.1007/s11837-019-03359-1.
[110] Y. Zhang, Y. Huang, F. Feyerabend, S. Gavras, Y. Xu, R. Willumeit-Römer, K.U. Kainer, N. Hort, Metall. Mater. Trans. A Phys. Metall. Mater. Sci. 51 (2020) 5498–5515, doi:10.1007/s11661-020-05926-7.
[111] Y. Lu, Y. Huang, F. Feyerabend, R. Willumeit-Römer, K.U. Kainer, N. Hort, Magnes. Technol. 2016-Janua (2016) 347–351, doi:10.1002/9781119274803.ch67.
[112] N. Zidane, A.A. Addi, R.A. Akbour, J. Douch, R.N. Singh, M. Hamdani, Int. J. Electrochem. Sci. 10 (2015) 9395–9407.
[113] D.T. Chou, D. Hong, P. Saha, J. Ferrero, B. Lee, Z. Tan, Z. Dong, P.N. Kumta, Acta Biomater 9 (2013) 8518–8533, doi:10.1016/j.actbio.2013.06.025.
[114] Y. Fei, X.B. Zhang, Z.X. Ba, Z.Z. Wang, Mater. Sci. Forum. 849 (2016) 196–202, doi:10.4028/www.scientific.net/MSF.849.196.
[115] Q. Wang, J. Chen, Z. Zhao, S. He, Mater. Sci. Eng. A. 528 (2010) 323–328, doi:10.1016/j.msea.2010.09.004.
[116] R. Alizadeh, R. Mahmudi, A.H.W. Ngan, P.H.R. Pereira, Y. Huang, T.G. Langdon, Metall. Mater. Trans. A 47 (47) (2016) 6056–6069 2016, doi:10.1007/S11661-016-3765-3.
[117] R. Zhen, Y. Sun, F. Xue, J. Sun, J. Bai, J. Alloys Compd. 550 (2013) 273–278, doi:10.1016/j.jallcom.2012.08.045.
[118] X. Zhang, Z. Ba, Z. Wang, Y. Wu, Y. Xue, Mater. Lett. 163 (2016) 250–253, doi:10.1016/j.matlet.2015.10.084.
[119] M. Ma, K. Zhang, X. Li, Y. Li, G. Shi, J. Yuan, Mater. Des. 51 (2013) 73–78, doi:10.1016/j.matdes.2013.03.104.
[120] P. Maier, R. Peters, C.L. Mendis, S. Müller, N. Hort, Jom 68 (2016) 1183–1190, doi:10.1007/s11837-015-1762-4.
[121] Z. Gui, Z. Kang, Y. Li, J. Alloys Compd. 765 (2018) 470–479, doi:10.1016/j.jallcom.2018.06.185.
[122] S.J. Liu, G.Y. Yang, S.F. Luo, W.Q. Jie, Mater. Charact. 107 (2015) 334–342, doi:10.1016/j.matchar.2015.07.034.
[123] X.B. Liu, R.S. Chen, E.H. Han, J. Alloys Compd. 465 (2008) 232–238, doi:10.1016/j.jallcom.2007.10.068.
[124] H.R. Jafari Nodooshan, W. Liu, G. Wu, R. Alizadeh, R. Mahmudi, W. Ding, J. Alloys Compd. 619 (2015) 826–833, doi:10.1016/j.jallcom.2014.09.102.
[125] J. Li, Z. He, P. Fu, Y. Wu, L. Peng, W. Ding, Mater. Sci. Eng. A. 651 (2016) 745–752, doi:10.1016/j.msea.2015.11.021.
[126] H. Li, F. Lv, X. Liang, Y. Qi, Z. Zhu, K. Zhang, Mater. Sci. Eng. A. 667 (2016) 409–416, doi:10.1016/j.msea.2016.05.014.
[127] H. Zhang, J. Fan, L. Zhang, G. Wu, W. Liu, W. Cui, S. Feng, Mater. Sci. Eng. A. 677 (2016) 411–420, doi:10.1016/j.msea.2016.09.044.
[128] V. Gärtnerová, Z. Trojanová, A. Jäger, P. Palček, J. Alloys Compd. 378 (2004) 180–183, doi:10.1016/j.jallcom.2003.11.172.
[129] D. Wu, Y.Q. Ma, R.S. Chen, W. Ke, J. Magnes. Alloy. 2 (2014) 20–26, doi:10.1016/j.jma.2014.01.006.
[130] N. Hort, Y. Huang, D. Fechner, M. Störmer, C. Blawert, F. Witte, C. Vogt, H. Drücker, R. Willumeit, K.U. Kainer, F. Feyerabend, Acta Biomater 6 (2010) 1714–1725, doi:10.1016/j.actbio.2009.09.010.
[131] M. Ren, S. Cai, G. Xu, X. Ye, Y. Dou, K. Huang, X. Wang, J. Non. Cryst. Solids. 369 (2013) 69–75, doi:10.1016/J.JNONCRYSOL.2013.03.022.
[132] K. Hong, H. Park, Y. Kim, M. Knapek, P. Minárik, K. Máthis, A. Yamamoto, H. Choe, J. Mech. Behav. Biomed. Mater. 98 (2019) 213–224, doi:10.1016/j.jmbbm.2019.06.022.
[133] C. Liu, Y. Xin, G. Tang, P.K. Chu, Mater. Sci. Eng. A. 456 (2007) 350–357, doi:10.1016/j.msea.2006.12.020.
[134] W. Zhou, T. Shen, N.N. Aung, Corros. Sci. 52 (2010) 1035–1041, doi:10.1016/j.corsci.2009.11.030.
[135] F. Lu, A. Ma, J. Jiang, Y. Guo, D. Yang, D. Song, J. Chen, Corros. Sci. 94 (2015) 171–178, doi:10.1016/j.corsci.2015.01.052.
[136] X. Gu, Y. Zheng, Y. Cheng, S. Zhong, T. Xi, Biomaterials 30 (2009) 484–498, doi:10.1016/J.BIOMATERIALS.2008.10.021.
[137] V.P. Sokoloff, B.V. Brajnikov, Review Section, Int. Geol. Rev. 9 (1967) 371–374, doi:10.1080/00206816709474477.
[138] R. Ambat, N.N. Aung, W. Zhou, Corros. Sci. 42 (2000) 1433–1455, doi:10.1016/S0010-938X(99)00143-2.
[139] Y. Ma, H. Xiong, B. Chen, Corros. Sci. 191 (2021) 109759, doi:10.1016/j.corsci.2021.109759.
[140] S.C. V, R. Dumpala, A.K. S, K. VV, R.S. B, J. Magnes. Alloy. 6 (2018) 52–58, doi:10.1016/j.jma.2017.12.001.
[141] N.N. Aung, W. Zhou, Corros. Sci. 52 (2010) 589–594, doi:10.1016/j.corsci.2009.10.018.
[142] P. Pradeep Kumar, A. Raj Bharat, B. Sesha Sai, R.J. Phani Sarath, P. Akhil, G. Pradeep Kumar Reddy, V.V. Kondaiah, B. Ratna Sunil, Mater. Today Proc 18 (2019) 175–181, doi:10.1016/j.matpr.2019.06.291.
[143] C.T. Lih, M.Z.M. Zamzuri, S. Norbahiyah, K.A. Ismail, M.N.B. Derman, S. Illias, Adv. Mater. Res. 685 (2013) 102–106, doi:10.4028/www.scientific.net/AMR.685.102.
[144] W. Chen, Y. Liu, H.S. Courtney, M. Bettenga, C.M. Agrawal, J.D. Bumgardner, J.L. Ong, Biomaterials 27 (2006) 5512–5517, doi:10.1016/J.BIOMATERIALS.2006.07.003.
[145] P.S. Murphy, G.R.D. Evans, Plast. Surg. Int. 2012 (2012) 190436, doi:10.1155/2012/190436.
[146] N.A. Agha, Z. Liu, F. Feyerabend, R. Willumeit-Römer, B. Gasharova, S. Heidrich, B. Mihailova, Mater. Sci. Eng. C. 91 (2018) 659–668, doi:10.1016/J.MSEC.2018.06.001.
[147] K. Bryła, J. Horky, M. Krystian, L. Lityńska-Dobrzyńska, B. Mingler, Mater. Sci. Eng. C. 109 (2020) 110543, doi:10.1016/J.MSEC.2019.110543.
[148] D. Tie, F. Feyerabend, W.D. Müller, R. Schade, K. Liefeith, K.U. Kainer, R. Willumeit, Eur. Cell. Mater. 25 (2013) 284–298 discussion 298, doi:10.22203/ECM.V025A20.
[149] H.L. Kim, J.S. Park, Y.W. Chang, Mater. Sci. Eng. A. 540 (2012) 198–206, doi:10.1016/J.MSEA.2012.01.126.
[150] S.Q. Luo, A.T. Tang, B. Jiang, W.J. Liu, R.J. Cheng, F.S. Pan, Mater. Res. Innov. 19 (2015) S133–S137, doi:10.1179/1432891715Z.0000000001529.

[151] J.A. Yasi, L.G. Hector, D.R. Trinkle, Acta Mater 58 (2010) 5704–5713, doi:10.1016/J.ACTAMAT.2010.06.045.
[152] S. Gorsse, C.R. Hutchinson, B. Chevalier, J.F. Nie, J. Alloys Compd. 392 (2005) 253–262, doi:10.1016/J.JALLCOM.2004.09.040.
[153] A. Akhtar, E. Teghtsoonian, Philos. Mag. 25 (2006) 897–916, doi:10.1080/14786437208229311.
[154] C.J. Hashemi N, Phase diagrams of binary magnesium alloy, ASM International, 1988.
[155] M. Taheri, R.C. Phillips, J.R. Kish, G.A. Botton, Corros. Sci. 59 (2012) 222–228, doi:10.1016/J.CORSCI.2012.03.001.
[156] M. Liu, S. Zanna, H. Ardelean, I. Frateur, P. Schmutz, G. Song, A. Atrens, P. Marcus, Corros. Sci. 51 (2009) 1115–1127, doi:10.1016/J.CORSCI.2009.02.017.
[157] F. Cao, G.L. Song, A. Atrens, Corros. Sci. 111 (2016) 835–845, doi:10.1016/J.CORSCI.2016.05.041.
[158] M. Haghshenas, J. Magnes. Alloy. 5 (2017) 189–201, doi:10.1016/J.JMA.2017.05.001.
[159] Y. Yan, H. Cao, Y. Kang, K. Yu, T. Xiao, J. Luo, Y. Deng, H. Fang, H. Xiong, Y. Dai, J. Alloys Compd. 693 (2017) 1277–1289, doi:10.1016/J.JALLCOM.2016.10.017.
[160] Y. Zamani, H. Ghazanfari, G. Erabi, A. Moghanian, B. Fakić, S.M. Hosseini, B.P.M. Fakić, J. Compos. Compd. 3 (2021) 71–83, doi:10.52547/JCC.3.1.7.
[161] Y. Wang, P. Fu, N. Wang, L. Peng, B. Kang, H. Zeng, G. Yuan, W. Ding, Engineering 6 (2020) 1267–1275, doi:10.1016/J.ENG.2020.02.015.
[162] N. Sezer, Z. Evis, M. Koç, J. Magnes. Alloy. 9 (2021) 392–415, doi:10.1016/J.JMA.2020.09.014.
[163] S. Ganesan, M. Yaghoobi, A. Githens, Z. Chen, S. Daly, J.E. Allison, V. Sundararaghavan, Int. J. Plast. 137 (2021) 102917, doi:10.1016/J.IJPLAS.2020.102917.
[164] M. Zhang, J. Wang, J. Han, H. Sui, H. Huang, K. Jin, F. Qian, Calphad 67 (2019) 101684, doi:10.1016/J.CALPHAD.2019.101684.